TECHNISCHE UNIVERSITÄT MÜNCHEN

Fakultät für Medizin

Inhalational anesthetics do not deteriorate Amyloid-β-derived pathophysiology of Alzheimer's disease: investigations on the molecular and neuronal level

Carolin Hofmann

Vollständiger Abdruck der von der Fakultät für Medizin der Technischen Universität München zur Erlangung des akademischen Grades einer Doktorin der Naturwissenschaften genehmigten Dissertation.

Vorsitz: Prof. Dr. Ulrike Protzer

Prüfer*innen der Dissertation:

1. apl. Prof. Dr. Gerhard Rammes
2. Prof. Dr. Aphrodite Kapurniotu

Die Dissertation wurde am 04.04.2022 bei der Technischen Universität München eingereicht und durch die Fakultät für Medizin am 11.10.2022 angenommen.

Klinikum rechts der Isar

Inhalational anesthetics do not deteriorate Amyloid-β-derived pathophysiology in Alzheimer's disease: investigations on the molecular and neuronal level

von
Carolin Hofmann

Zur Erlangung des Grades
Doktor der Naturwissenschaften (Dr. rer. nat.)

Always remember for those who cannot.

Parts of this dissertation were published in:

Hofmann C., Sander A. et al., **Inhalational anesthetics do not deteriorate Amyloid-β-derived pathophysiology in Alzheimer's disease: investigations on the molecular, neuronal and behavioral level.** J Alzheimers Dis. 2021;84(3):1193-1218.

Table of contents

Abbreviations

aCSF	Artificial cerebral spinal fluid
AD	Alzheimer's disease
AMPA	α-Amino-3-hydroxy-5-methyl-4-isoxazolpropionacid
ApoE	Apoliprotein E
APS	Ammonium Persulfate
Aβ	Amyloid-beta
AβPP	Amyloid-beta Precursor Protein
AβpE3	pyroglutamate-modified amyloid-β
Atg	Autophagy-related-protein
BACE1	Beta-Secretase 1 (ß-site of APP cleaving enzyme)
CA	*Cornu Ammonis*
CI	Confidence interval
CNS	Central Nervous System
CSF	Cerebral spinal fluid
ddH_20	Double distilled water
DG	Dentate gyrus
DMSO	Dimethyl sulfoxide
ECL	Enhanced Chemiluminescence
EGFP	Enhanced green fluorescent protein
ELISA	Enzyme-Linked-Immunosorbent-Assay
FAD	Familial Alzheimer's disease
GA	General anesthesia
GCL	Granule cell layer
GFP	Green fluorescent protein
h	Hours
HCN	Hyperpolarization-activated, cyclic nucleotide-gated
HFIP	Hexafluorisopropanol
HRP	Horseradish-peroxidase
KDa	Kilodalton
LTD	Long-Term Depression
LTP	Long-Term Potentiation
MCI	Mild Cognitive Impairment
ML	Molecular layer
NFTs	Neurofibrillary tangles
NGS	Normal goat serum
NMDARs	*N*-methyl-D-aspartate receptors
PAGE	Polyacrylamide gel electrophoresis

PBS	Phosphate buffer saline
PI3K-Class III	Phosphatidylinositol3-Kinase Class III
Pl	Placebo
PP	Perforant Path
PSEN	Presenilin
RIPA	Radioimmunoprecipitation Assay
ROI	Region of interest
ROS	Reactive oxygen species
RT	Room temperature
SDS-PAGE	Sodium dodecyl sulfate-polyacrylamide gel electrophoresis
TBS/T	Tris-buffered-saline with Tween20
TR-FRET	Time-resolved fluorescence resonance energy transfer
ULK	Unc-51-like-Kinase
VSDI	Voltage sensitive dye imaging
WB	Western Blot
WT	Wildtype
3NTyrAβ	3-Nitrotyrosine-Aβ

Abstract

Background: Inhalative anesthetics are routinely used for general anesthesia in humans including patients suffering from Alzheimer's disease (AD). Several studies suggest that anesthetics such as isoflurane and sevoflurane may induce changes consistent with AD neuropathogenesis, e.g., increased amyloid-beta (Aβ) protein aggregation resulting in an increased neurotoxicity. In contrast, other studies showed some neuroprotective effects, e.g. with the noble gas xenon.

Objective: In the present study, possible interactions of xenon, isoflurane and sevoflurane with different Aβ species were investigated regarding Aβ aggregation, neuronal activity and synaptic plasticity of the hippocampus, as well as changes in the expression levels of autophagy proteins.

Methods: By means of time-resolved fluorescence resonance energy transfer (TR-FRET) and silver staining, Aβ aggregation was investigated in the presence of anesthetics. Changes in neuronal plasticity due to application of anesthetics and Aβ-amyloid species 1-42 ($Aβ_{1-42}$) and the post-translationally modified forms pyroglutamate-modified amyloid-(AβpE3) and nitrated Aβ (3NTyrAβ) were detected by quantification of long-term potentiation (LTP) and spine density in the murine hippocampus. Network activity in the tri-synaptic hippocampal circuit was monitored via voltage-sensitive dye imaging (VSDI) and changes in the expression level of autophagy proteins via western blotting.

Results: TR-FRET and silver staining revealed that isoflurane and sevoflurane did not affect Aβ aggregation whereas xenon even alleviates the propensity for Aβ to aggregate. Xenon partially reversed AβpE3-induced synaptotoxic effects on LTP and $Aβ_{1-42}$-induced spine density attenuation, thereby showing neuroprotective activity. In the presence of $Aβ_{1-40}$ and AβpE3, anesthetic-induced depression of neuronal activity propagation monitored by VSDI, recovered after xenon, but not isoflurane and sevoflurane removal. When slices were pretreated with $Aβ_{1-42}$ or 3NTyrAβ neuronal activity did not recover after washout of xenon, sevoflurane or isoflurane. Anesthetics as well as Aβ had no influence on the expression level of proteins important for autophagy.

Conclusions: Different anesthetics in the specific context of Aβ-induced neurotoxicity were tested, investigating different levels of complexity. Either anesthetic tested did not aggravate AD pathology *in vivo* and *in vitro* through acceleration of oligomerization or changes in the expression of autophagy proteins, whereas xenon showed some beneficial effects.

Abstract in German

Hintergrund: Inhalationsanästhetika werden routinemäßig zur Einleitung und Aufrechterhaltung einer Vollnarkose in Menschen verwendet. Unter diesen Patienten sind auch Patienten, die an der Alzheimer Erkrankung leiden. Einige Studien weisen darauf hin, dass die verwendeten Anästhetika (z. B. Isofluran und Sevofluran) pathologische Veränderungen hervorrufen können, die mit der Alzheimer-Pathologie in Zusammenhang stehen: etwa eine erhöhte Amyloid-beta(Aβ)-Aggregation, die zu einer erhöhten Synaptotoxizität führen kann. Im Gegensatz dazu haben andere Studien gezeigt, dass Inhalationsanästhetika neuroprotektive Eigenschaften aufweisen, wie etwa das Edelgas Xenon.

Ziel: Untersuchungen möglicher Interaktionen von Xenon, Isofluran und Sevofluran mit verschiedenen Aβ-Spezies. Der Fokus lag auf Aβ-Aggregationen, neuronaler Aktivität und synaptischer Plastizität des Hippokampus, sowie Veränderungen der Expression von Autophagie-Proteinen.

Methoden: Mittels time-resolved fluorescence resonance energy transfer (TR-FRET) und Silberfärbungen wurde der Einfluss von Anästhetika auf die Aβ-Aggregation untersucht. Veränderungen der neuronalen Plastizität durch Anästhetika und der Amyloid-Spezies 1-42 ($Aβ_{1-42}$) und die posttranslational modifizierten Formen Pyroglutamat-modifiziertes Amyloid-(AβpE3) und nitriertes Aβ (3NTyrAβ) wurden durch Untersuchung der Langzeitpotenzierung (LTP) und der Spine Density im murinen Hippokampus nachgewiesen. Die neuronale Aktivität des trisynaptischen Hippokampus-Schaltkreises wurde mittels Voltage-Sensitive-Dye-Imaging (VSDI) und Veränderungen in der Expression von Proteinen, die für die Autophagie wichtig sind, mittels Western Blotting getestet.

Ergebnisse: Ergebnisse der TR-FRET-Assays und Silberfärbungen zeigten, dass Isofluran und Sevofluran die Aggregation von Aβ nicht beeinflussen. Xenon hingegen reduzierte die Aggregation von Aβ signifikant. In den LTP-Experimenten konnte Xenon die synaptotoxischen Effekte von $Aβ_{1-42}$ teilweise reversieren. Zudem zeigte Xenon neuroprotektive Eigenschaften gegenüber AβpE3-induzierter Synaptotoxizität in Spine-Density-Experimenten. VSDI-Experimente zeigten, dass sich die neuronale Aktivität der Hirnschnitte die in $Aβ_{1-40}$ und AβpE3 inkubiert waren nach dem Entfernen von Xenon, aber nicht von Isofluran und Sevofluran, wieder regeneriert. Wenn die Schnitte mit $Aβ_{1-42}$ oder 3NTyrAβ inkubiert wurden, erholte sich die neuronale Aktivität nach dem Auswaschen von Xenon, Sevofluran oder Isofluran nicht. Sowohl Anästhetika als auch $Aβ_{1-42}$ hatten keinen Einfluss auf die Expression von Autophagie-Proteinen.

Schlussfolgerung: Keines der untersuchten Anästhetika verschlechterte die Alzheimer-Pathologie *in vivo* und *in vitro* durch Erhöhung der Oligomerisierung oder Veränderungen der Expression von Autophagie-Proteinen. Xenon zeigte neuroprotective Wirkungen auf die Aβ-Aggregation, LTP und Spine Density.

Dedicated to my family

1. Introduction

1.1 Alzheimer's disease – the discovery of 'presenile dementia'

The German psychiatrist Dr. Aloysius Alzheimer started describing and investigating the first registered case of 'presenile dementia' in his 51-year old patient Auguste Deter in 1901 (Fig. 1). Dr. Alzheimer observed and recorded her clinical symptoms over several years in a psychiatric asylum in Frankfurt (Germany) until Mrs. Deter died at age 56 in 1906. He investigated her brain in Emil Kraepelin's laboratory in Munich and found 'amyloid plaques' and 'neurofibrillary tangles', which he stained with the newly developed Bielschowsky's silver staining method (Alzheimer 1911, Alzheimer, Stelzmann et al. 1995) (Fig. 1, right). He first presented his findings at a meeting in Munich in 1906 (Graeber and Mehraein 1999). In 1910, Kraepelin named the disease 'Alzheimer's disease' (AD).

Until today, the cause of the disease remains poorly understood, only some of the psychiatric symptoms can be treated, and there is no cure for patients suffering from this devastating disease.

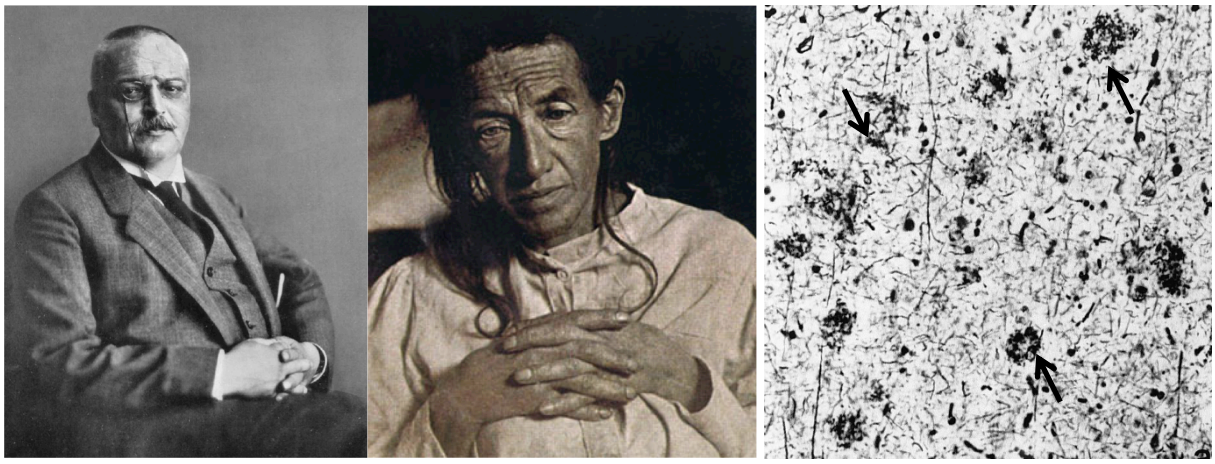

Fig. 1: Dr. Aloysius Alzheimer (left), his patient Auguste Deter (middle) and a section of her cerebral cortex stained with the Bielschowsky's silver staining method showing amyloid-plaques and tangles (right, arrows) (modified after Alzheimer (1911)).

1.2 Prevalence and symptoms of AD

AD is a slowly progressing irreversible neurodegenerative disease that affects about 44 million people worldwide. The number of affected people is predicted to increase up to 139 Mio until 2050 because of the increasing life expectancy due to medical progresses and higher birth rates of humans (Gauthier, Rosa-Neto et al. 2021). AD is the most common form of dementia and the incidence to develop sporadic AD rises almost logarithmically with age (Selkoe 2001).

Findings suggest that the neuropathological progression and clinical manifestation of AD differs between men and women. The prevalence to develop AD seems to be higher in women than in men (women account for two-thirds of AD patients) (Herbert, Weuve et al. 2013). This is on the one hand

due to the increased life expectancy of women (Austad 2006) but scientists believe that there is more to this and future studies need to address this important question.

Alzheimer's first patient was a woman and showed cardinal symptoms of the disease that we still observe in most AD patients nowadays (Selkoe 2001). The onset of sporadic AD is at about 65 years. The first symptoms patients realize are memory deficits in everyday life that are untypical for their age. Psychiatrists may diagnose patients with 'Mild Cognitive Impairment' (MCI) if there are no other clinical symptoms such as brain atrophy or other abnormalities. MCI is the intermediate neuropathology between normal aging and AD (Fig. 2). The cognitive decline then progresses steadily within several years. MCI nowadays represents early-stage AD (Morris, Storandt et al. 2001) and is usually followed by moderate-stage AD. This so called 'mid-stage AD' is the longest phase of the disease and can last many years. Symptoms are an unusual degree of confusion, difficulty to find words, reduced vocabulary and problems with routine tasks in everyday life. Patients often react angry, frustrated and anxious. Due to those symptoms, patients require a great level of care. In the last and most severe stage of AD (Fig. 2), patients cannot recognize people or communicate in any way. Additional symptoms are weight loss, seizures, increased sleeping, hallucinations, difficulty swallowing and lack of bladder and bowel control. The most frequent cause of death is aspiration pneumonia. Patients live four to eight years after diagnosis on average, but as long as about 20 years after diagnosis of AD (Association 2021).

Other forms of dementia have to be excluded before AD can be diagnosed. The second leading form of dementia after AD is vascular dementia (about 40% of all dementia cases). A blockage or damage to a blood vessel leads to a stroke (infarct) or bleeding that damages brain tissue. Depending on where the damage occurs, neurons die and certain cognitive dysfunctions develop. AD and vascular dementia often coexist. Sleep disturbances, hallucinations and parkinsonian movement features are hallmarks of Lewy body dementia. These symptoms also occur in the absence of memory impairment. Alpha-synuclein proteins aggregate in the brain and damage neurons. DLB can also coexist with AD. Another form of dementia is the fronto-temporal lobar degeneration. Patients show changes in their personality and behavior and experience severe language problems resulting from atrophy of the frontal and temporal lobes of the brain through abnormal tau-protein (will be further explained in 1.3.4) inclusions in neurons (Association 2021).

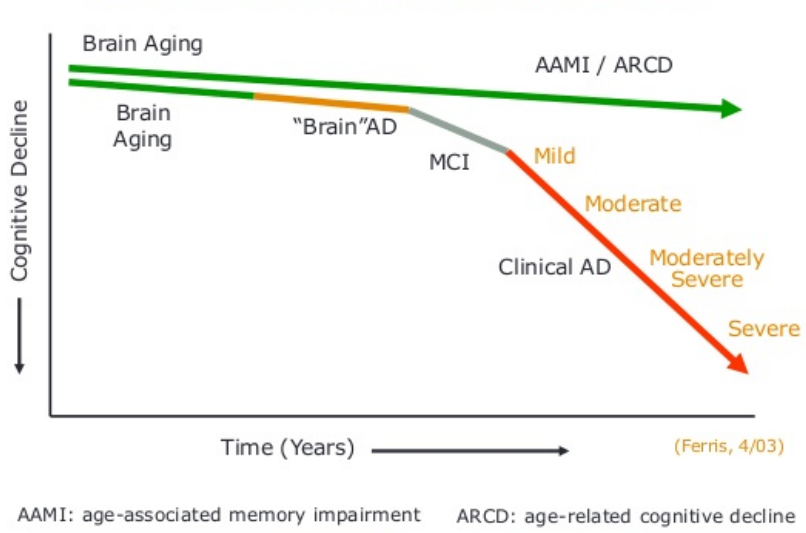

Fig. 2: Development of cognitive decline over time (in years). Normal aging of the brain leads to AAMI/ARCD. AD develops from MCI to severe cognitive decline over years (modified after Golomb, Kluger et al. (2004)).

1.3 Pathology of AD

The symptoms of AD are caused by the progressing loss of neurons in the brain. The frontal, temporal and parietal lobes and especially the hippocampus, to name just a few affected areas of the brain, show a severe atrophy over time (Pini, Pievani et al. 2016) (Fig. 3). Scientists believe that synaptic dysfunctions in early stages of the disease lead to this neurodegeneration in mid to late stages of AD, but the groundbreaking discovery of the 'real' cause is not yet in sight. AD is regarded as being a multigenic degenerative disease, because of the many different pathologies scientists were already able to discover (Selkoe 2001). The current state of scientific knowledge of the pathology of AD will be explained in the following chapters.

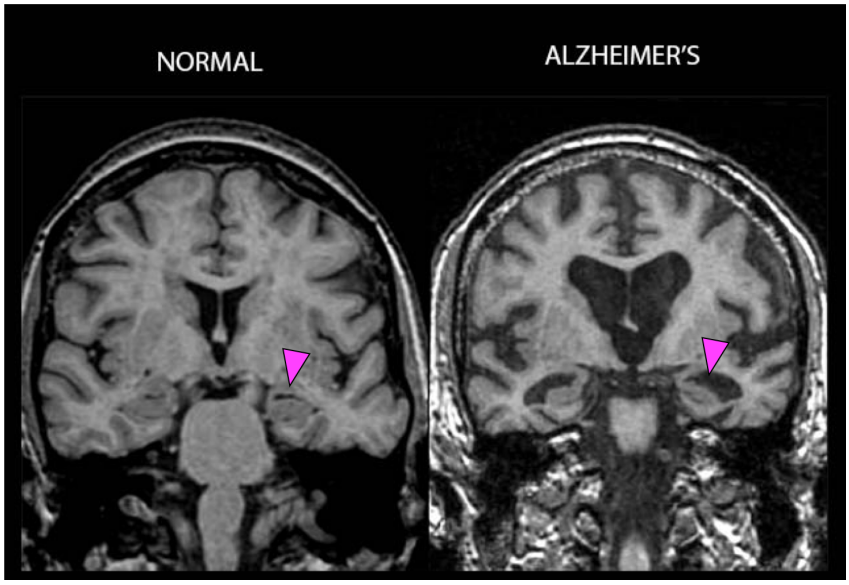

Fig. 3: Magnetic Resonance Image of a healthy brain compared to an AD patient showing severe atrophy in the hippocampus (arrows) and other brain regions (dark areas) (from: https://www.hopkinsmedicine.org/research/advancements-in-research/fundamentals/in-depth/we-need-to-talk-about-alzheimers-disease; last accessed February 2021).

1.3.1 The Aβ-hypothesis of Alzheimer's disease

One of the most unifying hypotheses about the cause of AD is the 'Amyloid-beta hypothesis'. In the original hypothesis scientists propose that altered processing and imbalanced clearance of the Aβ protein lead to an accumulation and aggregation of the protein to extracellular insoluble plaques in the brain and cause AD before other pathologies occur (e.g. tau pathologies, neurodegeneration) (Hardy and Allsop 1991, Selkoe 2001).

Aβ derives from the proteolysis of the Amyloid-Precursor-Protein (AβPP) via the so called amyloidogenic pathway. In a first step AβPP gets cleaved by the β-secretase and a 99-residue C-terminal fragment (C99) is generated (BACE1). The fragment gets cleaved by the γ-secretase and generates Aβ peptides (Sinha, Anderson et al. 1999, Vassar, Bennett et al. 1999) (Fig. 4). Aβ can then exist in different forms such as monomers, dimers, higher oligomers, polymers and fibrils (Selkoe 2000). Aβ in its monomeric form and at low concentrations is thought to be neuroprotective and to have several important physiological functions (Giuffrida, Caraci et al. 2010, Giuffrida, Tomasello et al. 2015).
Aβ consists of 36-43 amino acids with $A\beta_{1-42}$ and $A\beta_{1-40}$ being the most prevalent Aβ isoforms in plaques (Selkoe 2001). If AβPP is instead cleaved by the α- and γ-secretase through the non-amyloidogenic pathway, the generation of toxic Aβ proteins is prevented (Lammich, Kojro et al. 1999, Hiltunen, van Groen et al. 2009) (Fig. 4). AβPP is a highly conserved, large protein (4 KDa), which is expressed in the complete central nervous system (Hiltunen, van Groen et al. 2009).
The function of AβPP and Aβ under normal conditions is not well understood, but researchers showed that the proteins are important for a normal neuronal metabolism and information processing in the brain (Puzzo, Privitera et al. 2008, Abramov, Dolev et al. 2009). They are important for the energy supply to neurons (Giuffrida, Tomasello et al. 2015) and might even have antimicrobial functions (Soscia, Kirby et al. 2010). In healthy mice, amounts of Aβ proteins are in the picomolar range. An Aβ concentration around 200 pM enhances synaptic plasticity and memory function (Puzzo, Privitera et al. 2008) and has several important functions for the brain such as adjustment of synaptic function and a faster recovery from brain injuries (Pearson and Peers 2006, Brothers, Gosztyla et al. 2018). A massive production of Aβ exceeding an amount of ~20 nM and aggregation to neurotoxic oligomers shows the change from a benign to a neurotoxic protein (Pearson and Peers 2006).

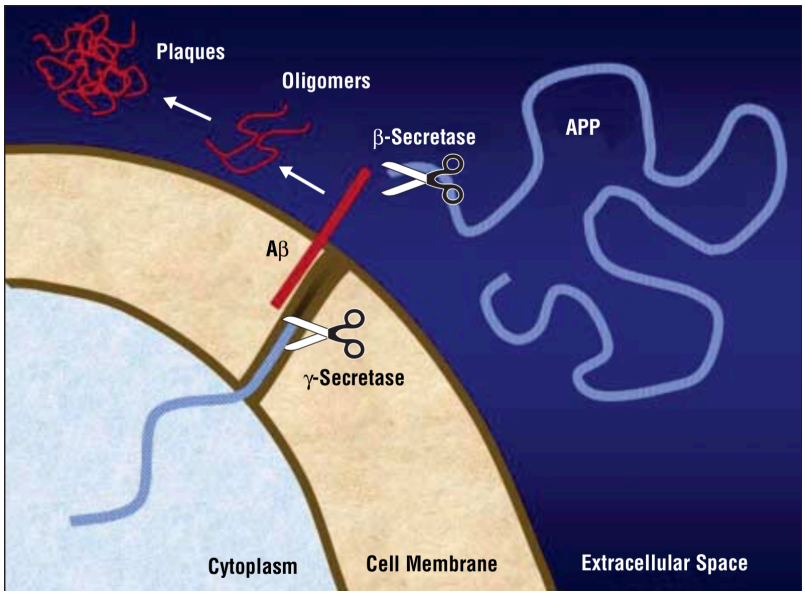

Fig. 4: The proteolytic processing of the β-amyloid precursor protein (APP) and the fate of Aβ (modified after Selkoe (2005)).

Glenner and Wong (1984) were the first scientists to extract, purify and sequence Aβ fragments from a human brain with Down's syndrome. They found the proteins to be the same as in AD brains and suggested that the genetic defect leading to AD is located on chromosome 21 (Glenner and Wong 1984). Patients suffering from Down's syndrome show AD-like symptoms and pathologies starting at about age 30 (Lai and Williams 1989).

1.3.2 The modified Amyloid Hypothesis and its role in Alzheimer's disease

Several years of research after the Aβ hypothesis was formulated, studies showed that not only the extracellular accumulation of Aβ peptides, but also the intracellular accumulation of Aβ plays a central role for the pathologic cascade of AD (Wirths, Multhaup et al. 2004). Intracellular Aβ was first discovered by Wertkin, Turner et al. (1993) in a neuronal carcinoma cell line. Scientists mostly agree that intracellular Aβ accumulation is one of the first neurodegenerative alterations in the AD brain and resemble early stage AD. The first intracellular accumulations can be found in pyramidal neurons of the hippocampus and entorhinal cortex, regions where later on the first Aβ plaques are found (Fernandez-Vizarra, Fernandez et al. 2004, Wirths, Multhaup et al. 2004).

Different types of AβPP transgenic mice show intracellular Aβ accumulation in early stages of pathology (showed by immunoreactivity with Aβ antibodies) but the reactivity in the cells declined with increased extracellular plaque formation (Wirths, Multhaup et al. 2002). These and other observations confirm that intracellular Aβ accumulation occurs before extracellular Aβ plaques or other pathologies develop (Oddo, Caccamo et al. 2003).

Twenty years ago, scientists found small, soluble (diffusible) $A\beta_{1-42}$ oligomers to be neurotoxic and one of the major contributors to neurodegeneration in AD-brains. They showed that nanomolar concentrations of these oligomers were neurotoxic for organotypic mouse brain slice cultures and found them to block formation of long term potentiation (LTP) in the CA1-layer of the hippocampus of

mice (Lambert, Barlow et al. 1998). LTP is the electrophysiological correlate for learning and memory and will be explained in detail later (1.6.2). Studies also found that Aβ oligomerization intracellularly occurs before memory dysfunctions develop. This indicates that the buildup of small and soluble Aβ oligomers might be the main event leading to neurotoxicity and neurodegeneration, but the reasons remain elusive (Gouras, Tsai et al. 2000, Gong, Chang et al. 2003, Schmitz, Rutten et al. 2004, Takahashi, Almeida et al. 2004, Wirths, Multhaup et al. 2004, Yang, Li et al. 2017) (Fig. 5). Oligomers with a low molecular weight of less than 50 kDa have been described as non-toxic and related to Aβ plaques, whereas high molecular weight oligomers greater than 50 kDa are toxic and the most common Aβ form in the AD brain under native conditions and unrelated to Aβ plaques (Cline, Bicca et al. 2018).

It is believed that Aβ triggers its toxicity for neurons mainly through N-methyl-D-aspartate receptors (NMDARs) (Fig. 6). These receptors play an important role in synaptic transmission and plasticity. NMDARs are transmembrane receptors with 3 subunits (NR1-3). These subunits are divided into subunits: NR2A-D and NR3A-B (Ulbrich and Isacoff 2008). They are located at the postsynaptic membrane and get activated through binding of the agonist glutamate and the co-agonists D-serine or glycine (Furukawa, Singh et al. 2005). Other important postsynaptic receptors that get activated through glutamate are α-amino-3-hydroxy-5-methyl-4-isoxazolpropionacid (AMPA)- and kainate-receptors (Traynelis, Wollmuth et al. 2010). Glutamate gets released into the synaptic cleft from the pre-synapse and then binds to the postsynaptic receptors to activate them. NMDARs open for the influx of Na^+, Ca^{2+} and K^+. After activation of the receptors, the cell recycles the glutamate. This process ensures that NMDARs, and glutamate-receptors in general, are only activated when necessary and not in resting states of the cell. During the resting states, Magnesium (Mg^{2+}) blocks NMDAR channels (Herman and Jahr 2007).

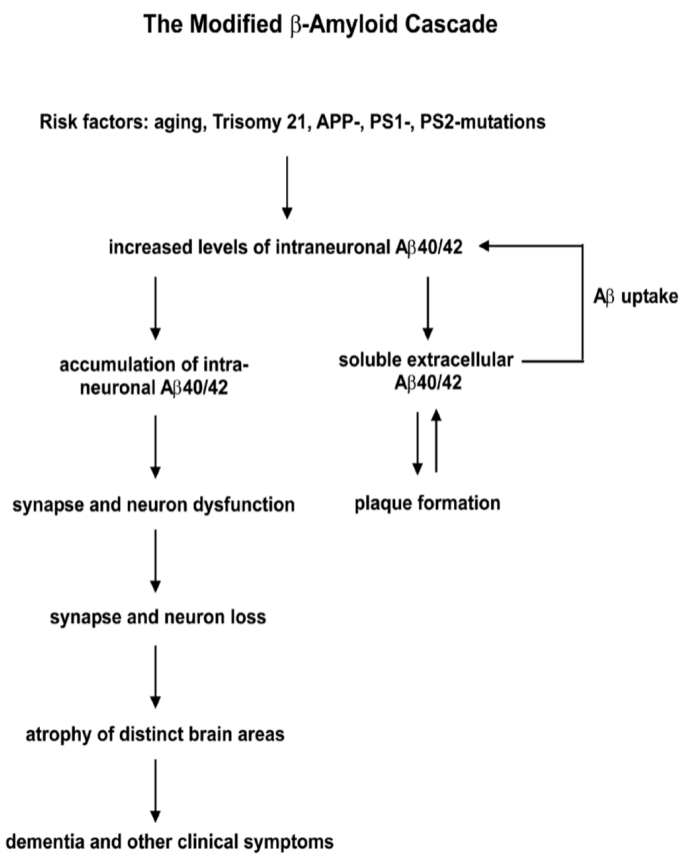

Fig. 5: Scheme of the modified β-amyloid cascade. Certain risk factors lead to increased intraneuronal Aβ which then causes plaque formation through extracellular proteins. This can then lead to synapse and neuron dysfunctions which in then end generates dementia such as AD (modified after Wirths, Multhaup et al. (2004)).

A balance between activation and deactivation is fundamental for a healthy function of synaptic plasticity and transmission, which resemble learning and memory production. Both hyperactivation and hypoactivation of the NMDARs can be neurotoxic and lead to neurodegeneration. Here is where the toxicity of Aβ comes into play. Studies showed that the accumulation of Aβ hyperactivates NMDARs through malfunction of glutamate release and degradation. An increased amount of glutamate stays in the synaptic cleft and activates the receptors continuously. This chronic activation leads to an increased signal-to-noise ratio. Relevant signals for learning and memory cannot be distinguished from the continuous background noise and memory dysfunctions develop (Selkoe 2001, Parsons, Stoffler et al. 2007) (Fig. 6).

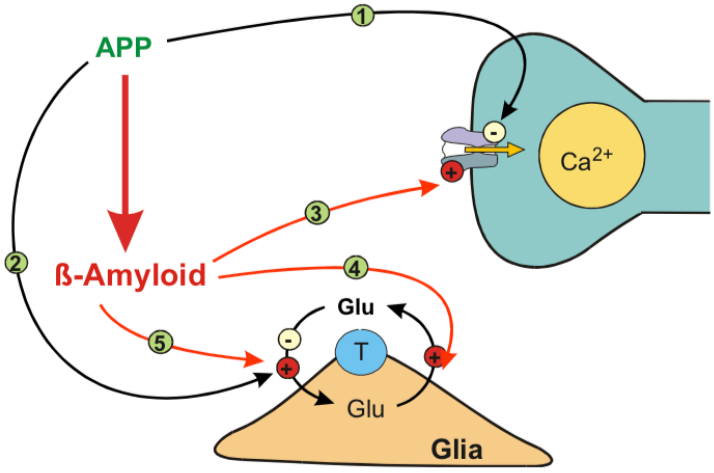

Fig. 6: Effects of β-Amyloid on the glutamate receptor. Under normal conditions, APP has antagonistic effects on glutamatergic receptors (1), removes glutamate from the synaptic cleft and activates glutamatergic signaling (2). When ß-amyloid is generated from AβPP, this has opposite effects on NMDARs (3) and glutamate (4). Glutamate is building up in the synaptic cleft (5) (Parsons, Stoffler et al. 2007)).

1.3.3 Most prevalent isoforms of Aβ in AD

$A\beta_{42}$ and $A\beta_{40}$ are the most prevalent isoforms of Aβ in the brain of AD patients. Studies showed that although $A\beta_{1\text{-}40}$ is the most frequent isoform of Aβ plaques (~80-90% of plaques consist of $A\beta_{1\text{-}40}$, ~5-10% of $A\beta_{1\text{-}42}$ (Jarrett, Berger et al. 1993, Iwatsubo, Odaka et al. 1994)), whereas $A\beta_{1\text{-}42}$ is much more likely to aggregate (Cappai and Barnham 2008) and its toxicity is even comparable to pre-aggregated $A\beta_{42}$ proteins. $A\beta_{40}$ is only likely to form toxic aggregates after pre-aggregation, only minimal cell death could be detected when cell cultures were treated with freshly solubilized $A\beta_{1\text{-}40}$, whereas $A\beta_{1\text{-}42}$ directly caused dose-dependent cell death in cell cultures (Tekirian, Yang et al. 1999).

Aβ can undergo many different posttranslational modifications in the brain that generate proteins such as pyroglutamate-modified $A\beta_{3\text{-}43}$ (AβpE3) and nitrated Aβ (3NTyr-10Aβ/3NTyrAβ) (Fig. 7). Studies showed that a truncation of Aβ can lead to an increase in aggregation of the protein and an increase of the Aβ toxicity for the brain (Pike, Burdick et al. 1993). When full length Aβ loses its first two amino acids through aminopeptidase A activity, followed by glutamyl cyclase at position 3, AβpE3 is formed. Extra-cytoplasmic aminopeptidases cannot degrade the Aβ peptide sufficiently because it is protected by L-glutamate, which converses to pyroglutamate. Additionally, scientists found less aminopeptidase activity in sporadic AD suggesting that even more AβpE3 accumulates and becomes a major part of senile plaques (Tekirian, Saido et al. 1998). AβpE3 is not specific to AD brains and can be found in the tissue of healthy patients, canine and polar bear brains (Tekirian, Saido et al. 1998). Still, AβpE3 is the most abundant truncated form of Aβ protein found in extracellular Aβ plaques in the brain of AD patients (Russo, Saido et al. 1997).

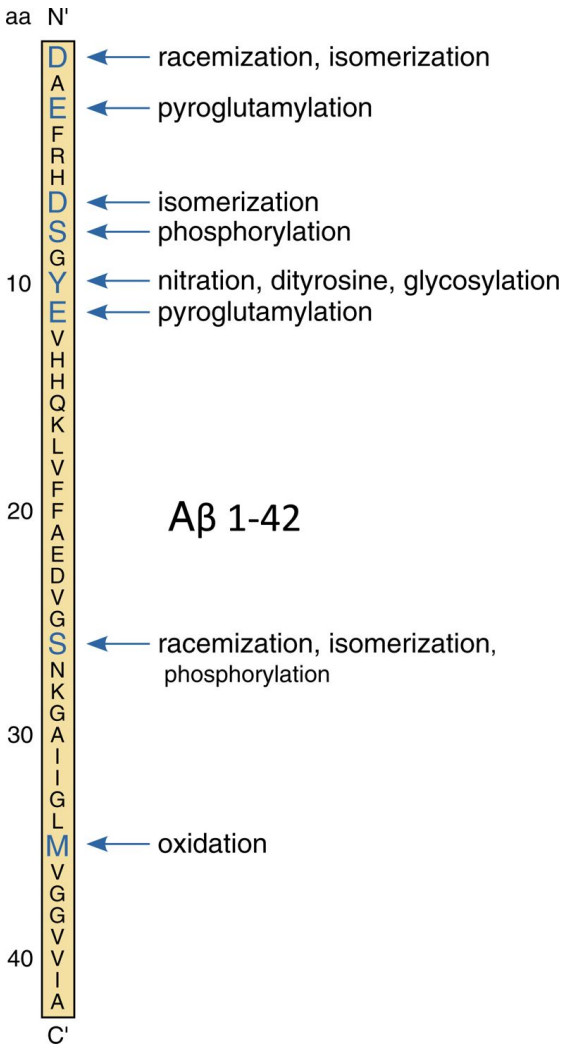

Fig. 7: Positions of post-translational modifications in $Aβ_{1-42}$. Blue letters show amino acid residues that are subject to post-translational modifications. Red circles mark the modified residues that lead to AβpE3 and 3NTyrAβ, both were investigated in this work (modified after Kummer and Heneka (2014)).

Tekirian, Yang et al. (1999) tested the effect of different truncated Aβ isoforms on primary cortical and hippocampal cell cultures and found pre-aggregated AβpE3 to have no difference in the level of toxicity compared to pre-aggregated $Aβ_{42}$, and AβpE3 to have no differences to $Aβ_{40}$. The scientists suggested that AβpE3 plays a critical role in extracellular plaque formation and neurodegeneration in AD although they showed in vitro that the truncated Aβ is not more toxic than full length $Aβ_{42}$ (Tekirian, Yang et al. 1999). In contrast to that, following studies proved that AβpE3 is more toxic and amyloidogenic than full-length Aβ. The protein even influenced the aggregation process of other Aβ isoforms and led to quicker protein seed formation (Schlenzig, Manhart et al. 2009, Nussbaum, Schilling et al. 2012, Schlenzig, Ronicke et al. 2012).

Elevated calcium levels (e.g. through chronic activation of NMDARs) lead to an increase in nitric oxide synthase through Ca^{2+}-calmodulin and production of nitric oxide (NO). NO is able to nitrate other proteins together with free radicals by adding a nitro group irreversibly to an amino acid, most likely

to tyrosine (Dawson and Dawson 1996, Rossi and Bianchini 1996). Guix, Uribesalgo et al. (2005) stated that Aβ is very likely to be nitrated at its tyrosine 10. 3NTyrAβ forms stable oligomers over time and prevents the formation of less toxic Aβ fibrils, therefore preserving its neurotoxicity. It also leads to an increase in aggregation and is found in the core of Aβ plaques of AD brains and transgenic mice (Kummer, Hermes et al. 2011, Guivernau, Bonet et al. 2016).
All previously mentioned forms of Aβ reduce the ability to induce LTP in acute murine hippocampal slices concentration-dependently (Rammes, Hasenjager et al. 2011, Rammes, Seeser et al. 2018, Bürge, Kratzer et al. 2019). Because of these findings and the high prevalence of the described Aβ isoforms in the AD brain, all four isoforms were investigated in this work.

1.3.4 Tau Pathology

Another typical brain lesion in brains of Alzheimer's patients and FTD are neurofibrillary tangles (NFTs) that consist of hyper-phosphorylated tau proteins (Fig. 8). Tau proteins are normally associated with microtubules, but in diseased brains they detach from microtubules, destabilize them and lead to failures in transport mechanisms of non-myelinated axons. The high expression of tau proteins mainly occurs in brains parts where memory and learning is processed (e.g. hippocampus, prefrontal cortex) (Hampel, Blennow et al. 2010).
Studies showed that tau tangles are most likely established after the development of Aβ plaques and it is not clear if they contribute to the development of AD or if they form as a result of other pathologies of AD (Ballatore, Lee et al. 2007). For diagnosis of dementia, the levels of *t-tau* and *p-tau* are measured in the CSF of patients to distinguish between AD and other forms of dementia (Hulstaert, Blennow et al. 1999).
In this dissertation however, Aβ proteins were the main focus.

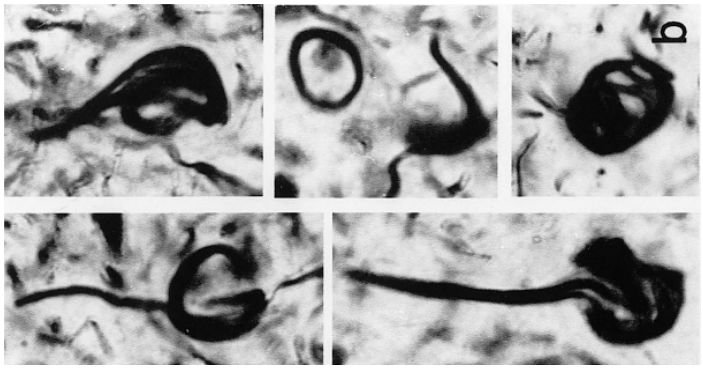

Fig. 8: Different types of tau tangles in the brain of August Deter stained with Bielschowsky' silver staining (modified after Graeber, Kosel et al. (1998)).

1.4 Familial Alzheimer's disease (FAD)

A very rare form of AD (only about 5% of all AD cases), called Familial Alzheimer's disease (FAD), is caused by autosomal dominant mutations of different genes. Mutations in the AβPP and presenilins

(PSEN) lead to a very similar pathology and similar symptoms compared to the sporadic form of AD as already explained in earlier chapters. Presenilins build the catalytic core to AβPP processing and γ-secretases in a healthy brain to generate Aβ proteins (Chavez-Gutierrez, Bammens et al. 2012). Sherrington, Rogaev et al. (1995) found more than 150 different mutations in these presenilins to be the reason for FAD. About 20 different pathogenic mutations have been found in the AβPP (Gotz and Ittner 2008, Lu, Wu et al. 2010). Still, the mechanisms by which the genetic alterations occur remain elusive and controversial (Chavez-Gutierrez, Bammens et al. 2012).
Studies showed that these mutations lead to an altered Aβ processing in the brain that ultimately progresses to the typical AD histopathology which can only be discriminated from the sporadic form of AD by its early onset at an age of about 30. That is why the disease is also called early-onset AD. Decades after Dr. Alzheimer described the disease in Auguste Deter, researchers investigated the remaining parts of her brain and found her to have the familial form of Alzheimer's disease (Graeber, Kosel et al. 1998).

1.5 General Anesthesia

In 1804, the Japanese surgeon Hanaoka Seishu was the first person to successfully perform general anesthesia (GA) during surgery (Novel: A Sawako, *The Doctor's Wife* (Tokyo: Kodansha International, 1978)). GA is a state of reversible unconsciousness (hypnosis) accompanied by immobility (loss of protective and motor reflexes), analgesia (relief from pain) and amnesia (deficit in memory). Different anesthetic drugs induce this loss of consciousness. They are administered to patients to induce and maintain GA to facilitate surgeries. They are inhalational (gases or volatile liquids) – or intravenous anesthetics. The most common form of GA combines these, using intravenous drugs to induce hypnosis and hence volatiles to maintain GA. Drug and dose are adjusted to each patient and the type of surgery and health background of the patient (Brown, Lydic et al. 2010).

Hypnosis-inducing drugs are a very diverse group of chemicals ranging from simple gases to complex steroids. Most of them have only one thing in common: producing the loss of consciousness in humans and animals. How exactly these drugs do that on the molecular level is not well understood. For some time, scientists suggested that lipid bilayers in the central nervous system (CNS) are disrupted somehow and anesthetic mechanisms are non-specific. In recent years, studies have shown that anesthetic drugs indeed act on specific selected targets such as ion channels, receptors and enzymes. A commonly accepted target is the neuronal GABA (gamma-aminobutyric-acid) type A ($GABA_A$) receptor, which is found at synapses throughout the CNS. It is composed of alpha, beta, and gamma subunits. The composition of the subunits varies with the location in the CNS and their function. GABA, one of the most important inhibiting neurotransmitters, activates the receptor. When activated, the receptor conducts Calcium through its pores, which lead to a hyperpolarization of the neuron and an inhibition of action potentials (Franks and Lieb 1993, Rudolph and Antkowiak 2004, Franks 2008). Several different drugs such as inhaled anesthetics, benzodiazepines, neuroactive steroids, barbiturates, ethanol and others bind to certain binding sites that are located among the

GABA-binding sites. Commonly used anesthetics such as the intravenous anesthetic propofol (Nagashima, Zorumski et al. 2005) and etomidate (Martin, Oh et al. 2009), as well as the volatile anesthetics isoflurane (Simon, Hapfelmeier et al. 2001) and sevoflurane (Ishizeki, Nishikawa et al. 2008) attenuate hippocampal synaptic plasticity through activation of GABARs. This strong inhibition is suggested to induce amnesia during general anesthesia (Campagna, Forman et al. 2003).
Another target of some anesthetics is the NMDAR. NMDARs are located both pre-synaptically and post-synaptically in neurons of the CNS. The receptor consists of the NR1 subunit, at least one of four NR2 subunits and two NR3 subunits. They are glutamate receptors and are activated when glutamate or glycine bind to its binding sites. When activated, positively charged ions flow through the cell membrane and excite the neuron. Most inhalational anesthetics inhibit the activation of NMDARs to some extend (Antkowiak 2001, Franks 2008, Brosnan 2012, Dong, Wu et al. 2013).

I focused on isoflurane and sevoflurane in this dissertation. They are halo ethers and produce their anesthetic effect via a strong potentiation of GABARs, a less potent inhibition of NMDARs and modulation of other ion channels and receptors that still need to be identified (Brosnan 2012).
Another focus of this dissertation is on the noble gas xenon. The mechanism on how xenon produces anesthesia will be explained in chapter 1.5.2.

An essential pharmacological parameter of inhalation anesthetics is the minimum alveolar concentration (MAC) at 1 atmosphere. The MAC is defined as the alveolar concentration of an inhalation anesthetic at which 50% of patients show no motor defense reaction to a defined pain stimulus. The MAC varies according to the species, its physical characteristics (e.g. age, weight) and type of anesthetic. Figure 9 shows how the MAC of sevoflurane, isoflurane and desflurane decreases with the patient's age.

	Sevoflurane	**Isoflurane**	**Desflurane**	**Xenon**
MAC_{human}	1.9% - 2.29%	0.91% - 1.49%	5.1% – 8.3%	63% - 71%
MAC_{mouse}	~ 3.22%	~ 1.4%	~ 8.6%	~ 160%

Tab. 1: MAC ranges in clinically used inhalational anesthetics in human and mice. Low concentrations represent the MAC for an 80-year-old patient, high concentrations represent the MAC for a 1-year-old patient (modified after (Mapleson 1996, Sonner, Gong et al. 2000, Haseneder, Kratzer et al. 2009).

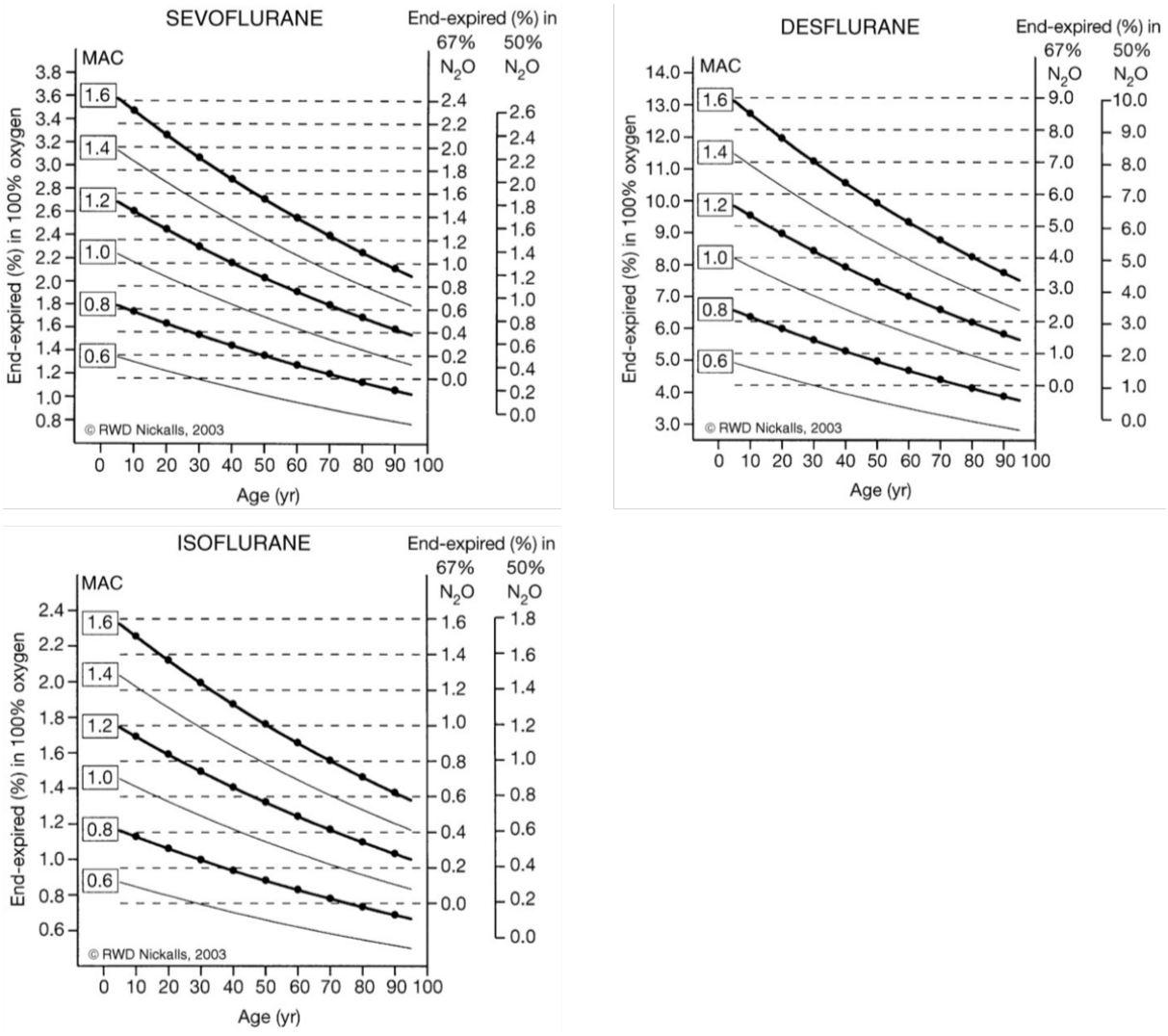

Fig. 9: Iso-MAC charts for sevoflurane, isoflurane and desflurane (age ≥1 year). The iso-MAC curves are drawn for MAC (y-axis) using an equation. Dots on the iso-MAC curves are to help alignment. The left-hand ordinate scale indicates the end-expired anesthetic concentration when using 100% oxygen. The two right-hand ordinate scales indicate the end-expired anesthetic concentration when using nitrous oxide (N_20) 50% and 67% in oxygen. For a given age (x-axis) and MAC, the associated end-expired anesthetic concentration is read from the appropriate ordinate scale. For example, a MAC of 1.2 for a 60-year-old patient using isoflurane and nitrous oxide 67% in oxygen requires an end-expired isoflurane concentration of ~ 0.5% (modified after Nickalls and Mapleson (2003)).

1.5.1 General anesthesia and Alzheimer's disease

Every day, thousands of patients undergo GA. Commonly used inhalative anesthetics have been hypothesized to increase the risk to develop AD or to accelerate the onset and progression of the disease, but there are no conclusive articles describing the association between anesthetics and AD (Jiang and Jiang 2015). Many different studies found contradictive results:

The commonly used volatile anesthetic isoflurane has been found to induce the activation of caspase-3, alter the processing of AβPP and increase levels of BACE and Aβ in H4-AβPP cell lines (Xie, Dong et al. 2007) It was also found to enhance the oligomerization of Aβ (Eckenhoff, Johansson et al. 2004)

and to induce DNA damage through oxidative stress and the p53 pathway (Ni, Li et al. 2017). Dong, Zhang et al. (2009) and Lu, Wu et al. (2010) described similar results for sevoflurane (one of the most commonly used volatile anesthetics) and also increased levels of caspase-3, AβPP, Aβ and BACE in naive mice and H4-AβPP cells.

In contradiction to these negative results about general anesthetics, studies in our lab showed that clinically relevant concentrations of isoflurane (Rammes, Starker et al. 2009) and sevoflurane (Haseneder, Starker et al. 2013) improved the cognitive performance of mice and increased the expression of certain subunits of NMDARs. Isoflurane even enhanced hippocampal LTP 24 h after anesthesia. Several studies found sevoflurane and isoflurane to block LTP in acute murine hippocampal slices, even when applied at concentrations below 1 MAC. This blockage would result in the memory deficits patients suffer from after GA (Dwyer, Bennett et al. 1992). In contradiction, Haseneder, Kratzer et al. (2009) investigated the effect of different concentrations of sevoflurane and isoflurane on CA1 LTP of and found only high concentrations to block LTP completely. The scientists suggest that additional mechanisms influencing synaptic plasticity in other brain regions important for memory formation contribute to memory deficits resulting from general anesthesia via sevoflurane or isoflurane. Jiang, Sun et al. (2017) suggest that isoflurane even acts neuroprotective in mice. They believe that low concentrations of isoflurane for a short time act neuroprotective (e.g. after brain injuries), and high concentrations for a long time neurotoxic. Repeated exposure to isoflurane in mid-adulthood even attenuated age-related cognitive impairments in transgenic AβPP/PS1 mice and slowed down the formation of Aβ plaques (Su, Zhao et al. 2012). Similarly, Liu, Zhang et al. (2015) found an exposure of mice to sevoflurane for one to three hours to improve their cognitive performance, and more than three hours to activate caspase-3 and apoptosis.

Trials in humans showed inconsistent results. It is well known that many elderly patients experience memory problems after GA (especially after cardiac surgery), this is commonly referred to as postoperative cognitive dysfunction (POCD). The reasons for the development of POCD remain elusive as well as if there is a relationship between POCD and AD (Bittner, Yue et al. 2011). Gasparini (2002) and Bohnen, Warner et al. (1994) did not find an association between exposure to GA and AD in a retrospective study. Several years later, scientists found exposure to GA in early and midlife to accelerate the onset of sporadic AD and also markers of neuroinflammation (interleukin (IL)-6, IL-10, tumor necrosis factor (TNFα) and total tau/A$\beta_{1\text{-}42}$ ratio in the CSF of patients to be increased (Tang, Baranov et al. 2011). Inhaled sevoflurane accelerated the progression of amnesic mild cognitive impairment (aMCI) to progressive MCI in a selected population (Liu, Pan et al. 2013). Chen, Lin et al. (2014) found especially patients with diabetes mellitus, hypertension, atherosclerosis or patients after a stroke to be at greater risk to develop dementia after GA. A randomized trial study comparing sevoflurane and isoflurane during cardiac surgery did not find any significant differences in the general clinical outcome (Jones, Bainbridge et al. 2016). The only significant difference was the faster recovery of response to command in patients that inhaled sevoflurane (7.5 +/- 5 min) compared to

isoflurane (18.6 +/- 5 min) because sevoflurane is less soluble in the blood (Frink, Malan et al. 1992). This feature allows a more rapid recovery (Gupta, Stierer et al. 2004).

It is of great interest to find out if anesthetics lead to the development of AD related pathologies or weather they could even help to prevent them, because anesthesiologists will encounter an increasing number of patients suffering from AD or MCI in the coming years (Palotas et al., 2010). This is due to the increasing average age of population (Statistisches Bundesamt; Fig. 10).

In the current study, I focused on the effects of sevoflurane, isoflurane and xenon.

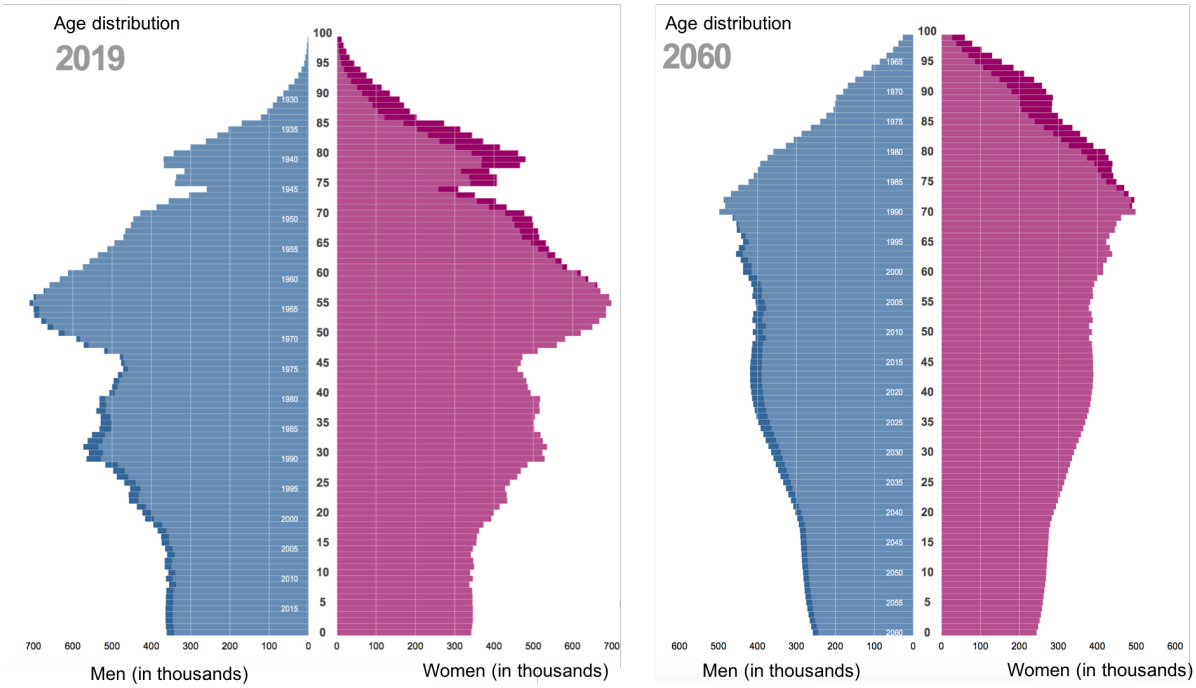

Fig. 10: Population pyramids for 2019 and 2060. Estimated population in year 2019 and 2060 focusing on age and gender. In 2019, the average age of population is around 50-60, whereas in 2060 the average age is estimated to be around 70-75 (modified after Statistisches Bundesamt DE; from: https://service.destatis.de/bevoelkerungspyramide/index.html#!y=2053; last accessed February 2022).

1.5.2 The noble gas xenon and its neuroprotective features

The Scottish chemist Sir William Ramsay and the English chemist Morris William Travers discovered the noble gas xenon (Xe, atomic number 53) in 1898 in the residue left over from evaporating components of liquid air. Together with krypton, argon, neon, helium and radon, xenon forms the chemical group of noble gases. Albert R. Behnke Jr. found it to have anesthetic features in 1931 (Behnke and Yarborough 1939). It was not until 1951 that xenon was used for general anesthesia during surgery. Xenon is a very rare (one part in 20 million (Ramsay 1903); 0,0000087% in the atmosphere), odorless and non-explosive noble gas in our atmosphere and its extraction is very cost and time intensive. It is purified by fractional distillation of liquefied air (Joyce 2000).

Xenon produces its anesthetic effect through competitive blocking (inhibition) of NMDARs and has almost no effect on GABA receptors and shows therefore no potentiation of inhibiting synaptic transmission (Franks, Dickinson et al. 1998, de Sousa, Dickinson et al. 2000, Haseneder, Kratzer et al. 2008, Kratzer, Mattusch et al. 2012). Only at heterologously transfected $GABA_A$-receptors at low GABA concentrations, a potentiation of the current responses by xenon could be observed (Hapfelmeier, Zieglgansberger et al. 2000).
A study in our lab showed that xenon concentration-dependently impairs hyperpolarization-activated, cyclic nucleotide-gated (HCN) cation channel function and reduces signal propagation in the thalamus (also referred to as 'gate to consciousness'), this may contribute to the hypnotic effect of xenon (Mattusch, Kratzer et al. 2015).

Xenon has many beneficial properties as a volatile anesthetic such as cardiovascular stability during surgery (Coburn, Kunitz et al. 2005), myocardial protection (Preckel, Schlack et al. 2002), analgesia (Nakata, Goto et al. 2001), a low blood:gas solubility and quicker introduction and faster awakening from anesthesia (Goto, Saito et al. 1997). Bronco, Ingelmo et al. (2010) found that xenon might have the ability to even reduce POCD after surgery when compared to sevoflurane anesthesia.
Studies on xenon showed that it acts neuroprotective in pre-clinical models of brain-injury and global cerebral hypoxia-ischemia (e.g. after resuscitation or in neonates after birth) through reduction of ischemia-induced neurotransmitter release and blockage of NMDARs (preventing overstimulation) (Esencan, Yuksel et al. 2013). Xenon also protected cultured cortical and subcortical neurons against mild excitotoxic stress (also a component of neuronal death in AD), suggesting a potential therapeutic effect of xenon (Lavaur, Lemaire et al. 2016). Recent studies in our lab showed that sub-anesthetic concentrations of xenon partially reverse the neurotoxic effects of $A\beta_{1-40}$ and $A\beta_{1-42}$ on LTP. This might result from the blockage of NMDARs through xenon which inhibits overstimulation of these receptors that lead to hyperexcitability (Bürge, Kratzer et al. 2019).

Although xenon has mostly positive features, there are some limitations besides the high cost. The potency of xenon is very high with a MAC of between 63% and 71% in adults and possibly even higher in children. The higher the MAC is, the less oxygen can be applied which is of course essential, especially for the developing brain of an infant (Goto, Saito et al. 1997). Additionally, due to its high density and viscosity, xenon leads to an increase in airway resistance in animal experiments (Zhang, Ohara et al. 1995), although the clinical relevance of this phenomenon seems to be rather low (Baumert, Hein et al. 2007). Another drawback of xenon anesthesia is a higher incidence of postoperative nausea and vomiting (PONV) compared to other frequently used anesthetics (Schaefer, Apfel et al. 2015, Fahlenkamp, Stoppe et al. 2016).

1.6 Learning and memory

1.6.1 The anatomy of the hippocampus and its role in memory formation

The hippocampus (plural: hippocampi) is an essential and well-conserved part of the vertebrate brain, is located in the medial temporal lobe below the cerebral cortex and belongs to the limbic system. There are two hippocampi, located in each brain hemisphere. The hippocampus resembles the shape of a seahorse (greek 'hippos'= horse; 'kampos'= sea monster) and forms together with the dentate gyrus (DG) and the subiculum the hippocampal formation (Fig. 11A).

In cross-sections of the hippocampus, several different cell layers show. The DG includes the molecular layer (ML; almost cell-free, occupied by different fibers and dendrites), the granule cell layer (GCL) and the polymorphic cell layer (PCL; mostly mossy cells) and tends to have a V-shape septally and a U-shape temporally (Amaral 2007).

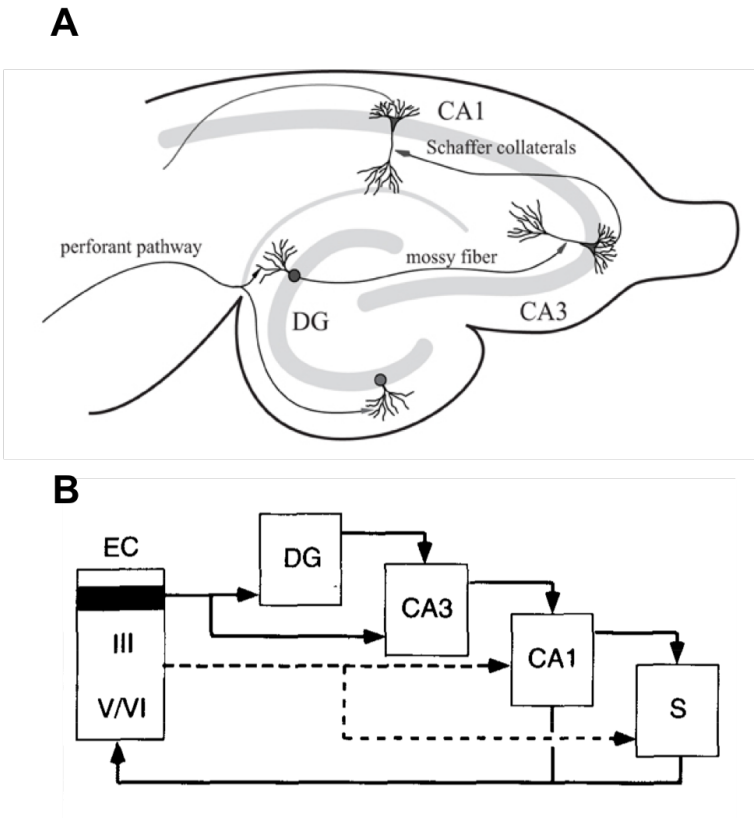

Fig. 11: Schematic drawing of the trisynaptic circuit in the hippocampus. A: The perforant path as the main input region sends information to the dentate gyrus (DG) from where mossy fibers connect to the CA1 and the Schaffer collaterals to the CA1 region of the hippocampus (modified after Hsiao (2013)). **B:** Schematic diagram illustrating the organization of the two perforant pathway projections to the other fields of the hippocampus. Cells in layer II of the entorhinal cortex (EC) project to the DC and to the CA3. Cells in layer Ill of the EC give rise to a distinct pathway that innervates the CA1 field of the hippocampus and the subiculum (S). Monosynaptic links between various fields of the hippocampal formation (DC → CA3 → CA1 → S) are indicated. The CA1 region has the distinction of being the first stage in the hippocampal circuitry where information from the layer II and layer III perforant pathways converge. Information carried by layer II projection will ultimately attain CA1 by both trisynaptic (through the DC) and disynaptic (directly from CA3) pathways. There is a return projection from CA1 and the subiculum to the deep layers of the entorhinal cortex (modified after (Amaral 1993)).

The DG gets its major input from the entorhinal cortex via fibers of the perforant path (PP). The incoming information is processed through mossy fibers of the DG and further send to pyramidal cells of the first subfield of the hippocampus, the *Cornu Ammonis* (CA) 3 region. From here, neuronal activity is sent via Schaffer collateral connections through the CA2 and on to the CA1 region. The CA1 region in-turn projects to the subiculum and back to the entorhinal cortex, thereby completing the so-called trisynaptic circuit of the hippocampus (Amaral 1993). The flow of information is largely unidirectional (Fig. 11). There are only a few axons directly connecting the DG with the CA1 region.

The function of the hippocampal formation was unclear until a patient named Henry Molaison (in literature known as 'patient H. M.') had a temporal lobectomy in 1953. His doctors believed they could cure his epilepsy by simply removing a part of the brain they thought may play a role in his disease. After the surgery, his epilepsy was controlled, but he completely lost the ability to form new memories (anterograde amnesia). He could not remember any events that happened shortly before the surgery (retrograde amnesia), but was able to remember childhood memories or events that happened several years before the surgery (Scoville 1957, Squire 2009). Since this famous surgery, many studies confirmed the role of the hippocampus in episodic memory formation (Squire and Cave 1991, Tulving and Markowitsch 1998) and spatial memory formation (O'Keefe 1978).

As already mentioned in the story about patient H. M., damage and also shrinkage of the hippocampus is related to memory dysfunctions (Eckerstrom, Andreasson et al. 2010). It is under great debate whether age itself contributes to the loss of hippocampal neurons in elderly which lead to memory decline or whether the environment and life conditions may play a more pivotal role (Baumgart, Snyder et al. 2015). Clear is, that neurodegenerative diseases such as AD lead to severe hippocampal atrophy, but also depression (Sapolsky 2001), chronic stress (increased levels of cortisol) (Watanabe, Gould et al. 1992), schizophrenia (Okasha and Madkour 1982) and post-traumatic stress disorder (PTSD) (Sapolsky 2001). The loss of hippocampal volume is also due to the retraction of dendritic spines. The involvement of dendritic spines will be explained later.

1.6.2 Long-Term Potentiation

Donald Hebb described in 1949 that 'memories are stored in the mammalian brain as stronger synaptic connections between neurons active during learning' (Hebb 1949). What was already theoretically described by Hebb, was proven right by a group of scientists in Great Britain that unraveled the cellular correlate of learning and memory in the brain. They repetitively activated synapses in the PP of the hippocampus of anesthetized and non-anesthetized rabbits through conditioning stimulation trains and found the increased synaptic response of the cells to last for 30 min to up to 10 hours (h). Because of this long-lasting potentiation, they named the effect 'long-term potentiation' (LTP) (Bliss and Lomo 1973). This lasting change in synaptic strength can also be found

in other brain tissues, but the hippocampus is a favorable site for studying it since it is densely packed with different layers of neurons (Cooke and Bliss 2006).

To evoke LTP in the hippocampus, both presynaptic and the postsynaptic neurons need to be active simultaneously (Fig. 12). This can be induced in a various number of ways. In most experimental settings, a train of high frequency tetanus stimuli (e.g. 50-100 Hz) triggers LTP through stimulation of the Schaffer collaterals between the CA3 and CA1 region of the hippocampus in acute murine brain slices (Malenka and Nicoll 1999). NMDARs on the post-synapse open for the strong influx of CA^{2+} and lead to a long lasting potentiation of synaptic activity (Luscher and Malenka 2012) (Fig. 12).

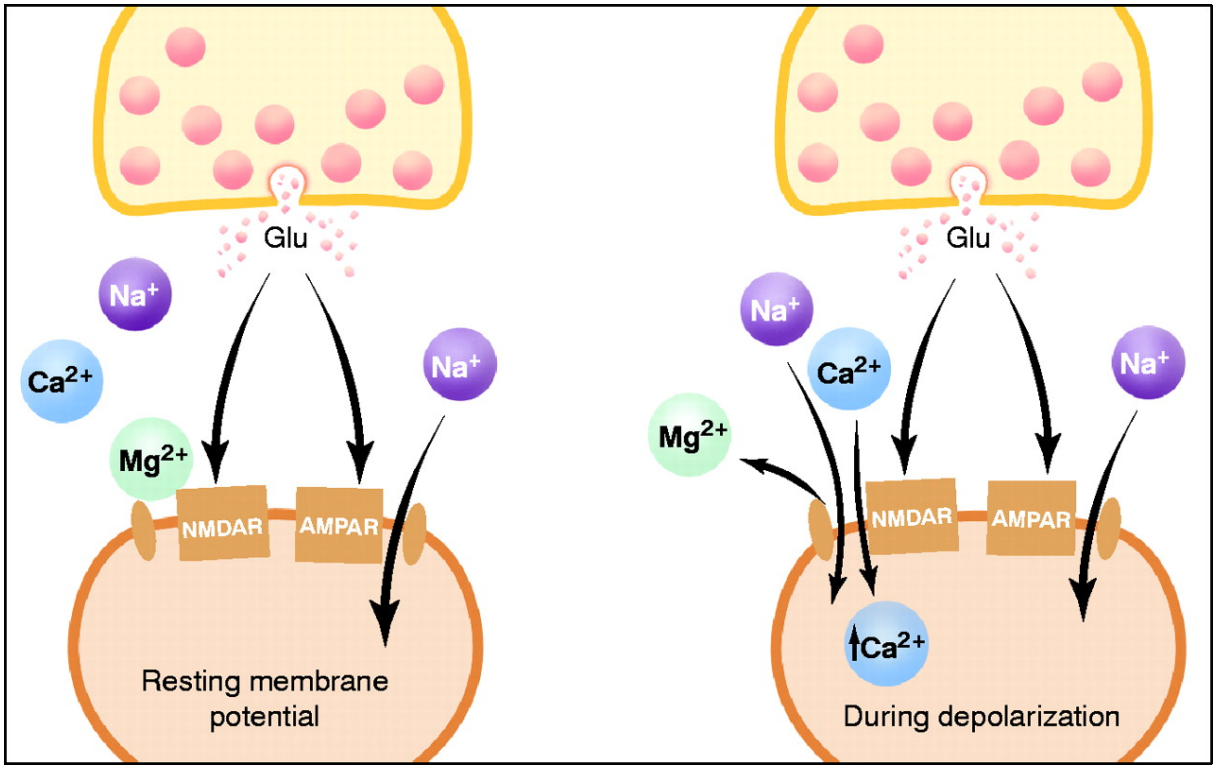

Fig. 12: Schematic drawing of LTP induction. During resting membrane potentials (normal synaptic transmission), glutamate gets released from the pre-synapse and acts on NMDARs of the post-synapse. Na^+ only enters the post-synapse through AMPARs, because Mg^{2+} blocks the influx through NMDARs. When the post-synapse depolarizes, Mg^{2+} gets released from NMDARs and Ca^{2+} and Na^{2+} ions can enter the post-synapse through NMDARs. The rise in Ca^{2+} in the post-synapse is the trigger for LTP (modified after Malenka and Nicoll (1999)).

Many studies have shown that altered LTP may lead to brain diseases such as depression, anxiety- and movement disorders, addiction and dementia. Early memory deficits in AD are likely caused by the accumulation of Aβ oligomers that disrupt induction of LTP (Sheng, Price et al. 2002, Walsh, Klyubin et al. 2002, Luscher and Malenka 2012) (Fig. 13). Rammes, Hasenjager et al. (2011), Rammes, Seeser et al. (2018) and Bürge, Kratzer et al. (2019) have shown that $Aβ_{1-42}$ and $Aβ_{1-40}$ concentration-dependently block LTP in acute murine hippocampal slices.

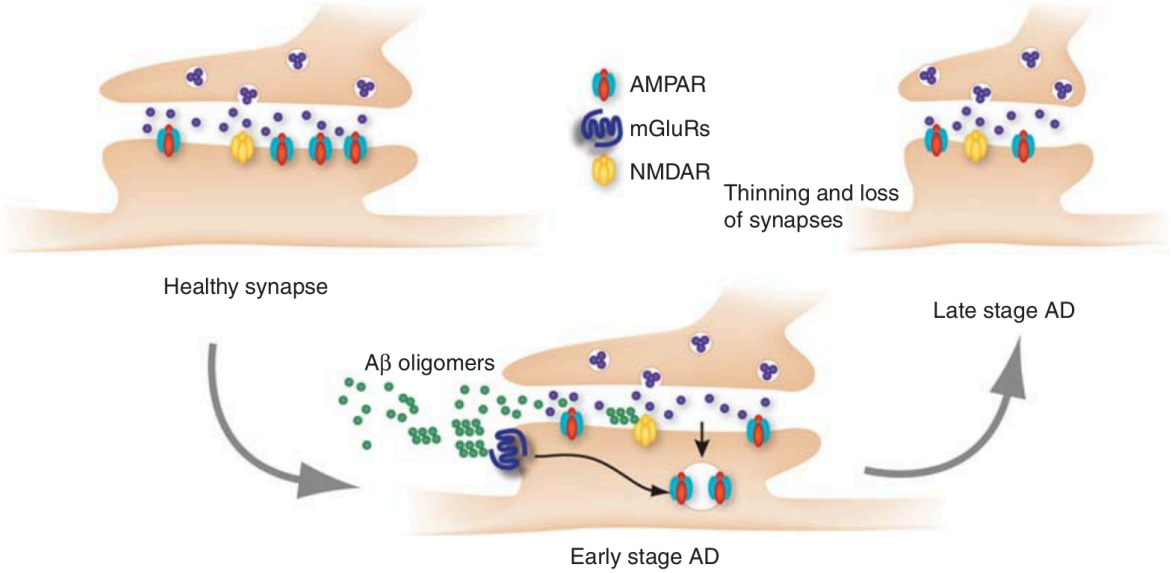

Fig. 13: Blockage of LTP by Aβ oligomers in AD. Soluble Aβ oligomers strongly activate metabotropic glutamate receptors (mGluRs), which leads to the internalization of AMPARs and LTD. Normal NMDAR-dependent long-term depression (LTD) is occluded. At the same time, Aβ oligomers inhibit NMDARs, preventing the induction of LTP. As a consequence, synapses become thinner, weaker and some disappear. It is believed that these changes underlie the early cognitive decline observed in AD (modified after Luscher and Malenka (2012)).

Bürge, Kratzer et al. (2019) have shown that the synaptotoxic effects induced by $A\beta_{1-42}$ could partially be ameliorated through the treatment with 30% xenon, the effects of $A\beta_{1-40}$ could not be reversed. I aimed to test whether 30% xenon can reverse the effects of AβpE3 and 3NTyrAβ on NMDAR-induced LTP.

1.6.3 Dendritic spines – classification, function and pathological changes

A change in synaptic plasticity (LTP, LTD) results in morphological changes of neurons. These can best be seen through changes in the density of dendritic spines (from the Greek word 'dendron'= tree). Dendritic spines are small membranous protrusions from neuronal dendrites that receive input from single axons on the synapse and help to transmit an electrical signal to the cell body of a neuron. They were first described by the neuroscientist Santiago Ramón y Cajal in the 19th century. They contain a head and a neck that connects the spine to the dendrite (Harris and Kater 1994) (Fig. 14). There can be over 10,000 spines on a single neuron (McCann and Ross 2017). The density of spines is defined as the number of visible spines per estimated micrometer of dendrite.

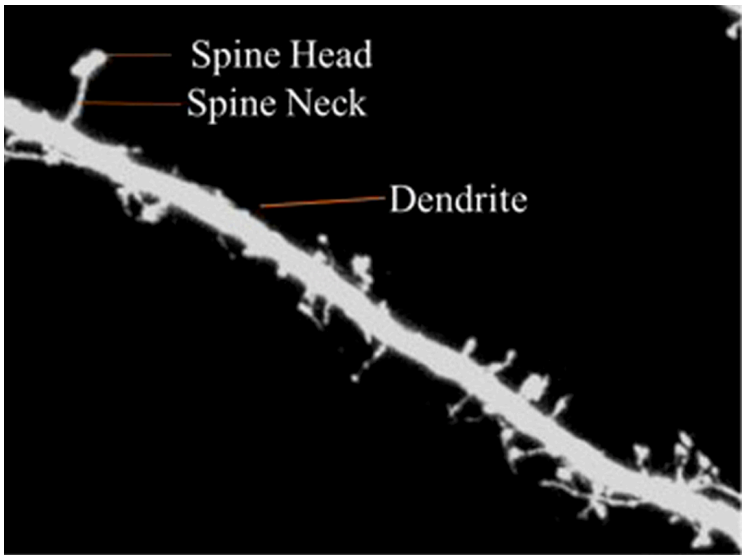

Fig. 14: CLSM-image of a dendrite with dendritic spines. The spine consists of the spine head and a spine neck that connects it to the dendrite (modified after Wang, Chen et al. (2016)).

There are different forms of spines including 'thin', 'stubby', 'mushroom' or 'branched' (Fig. 15) (Hering and Sheng 2002). Their surface expresses NMDARs, AMPA receptors and other receptors that transmit the received signal to the cell body. They are the morphological correlate of post-synapses. Their structure and density are very important for synaptic function (Ultanir, Kim et al. 2007). Dendritic spines are highly dynamic structures that change their volume and density depending on stimuli such as an induction of LTP or LTD within seconds. NMDAR signaling is thought to regulate spine density through recruitment of AMPA receptors (AMPARs). NMDAR antagonists such as memantine (approved to treat symptoms of moderate to severe AD cases (Danysz, Parsons et al. 2000, Reisberg, Doody et al. 2003)) therefore reduce spine density (Martinez-Coria, Green et al. 2010). The remodeling of spines provides a morphological basis of learning and memory. More stimulation leads to bigger, more stable and longer-lived spines (Engert and Bonhoeffer 1999, Saglietti, Dequidt et al. 2007, McCann and Ross 2017).

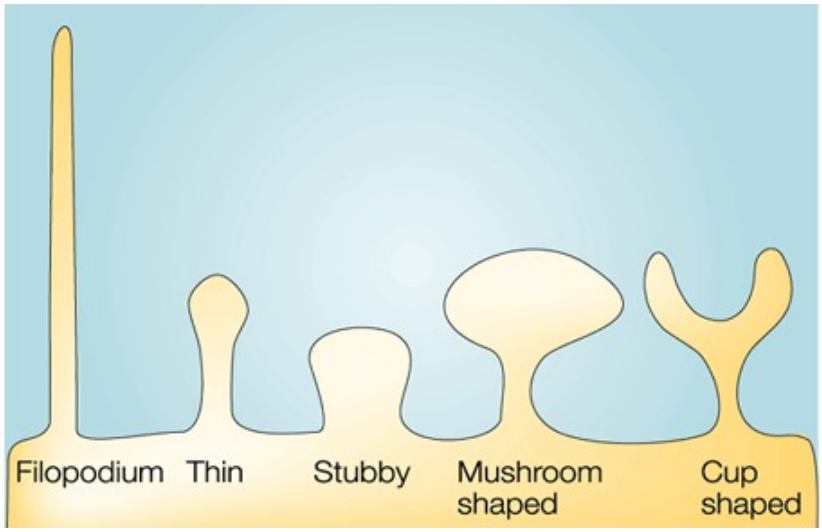

Fig. 15: Morphological classification of dendritic spines. Schematic overview of several shapes of dendritic spines: Filopodium, thin, stubby, mushroom- and cup-shaped (modified after Hering and Sheng (2002)).

A highly decreased density of spines is involved in neuropsychiatric disorders such as AD (el Hachimi and Foncin 1990, Knobloch and Mansuy 2008), autism spectrum disorders, schizophrenia (Penzes, Cahill et al. 2011) and ischemic stroke (Brown, Wong et al. 2008). A highly increased density of spines occurs in Fragile X Syndrome (mental retardation). Such abnormal changes in the structure lead to altered neuronal functions (Fu and Zuo 2011). These causes for spines density change are considered neuron-autonomous. Extra-neuronal factors leading to a loss of dendritic spines are for example trauma and inflammation (Dorostkar, Zou et al. 2015). In early stages of AD, strong synapse and dendrite loss can be found in several areas of the brain but primarily in the inferior temporal gyrus, in the CA1 region (Scheff, Price et al. 2007) and the DG of the hippocampus (Scheff, Price et al. 2006). DeKosky and Scheff (1990) were the first to describe that a loss of synapses and axons in post-mortem brains of AD (measured via electron-microscopy) correlated strongly with cognitive capabilities of the patients (tested via the 'Mini-Mental Status').

The role of soluble Aβ oligomers on the loss of dendritic spines was primarily discovered in neuronal cell culture and animal models several years later (Lambert, Barlow et al. 1998, Spires, Meyer-Luehmann et al. 2005, Shankar, Bloodgood et al. 2007). Removement of Aβ by an antibody resulted in increased formation of new spines (Spires-Jones and Hyman 2014). Memantine has been shown to reverse the neurotoxic effect of Aβ oligomers on dendritic spines (Rammes, Seeser et al. 2018).
The loss of spines in transgenic mice-models of AD is accompanied by changes in the morphology of the remaining spines. Normally, most spines are mushroom-shaped and only some are stubby. In AD models, there are more stubby spines and they become shorter in general (Merino-Serrais, Knafo et al. 2011). The scientists also found that the changes in spine morphology occur prior to neurodegeneration. Androuin, Potier et al. (2018) described similar phenomena in post-mortem AD brain tissue: lower density of spines = increased proportion of stubby spines and thicker spine necks. They suggest that thicker spine necks are a compensatory effect due to the reduction in spine density. Boros, Greathouse et al. (2017) found the plasticity of spines to be a mechanism of cognitive resilience. They compared the density and shape of spines in post-mortem brains of formerly healthy patients (controls), AD patients and healthy control patients with AD pathology. They discovered that spine density in control and patients with AD did not differ from each other but that mushroom-shaped and thin spines were highly reduced in AD brains. The scientists believe that the plasticity of spines protects older individuals with AD pathology from developing AD-related dementia.
Several studies investigating the effect of anesthetics on spine density found no changes on dendritic spines in mice at early developmental stages (De Roo, Klauser et al. 2009, Briner, De Roo et al. 2010, Yang, Chang et al. 2011), not many studies were done in adult animals up until now.

My aim was to elucidate the effects of the inhalational anesthetics sevoflurane, isoflurane and xenon alone and in combination with $A\beta_{1-42}$ on density of dendritic spines in the hippocampus (CA1 region) of adult GFP mice.

1.7 Autophagy – cellular and molecular mechanisms

Autophagy is a complex degradation process of intracellular constituents via a series of pathways in eukaryotic cells (Cuervo, Bergamini et al. 2005). There are three types of autophagy: macroautophagy, microautophagy and chaperone-mediated autophagy. Since the different types will not be of importance for this dissertation, they will not be further explained but can be reviewed in Cuervo (2004). I focused on proteins involved in macroautophagy and refer to it as autophagy. Normal autophagy is a vital protective factor in cells. It prevents damaged proteins and other cellular waste from accumulating in the cell, regulates energy homeostasis, survival in starvation and sustains metabolism (White, Mehnert et al. 2015). Autophagy was also found to suppress inflammation processes, tissue damage and genome instability and plays therefore an important factor in cancer (Takamura, Komatsu et al. 2011). In mammals, the regulation of autophagy is highly complex and there are many triggers that induce it. The depletion of amino acids, changes in insulin signaling, reactive oxygen species (ROS) and AMP-activated protein kinase (AMPK) are just some examples.

The first step of autophagy is the formation of autophagosomes (APSs), which are double membraned vesicles/organelles (Mizushima 2007). Therefore, the ULK1 (uncoordinated-51-like kinase 1) complex, consisting of ULK1 itself, autophagy-related protein 13 (Atg13), Atg101 and FIP200 (FAK family kinase interacting protein of 200 k Da), translocates to the initiation sites of autophagy. This complex then recruits the phosphatidylinositol 3-kinase (PI3K) complex (also VPS (vacuolar protein sorting) 34 complex), consisting of the class III PI3K, Beclin-1, VPS15 and Atg14L (Atg14-like) (Funderburk, Wang et al. 2010). These proteins together then lead to the formation of the APS. Another protein complex gathers at the site of the APS, the Atg12-Atg5-Atg16 complex (Cuervo, Bergamini et al. 2005, Suzuki, Kubota et al. 2007, Zachari and Ganley 2017) (Fig. 16, 17).

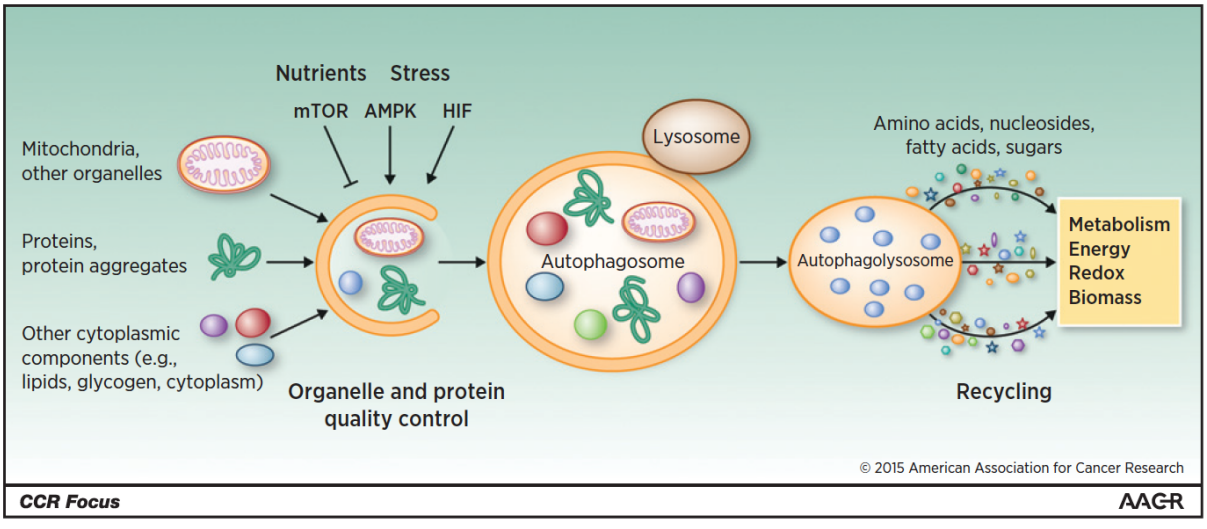

Fig. 16: Autophagy pathway. Organelles and proteins undergo quality controls, abnormal particles get engulfed by the autophagosome which then fuses with the lysosome to form the autophagolysosome. Particles get degraded and partially recycled White, Mehnert et al. (2015)).

The APs engulf the material that needs to be degraded. They then travel through the cytoplasm of the cell to lysosomes and the two organelles fuse together to form autolysosomes. Lysosomal hydrolases then degrade the material. After degradation, amino acids, sugars, fatty acids and other material is recycled and exported out of the autolysosome (Fig. 16) (Mizushima, Ohsumi et al. 2002, Mizushima 2007).

1.7.1 Normal autophagy is defect in AD

The degradation of damaged or aggregated cell material through autophagy is a highly important process for a normal and vital function of the nervous system and other systems in the body especially under stress or injury conditions. Autophagy may also prevent apoptosis of cells (Boya, Gonzalez-Polo et al. 2005). Therefore, a deregulation of autophagy impairs cell homeostasis and can lead to dysfunctions of the NS and neurodegeneration (Nixon and Yang 2011). It is known that normal autophagy function is somehow disrupted in patients suffering from neurodegenerative diseases such as AD. Terry, Gonatas et al. (1964) found dense lysosomes and many other intermediate stages of AVs to be present in the AD brain. These and other findings suggest that normal autophagy processing is impaired and AVs and lysosomes containing undigested cell material aggregate. In a healthy brain, AVs are only rarely present. Continuous clearance keeps their numbers low (Nixon, Wegiel et al. 2005, Nixon and Yang 2011). Scientists believe that the disruption of clearance AVs through lysosomes might be the main cause of autophagy dysfunction in AD. Even though autophagy function can be upregulated (e.g. through rapamycin), clearance of AVs containing undigested cell material did not increase (Cataldo, Barnett et al. 1996).

Mouse models of AD also show autophagy dysfunctions. PS1/AβPP transgenic mice do not only develop Aβ deposits, but also accumulate a very high number of AVs in their cortex and hippocampus, formerly early to late stage AVs in dystrophic neurites that are not degraded by lysosomes. These results indicate that autophagy is strongly induced, but the process cannot be finished due to dysfunctions somewhere in the pathway (Boya, Gonzalez-Polo et al. 2005, Nixon, Wegiel et al. 2005, Yu, Cuervo et al. 2005). Indicators for massive autophagy could be oxidative stress or the buildup of intracellular Aβ (Billings, Oddo et al. 2005). Yu, Cuervo et al. (2005) also found a high concentration of Aβ in aggregated AVs and described that Aβ is generated abundantly when the production of AVs is increased through elevated autophagy. In a healthy organism, only a low number of AVs generates Aβ which would be degraded subsequently. Genetic ablation of autophagy lead to a strongly reduced extracellular Aβ plaque load in AβPP transgenic mouse, which normally develop a high amount of Aβ plaques in their brain, but to an increased amount of intracellular Aβ aggregates. These results suggest that autophagy is directly involved in Aβ secretion and dysfunction of autophagy lead to a buildup of neurotoxic intracellular Aβ deposits (Nilsson and Saido 2014).

Studies have shown that autophagy decreases in elderly. The balance of production of damaged proteins and their disrupted clearance lead to accumulations and these contribute to the process of

aging. The accurate mechanisms underlying this phenomenon are not well understood but scientists found that caloric restriction can counteract aging through autophagy decrease (Cuervo, Bergamini et al. 2005). The autophagy pathway is highly complex and many different proteins are involved (Fig. 15). Depletion of genes essential for autophagy leads to the accumulation of cell material and cell death (Komatsu, Waguri et al. 2006).

Studies examining the effect of volatile anesthetics on autophagy are conflicting – some prognose an deleterious effect on the autophagy pathway through isoflurane (Perucho, Casarejos et al. 2010) and sevoflurane (Geng, Zhang et al. 2018), other studies do not find any effect and even others find sevoflurane (Shiomi, Miyamae et al. 2013) or isoflurane (Rao, Pan et al. 2017) to be protective.
It seems that the effect of inhalational anesthetics may depend on the concentration used and the duration of exposure. It is very important to use clinically relevant concentrations of isoflurane and sevoflurane as well as durations that closely represent everyday general anesthesia.
Very few studies examined the effect of xenon on autophagy. Zhu, Zhu et al. (2020) found xenon inhalation to increase autophagy and protect rats from neuronal injuries after seizures.

There is also only a small number of studies looking at the effect of volatile anesthetics on autophagy in combination with Aβ pathology. Perucho, Casarejos et al. (2010) observed that exposure of $A\beta PP_{swe}$ mice to isoflurane resulted in impaired autophagy: increased p62 and decreased LC3II/LC3B. They repeated exposure to isoflurane twice a week for three months in a row in 7-10-month-old AD mice. An extreme experimental setup like that, although they used clinically relevant concentrations of isoflurane (2%), is prone to have an effect on several important neurologic pathways in the brain and particularly in a diseased brain like the $A\beta PP_{swe}$ brain.
Another study focusing on sevoflurane found 3% sevoflurane exposure for 4 h to increase the expression of LC3B in the CA1 region of the hippocampus of APP/PS1 transgenic mice and to decrease p62 – representing the contrary to the isoflurane effect (Geng, Zhang et al. 2018).

This study focused on several important proteins that are crucially involved in the autophagy pathway. Most of them are highlighted through green circles in Fig. 17.

Besides proteins that are directly involved in autophagy, I also looked for the expression of p53. Ohyagi, Asahara et al. (2005) found elevated p53 levels in brains of AD patients. They discovered that intracellular $A\beta_{1-42}$ elevated the expression of p53 mRNA and therefore induced apoptosis of neurons that possibly lead to neurodegeneration of the disease.
The application of 2% isoflurane for 6 h decreased p53 levels in cultured cells. The scientists believe that isoflurane might induce DNA damage through oxidative stress and the inhibition of DNA repair through the p53 pathway (Ni, Li et al. 2017). They chose a relatively high concentration of isoflurane (2%) and applied it for a long time (6 h) directly onto the cells. Zhou, Guo et al. (2017) found that

anesthesia of neonatal rats with 2.3% sevoflurane for 6 h significantly increased the level of p-p53 in the hippocampus.

1.7.1.1 ULK1 and pULK1

The uncoordinated-51-like kinase 1 and 2 (ULK1/2) play an important part in the initiation of autophagy. Chan, Kir et al. (2007) identified ULK1 to be the primary autophagy modulator of the ULK complex in mammals. They knocked down ULK1 in GFP-LC3 mice and found the formation of autophagosomes to be inhibited (Chan, Kir et al. 2007). Scientists also discovered ULK1 to directly phosphorylate Beclin-1 and activate the phosphatidylinositol 3-kinase (PI3K) to induce autophagy (Russell, Tian et al. 2013).

1.7.1.2 Akt and pAkt

The PI3-kinase Akt pathway is activated by different stimuli, including insulin, growth factors, cytokines and cellular stresses, to regulate diverse biological processes such as cellular survival, proliferation, growth, motility and metabolic functions. Investigations show an increased and sustained PI3K/Akt pathway activation in AD patients, resulting in aberrant proteostasis of Aβ and tau, synaptic loss and cognitive decline (Griffin, Moloney et al. 2005, O' Neill 2013).

1.7.1.3 p62/SQSTM1

p62, also known as sequestosome-1 (SQSTM1), is a multidomain protein implicated as an important player in the survival or death of cells (Moscat and Diaz-Meco 2009). Liu, Kern et al. (2007) showed that p62 protects cells from oxidative stress. p62 levels are decreased in patients suffering from neurological disorders. This decrease leads to misfolded proteins and aggregated Aβ (Du, Wooten et al. 2009). Caccamo, Ferreira et al. (2017) increased the expression of p62 in AβPP/Presenilin1 transgenic mice and showed that their cognitive deficits recovered. Thus, increasing levels of p62 could work as a therapeutic approach to restore neuronal function in neuropathological disorders by inducing autophagy and therefore degrading Aβ (Caccamo, Ferreira et al. 2017).

1.7.1.4 Beclin-1

Beclin-1 is a component of the PI3K complex and is important for autophagosome formation (Funderburk, Wang et al. 2010). Together with its interacting proteins, Beclin-1 either accelerates or suppresses autophagy and has therefore an important control function (Salminen, Kaarniranta et al. 2013). Expression deficiencies of the Beclin-1 can lead to decreased autophagy and errors in the processing of AβPP as can be seen in AD patients. Studies indicate that a reduced synthesis and an increased degradation of Beclin-1 occur and lead to neuropathologies.

1.7.1.5 Atg12

Autophagy-related genes (Atg) and proteins are essential for the formation of autophagosomes. They are classified into six functional groups, one of them being the Atg12-Atg5-Atg16 complex (Suzuki,

Kubota et al. 2007). The groups are highly conserved in mammals (Kuma, Mizushima et al. 2002). Atg12 does not only play a critical role in the autophagy pathway, but also acts as a positive mediator of mitochondrial apoptosis (Rubinstein, Eisenstein et al. 2011).

1.7.1.6 PI3K Class III

The PI3K and Akt pathway promote cell survival, growth and differentiation through downregulation of apoptotic signals. The PI3K/Akt pathway targets and activates mTOR, which is an important down-regulator of autophagy (Brunet, Datta et al. 2001). There are three types: PI3K class I-III. PI3K-III–deficient mice show an impaired formation of autophagosomes and an accumulation of LC3 aggregates, but the main function of PI3K-III for autophagy remains unknown (Jaber, Dou et al. 2012). In AD patients, scientists found a somewhat altered PI3K/Akt pathway, leading to hyperactivation and incorrect clearance of Aβ proteins (Heras-Sandoval, Perez-Rojas et al. 2014).

1.7.1.7 LC3B

The microtubule associated light-chain 3 (LC3) protein has three isoforms: LC3A-C. During autophagy, the protein is synthesized to form cytosolic LC3-I and is then converted to LC3-II to become associated with autophagic vesicles on the membrane of autophagosomes. LC3-II was found to accumulate in transgenic mice overexpressing human AβPP (Kabeya, Mizushima et al. 2000, Nixon and Yang 2011). Additionally, Ma, Huang et al. (2010) found LC3 and other autophagy markers to be locally associated with Aβ plaques and tau pathologies in brains of AD patients, indicating that increasing deposition of Aβ in AD also leads to an increase in autophagy markers.

1.7.1.7 p53

The tumor suppressor protein p53 regulates the transcription of genes and eliminate cells, that cannot be repaired by apoptosis or senescence. The protein is activated via stressors such as oxidative stress through ROS, DNA damage or metabolic stress. In healthy cells, the level of p53 is low. Defective p53 leads to proliferation of abnormal cells, resulting in diseases such as cancer. Too much protein can lead to an acceleration of aging by excessive apoptosis - p53 must therefore be tightly regulated (Baker 1989). The p53 pathway is intertwined with the autophagy pathway. Autophagy suppresses p53 levels because it recycles cell material for DNA repairs and therefore prevents the activation of p53. Additionally, autophagy represses ROS which would activate p53. In contrast, when p53 is activated, autophagy is activated. The two pathways seem to regulate each other's activation and suppression (White 2016).

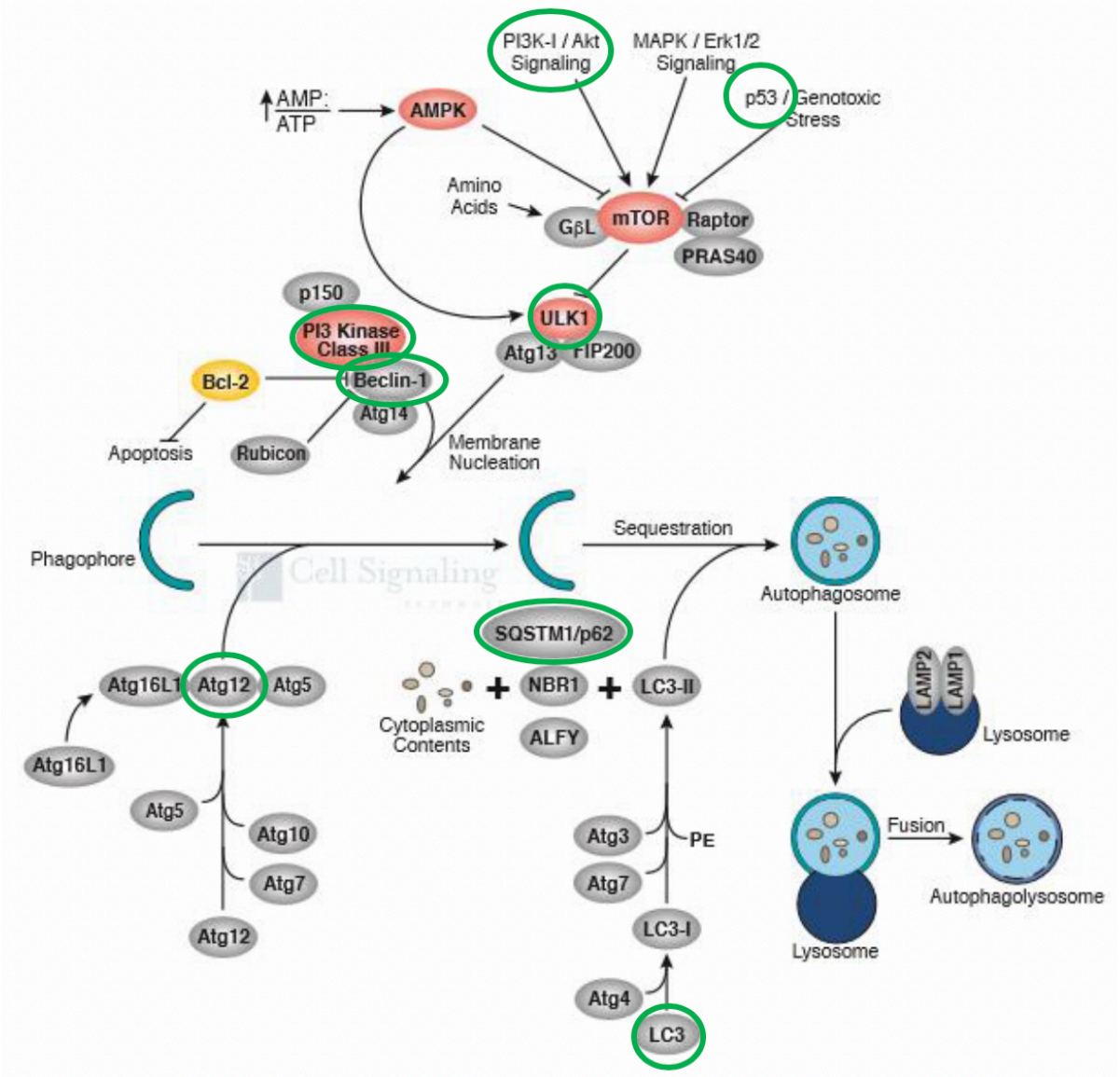

Fig. 17: Schematic image of the autophagy pathway. The autophagic pathway involves many different proteins and other pathways. Buildup of the autophagosome from the phagophore through sequestration of cellular compartments. Fusion of the autophagosome with the lysosome to the autophagolysosome. Important proteins involved and investigated in this work are circled in green: ULK1, PI3K-III, Beclin-1, Atg12, SQSTM/p62, LC3B-I and LC3B-II, Akt (Cell Signaling Technologies, 2017; from: https://www.cellsignal.de/contents/science-cst-pathways/autophagy-research-resources/science-pathways-autophagy/); last accessed February 2022.

2. Aim of the study

Thus far, Alzheimer's disease remains a devastating disease because the causes leading to it remain elusive and there is no cure in sight. In the past decades, many studies have shown very contradictive results regarding the effect of inhalative anesthetics on the development or progression of AD in patients undergoing general anesthesia. My doctoral project aimed to elucidate effects of the inhalational anesthetics isoflurane, sevoflurane and xenon on AD at different levels pf complexity. Several studies showed that isoflurane and sevoflurane might contribute to the development of sporadic AD in patients undergoing surgery. In contrast to that, other studies showed that anesthetics have no negative impact on patients but are rather neuroprotective. The reasons for these findings are not well understood and more studies need to be done to reveal the effect of anesthetics on the human brain during and after anesthesia.

I focused on the effects of isoflurane, sevoflurane and xenon on Aβ proteins. Aβ proteins are a major hallmark of AD and are said to cause neuronal loss due to their neurotoxicity. Scientists believe that anesthetics contribute to the intracellular oligomerization of Aβ and the aggregation of Aβ into extracellular plaques.

With the help of time-resolved fluorescence resonance energy transfer (TR-FRET) assays, I assessed the direct impact of the gases on aggregation properties of Aβ proteins in vitro by using a protocol modified after Parsons, Ruitenberg et al. (2015). Additionally, to further test the aggregation propensity of Aβ, I performed silver staining of Aβ proteins after treatment with anesthetics.

I used acute murine hippocampal slices to investigate the changes in basal neuronal activity after treatment with either anesthetics or Aβ alone or in combination, thereby mimicking a healthy patient versus a patient with increased amounts of Aβ in the brain (e.g. AD) undergoing general anesthesia in a laboratory setting.

Subanesthetic concentrations of xenon partially reverse the neurotoxic effects of $A\beta_{1-42}$ on LTP (Bürge, Kratzer et al. 2019). To further expand these findings, I tested whether xenon can also reverse the effects of AβpE3 and 3NTyrAβ.

Several studies showed that autophagy is impaired in AD (Nixon and Yang 2011, Metcalf, Garcia-Arencibia et al. 2012). I therefore looked at changes in expression of certain proteins involved in autophagy after treatment with Aβ, anesthetics or the combination of both. Finally, I used GFP mice to determine whether Aβ plus anesthetics affect the number of dendritic spines on axons in the CA1 region of the hippocampus.

3. Methods

3.1 TR-FRET-based oligomer specific assembly assay

Time-resolved fluorescence resonance energy transfer (TR-FRET) combines advantages from time-resolved fluorometry (TRF) and Foerster resonance energy transfer (FRET). With the help of TRF it is possible to investigate dynamic processes in materials and chemicals via spectroscopic techniques (e.g. illumination through lasers) that change the property of the studied compound (Stolow 2003). FRET describes the transfer of energy between chromophores (light-sensitive molecules). The donor chromophore, when excited by a laser or flash lamp, transfers energy to the acceptor chromophore only when they are in close proximity to each other (Fig. 18). The acceptor then emits light at its characteristic wavelength that gets measured by a plate reader (Yan and Marriott 2003). With this very sensitive method scientists investigate the interactions of molecules. TR-FRET combines these techniques which leads to a highly sensitive and reproducible assay.

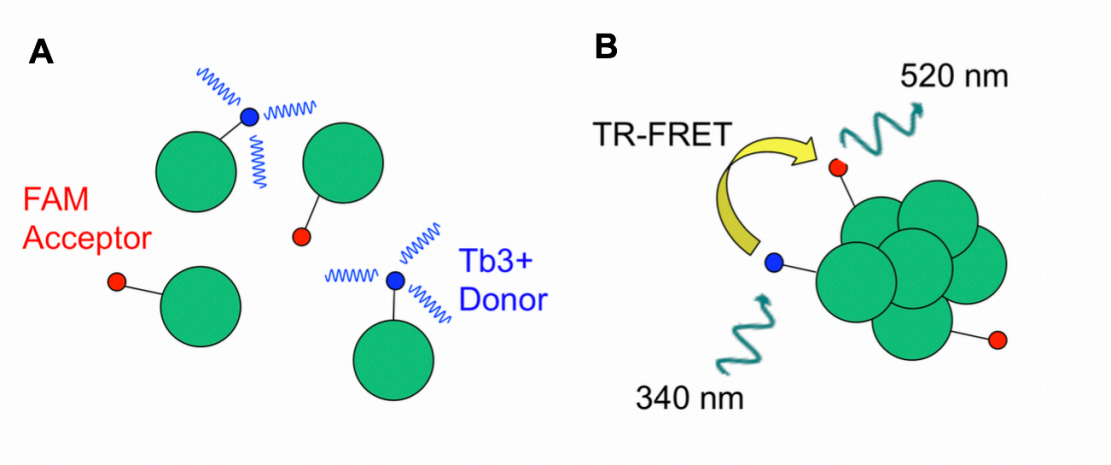

Fig. 18: Schematic drawing of TR-FRET. A: The fluorescent agent FAM is coupled to a protein (e. g. $A\beta_{1-42}$) and functions as the FRET-acceptor**,** Biotin-labeled molecules (e. g. $A\beta_{1-40}$) plus Terbium (Tb-) Streptavidin are the FRET-donor. The proteins are in no close proximity and no TR-FRET occurs. **B:** The proteins are in close proximity and under illuminance with 340 nm, an energy transfer occurs (TR-FRET). This can be measured at 520 nm.

The protocol used for these TR-FRET assays was modified after Parsons, Ruitenberg et al. (2015) and was performed in cooperation with the Assay Development and Screening Platform at the Institute of Molecular Toxicology and Pharmacology (Helmholtz Zentrum München, Neuherberg).

Biotin-labeled $A\beta_{1-42}$ (AnaSpec, Fremont, CA, USA) plus 1 mM Terbium-(Tb-) Streptavidin (Life Technologies, Paisley, UK) was used as the FRET-donor and a FAM-labeled $A\beta_{1-42}$ (AnaSpec) as the FRET-acceptor. Biotin (vitamin B7, vitamin H) is a very small vitamin (MW= 244.31 g/mol) and binds to streptavidin and avidin with extremely high affinity and specificity. The bondage is one of the strongest no*f*n-covalent interactions known in nature (Weber, Ohlendorf et al. 1989). Streptavidin is a protein purified from the bacterium *Streptomyces avidinii*. FAM (Fluorescein amidite) is an important synthetic equivalent of fluorescein dye used in oligonucleotide synthesis and molecular biology.

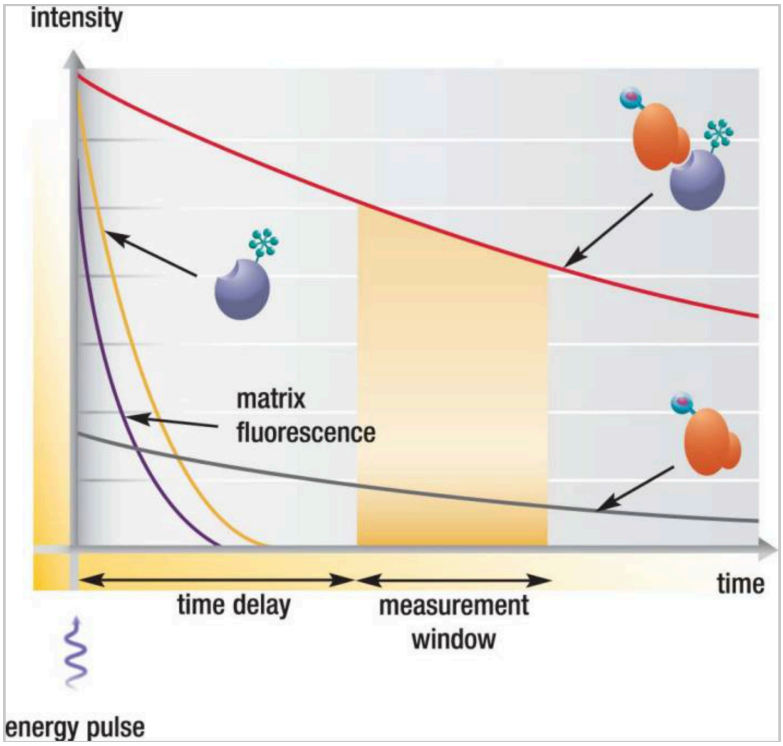

Fig. 19: TR-FRET. The energy pulse by a flash lamp/laser is followed by a time delay. This allows short-lived fluorescent proteins/compounds to decay. Grey line: emission of donor at a certain wavelength. Yellow line: Fluorescent signal from acceptor at a certain wavelength. Red line: FRET emission intensity generated at a certain wavelength (modified after Degorce, Card et al. (2009)).

For my experiments, I prepared MOPS/TRIS buffer (final 56.82 mM, pH 8.1) with $MgCl_2$ (113.64 mM). $MgCl_2$ is necessary to promote aggregation of Aβ proteins in this experimental setup. For control experiments, the buffer was untreated. For the actual experiments with anesthetics, the buffer was aerated directly with 65% xenon, 4% sevoflurane (~210 µM) or 2% isoflurane (~280 µM) for 30 min. The concentrations resemble ~1 MAC of each inhalative anesthetic (Haseneder, Kratzer et al. 2009; tested in cooperation with the peptide biochemistry workgroup at Weihenstephan of the Technical University of Munich). Then, 2 µM solution of biotin-labeled $Aβ_{1-42}$ was prepared in 1 µM Tb^{3+}-SA and of Fluorescein-amidites-(FAM)-labelled $Aβ_{1-42}$ as the FRET acceptor, $Aβ_{1-42}$ and AβpE3 in 20 mM sodium hydroxide (NaOH). These solutions were then mixed in a ratio of 1:5:10:4 (biotin-labeled $Aβ_{1-42}$: FAM-labelled $Aβ_{1-42}$: $Aβ_{1-42}$:AβpE3) resulting in a total concentration of 200 nM Aβ. 45 µl of the corresponding buffer was then mixed with 5 µl of the Aβ stock solution.

Since the compounds tested were inhalational anesthetics, I had to find a way to saturate the solutions with the certain gases. I tested different techniques until I found a method that did not interfere with the assay protocol. In the original assay, all compounds (stem buffers, Aβ solutions and other test substances) were pipetted together one after another on a black 384-well plate (Corning #3655, Corning, NY, USA) before incubation and measurement. In this case, when investigating gaseous anesthetics, the stem buffers were saturated first with these gases in falcons for 30 min before I mixed them in protein-low-binding Eppendorf tubes with the Aβ solution. The Tubes were then placed with open lids into a darkened gas incubation box. The corresponding anesthetics were

applied through an influx tube attached to the box for 1 h at RT. To ensure the efflux of gas from the box, another tube was attached (Fig. 20).

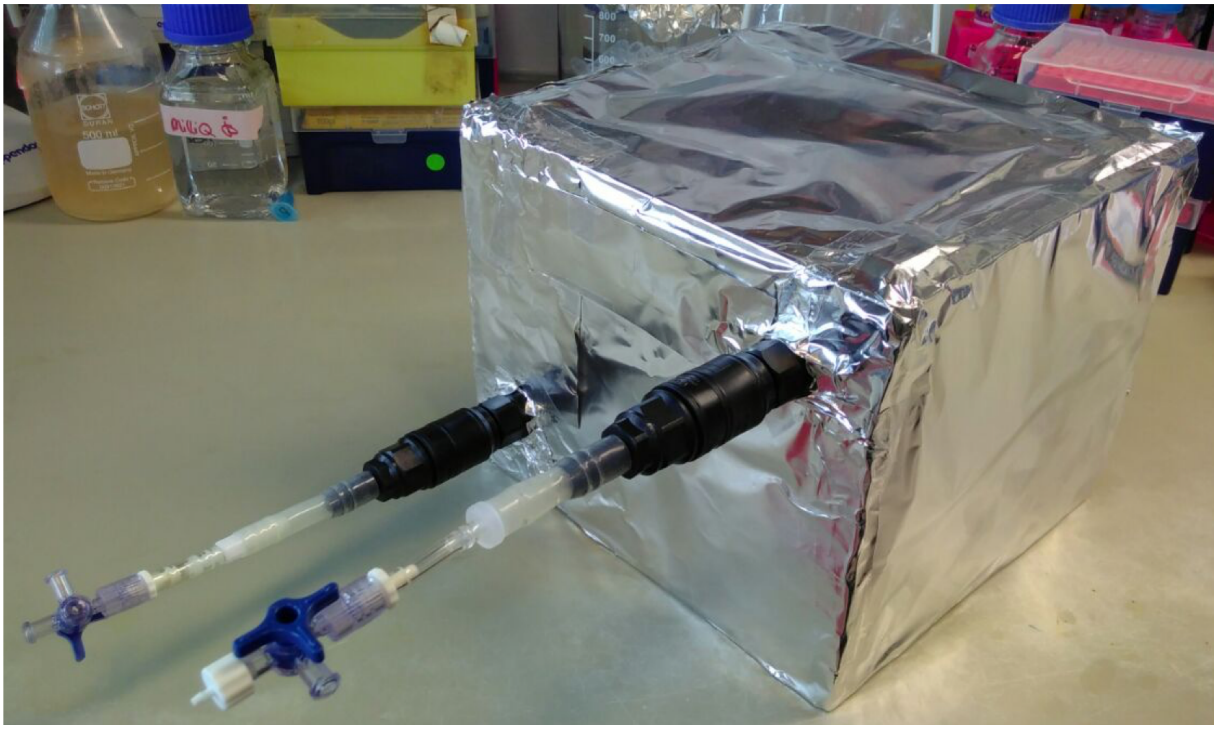

Fig. 20: Image of the incubation box including influx and efflux tubes.

A control box contained the control solutions. After incubation, the solutions were pipetted onto the assay plates and put into the EnVision multimode plate reader (PerkinElmer Inc, Waltham, Massachusetts, USA). The aggregation inhibitor MRZ13636 (Merz Pharmaceuticals, data not published; Fig. 21) as non-volatile test-compounds, were directly put into tubes containing stem buffers and Aβ solutions in a concentration of 3 µM, mixed and incubated at RT for the same amount of time as volatile compounds. Measurements were performed at RT.

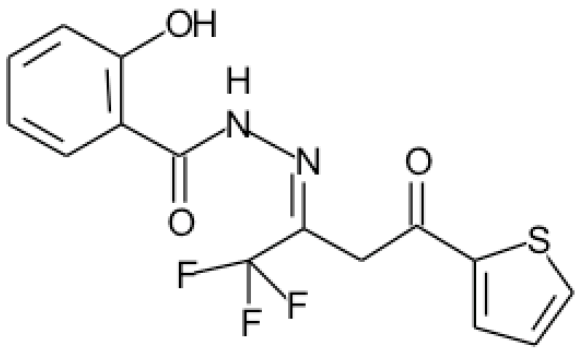

Fig. 21: Structural formula of MRZ13646. The compound was developed as an Aβ aggregation inhibitor by Merz Pharmaceuticals, but data was never published (kindly provided by Christopher Parsons).

The wavelengths with an excitation filter of 340/30 nm and emission filters of 490/10 nm and 520/25 nm were measured for for 20 min (interval 3 min). I averaged the data points for each emission wavelength of technical replicates and calculated the ratio for 520/490 nm. Afterwards, this ratio was corrected for the ratio in the absence of the FRET acceptor (after Parsons, Ruitenberg et al. (2015)).

3.2 Silver Staining of Aβ proteins

Silver Staining was first introduced and developed by Kerenyi and Gallyas in 1973. This technique uses silver nitrate to detect trace amount of proteins and nucleic acids in gels (Kerenyi and Gallyas 1973). In the following years, researchers further refined the process of silver staining to make it more sensitive, easy to handle and reproducible.
The current project used the protocol of Blum H. (1987) and the modified protocol of Parsons, Ruitenberg et al. (2015) as a basis.

The goal of the current study was to discover the effect of sevoflurane, isoflurane and xenon on aggregation levels of $A\beta_{1-42}$. Several studies showed before that sevoflurane and isoflurane increase oligomerization of $A\beta_{1-42}$ and therefore increase neurotoxicity of $A\beta_{1-42}$ (Jiang and Jiang 2015). What is already known is that $A\beta_{1-42}$ shows a time-dependent increase in high molecular weight (Tsigelny, Sharikov et al. 2014, Parsons, Ruitenberg et al. 2015). In my experiments, dissolved $A\beta_{1-42}$ was incubated for different lengths of time (0 min; 90 min; 6 h; 1 d; 3 d; 7 d) at RT in artificial cerebral spinal fluid (aCSF) to promote aggregation of the protein and determine possible differences in incubation lengths. At the end of the incubation time, the solutions were enriched with either 30 min of 2% sevoflurane, 1% isoflurane or 65% xenon (concentrations tested in cooperation with the peptide biochemistry institute of the TUM, Weihenstephan). The control solutions did not receive any treatment. Sample buffer was added to the solutions and mixed. Before start of electrophoresis, 1 µg peptide per lane was loaded onto NuPAGE Bis-Tris 4-12% Gels (Life Technologies, Paisley, UK). Images were taken afterwards with the ChemiDoc™ XRS+ System Imager and then analyzed with the Image Lab™ Software (Bio-Rad Laboratories, Hercules, CA, USA). To find differences between controls and pre-treated proteins, I evaluated the normalized volume intensity of the different bands (monomers, trimers, tetramers, higher oligomers) and compared them statistically.

3.3 Voltage-sensitive dye imaging of murine hippocampal slices

Voltage-sensitive dye imaging (VSDI) was first introduced by Tasaki, Watanabe et al. (1968) and represents an advanced technique that allows real-time imaging (down to 20-50 µm and a millisecond (Chemla and Chavane 2010) of neuronal network population activity through a voltage sensitive dye that binds externally to organic tissue like the membrane of cells without interrupting their function (Loew 2015). The dye molecules function as 'molecular transducers' and transform changes in membrane potentials into changes in fluorescence. These features of VSDI allow for a fast monitoring of neuronal signal transduction (Grinvald, Manker et al. 1982). Several studies have since validated

and confirmed the close correlation of the gained optical signal from VSDI and changes in membrane potential measured via conventional electrophysiology (Salzberg, V. et al. 1973, Morad and Salama 1979, Windisch, Muller et al. 1985).

3.3.1 Brain Slice Preparation

The ethical committee on animal care and use of the government of Bavaria, Germany, approved all experimental protocols including animals.

7-12 weeks old male mice (Black 6, C57B161N) were used for VSDI experiments. The animals were deeply anesthetized with isoflurane and decapitated using a guillotine. The head was placed quickly into ice-cold ringer solution saturated with carbogen (95% O_2, 5% CO_2). After removing the brain from the skull, the cerebellum was cut off and the brain separated into its hemispheres using a sharp razor blade. The following step is very important to preserve the intra-hippocampal tri-synapse-connectivity for VSDI measurements: Both hemispheres were prepared with a special cutting angle called the 'magic cut' (Fig. 22). I placed the hemispheres onto their medial face of the sagittal plane while the dorsal part of the brain was removed partly with defined angles (Bischofberger, Engel et al. 2006). The dorsal part was then fixated with histoacrylic glue to the tray of the microtome (Microm International, Walldorf, Germany). The hemispheres were cut into 350 µm thin slices and recovered afterwards for 30 min at 34 °C in a water bath.

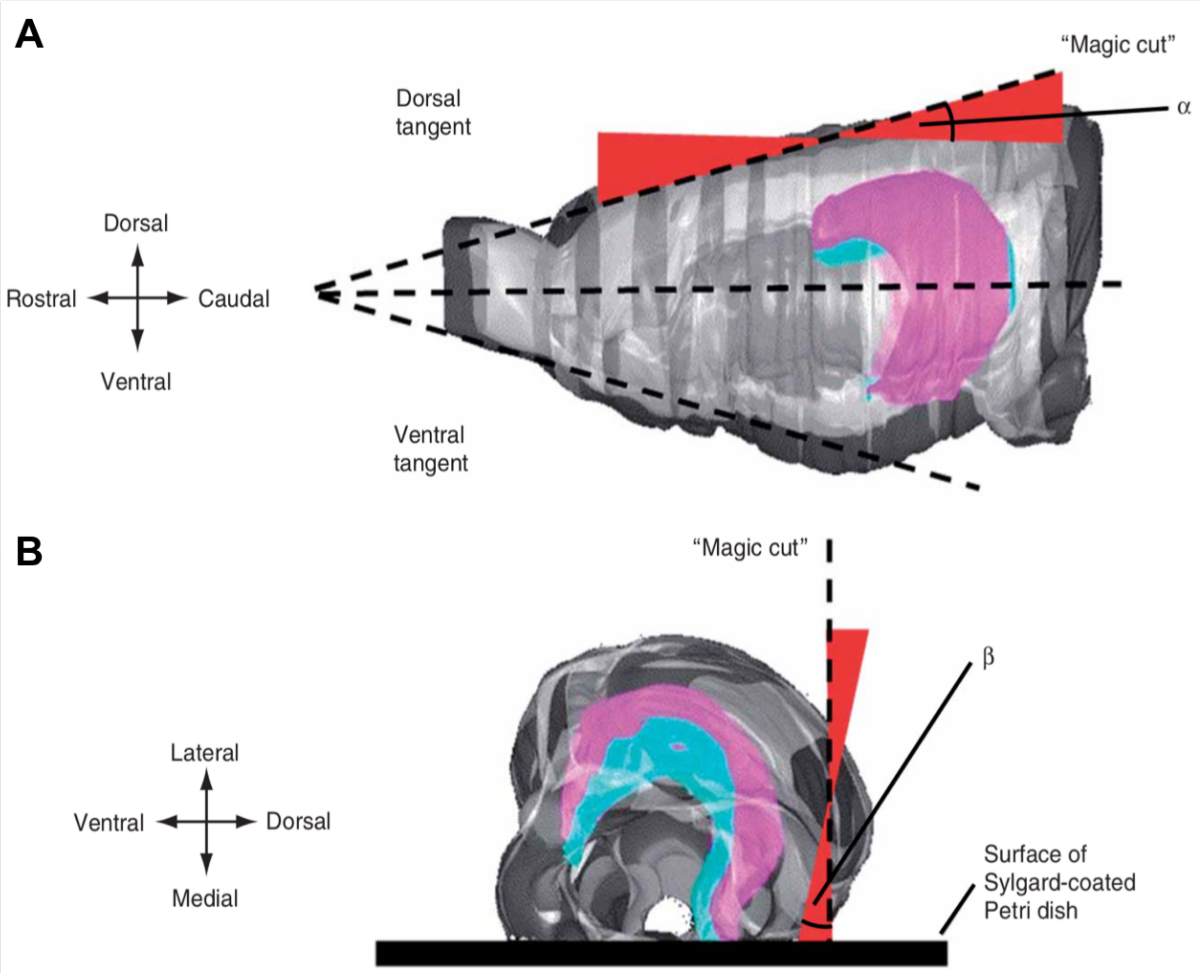

Fig. 22: Illustration of the 'magic cut'. A: Left hemisphere from top. Red markings represent the range of the 'magic cut'. The angle α should be close to 0. **B:** Left hemisphere from caudal. Red markings represent the range of the 'magic cut'. The angle β should be ~ 10°. CA3 and CA1 region are marked magenta, the dental gyrus in cyan (modified after Bischofberger, Engel et al. (2006)).

3.3.2 Preparation of the stock solution of *Di-4-ANEPPS* and staining of the slices

I dissolved 5 mg 4-(2-(6-(Dibutylamino)-2-naphthalenyl)ethenyl)-1-(3-sulfopropyl) pyridinium hydroxide inner salt (*Di-4-ANEPPS,* Sigma-Aldrich) in 500 µl DMSO to a stock solution of 20.8 mM. The solution was mixed, dissolved in an ultrasonic bath and then aliquoted into 10 µl portions to be stored for further use at -20 °C.

After cutting and recovery, I transferred the hippocampal slices into a small glass container where I stained them with *Di-4-ANEPPS* (final concentration 20.8 µM – 26 µM) for 20-30 min while being saturated with carbogen. The slices then recovered another 45 min in aCSF before start of experiments.

Di-4-ANEPPS is a commonly used and well-established voltage-sensitive dye. When excited with light between 350-550 nm, it emits light in longer wavelengths of about 500-800 nm. This phenomenon is called the 'stokes shift'. If the tissue gets excited, the fluorescence shifts to a lower wavelength

caused by the shift of absorption, excitation and emission spectra due to the dyes electrochromic characteristic (Loew 2015) (Fig. 23). In my experiments, I used certain filters that are further explained in the following chapters.

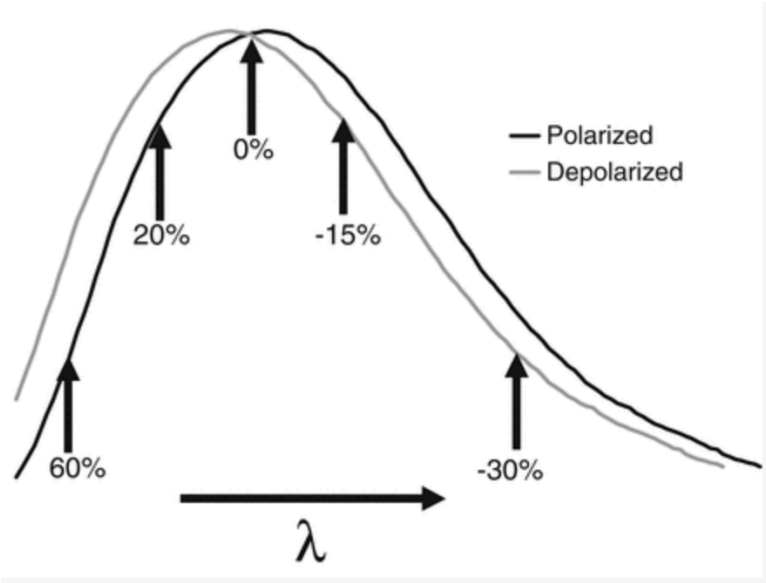

Fig. 23: The voltage-sensitive shift in VSDI. Spectra shown in this figure can represent absorbance, excitation or emission. The relative change in fluorescence, $\Delta F/F$ is shown as percentage change for different detection wavelengths (modified after Loew (2015)).

3.3.3 Amyloid-beta preparation

$A\beta_{1-42}$, $A\beta_{1-40}$ and AβpE3 (Bachem, CH-Bubendorf) were prepared in low-binding Eppendorf tubes to a 1 mg/400 µl solution with 100% hexafluoro isopropanol (HFIP) and either shaken at 37 °C for 20-30 min or 1 h at RT until the solution was clear. HFIP eliminates pre-existing structural inhomogeneities in Aβ proteins and acts as a hydrogen-bond breaker (Stine, Dahlgren et al. 2003). The solutions were then aliquoted into 20 µl portions á 50 µg Aβ on dry ice. HFIP was evaporated using a Lyophilizer for 60-90 min until a small white pellet was visible at the bottom of each tube.
On the day of an experiment, $A\beta_{1-42}$ and AβpE3 were dissolved in fresh DMSO to a concentration of 100 µM using a vortexer and 10 min of sonication in an ultrasonic water bath. $A\beta_{1-40}$ was dissolved in double distilled water (ddH_2O) to 100 µM. For VSDI experiments I used an $A\beta_{1-42}$ concentration of 50 nM (25 µl of the 100 µM aliquots in 50 ml aCSF). 3NTyrAβ was kindly provided by Dr. Markus Kummer (Bonn).

3.3.4 Experimental setup of VSDI

A single hippocampal slice was placed into the recording chamber of the setup (saturated with carbogen in a closed circuit and a flow rate of approx. 4-6 ml/min) and maintained with a platinum grid. During the whole experiment, its surrounding aCSF was saturated by carbogen. The recordings were performed at RT to ensure a better tolerance to hypoxia. I placed a concentric bipolar tungsten electrode onto the molecular layer of the DG (Fig. 24).

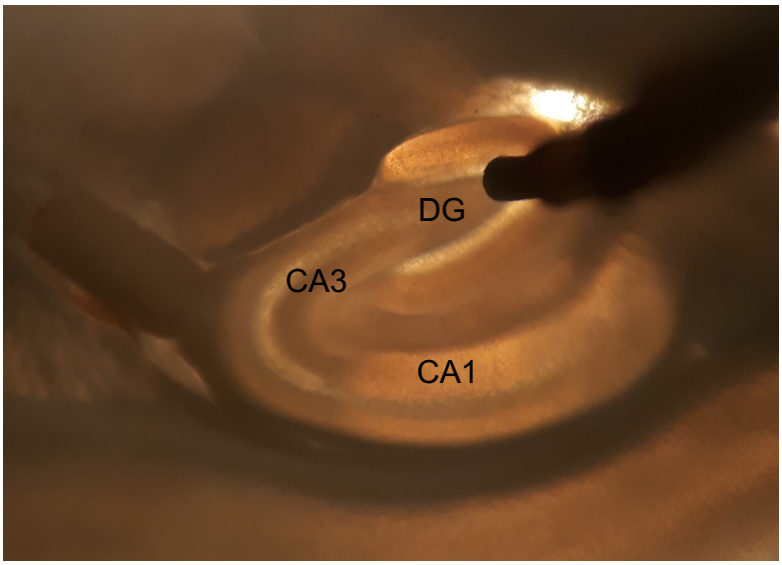

Fig. 24: Image of a murine hippocampal brain slice. View through the microscope showing the placement of the electrode into the granule cell layer of the dentate gyrus (DG) for VSDI experiments. Abbreviations: CA1/3= *Cornu Ammonis* 1/3)

A binocular epifluorescence microscope (BX51WI, Olympus, Hamburg, Germany) and a micromanipulator (Luigs and Neumann, Ratingen, Germany) enabled the placement of the electrode. Through illumination of the slice with an electronic shutter-controlled halogen lamp (MHAB-150 W; Moritex corp., China) through a filter cube with a band-pass filter (480-550 nm) for excitation, an emission long-pass filter (590 nm) and a dichroic mirror (570 nm), the camera MiCAM02 HR-charge-coupled device (CCD) (Brain Vision Inc., Tokyo, Japan; sampling rate of 2.2 ms, resolution of 88 x 60 pixels per frame and a pixel size of 8.4 µm x 9.8 µm) visualized the recording to the Brain Vision software (Brain Vision LLC, Morrisville, NC, USA) (Fig. 24 A). The recorded signal is then processed as normalized differences of fluorescence intensity *(ΔF/F)* in each pixel over time and presented as a color-coded sequence movie (Fig. 25 B). The Brain Vision and WinLTP (WinLTP Ltd., Centre for Synaptic Plasticity, School of Physiology & Pharmacology, University of Bristol, Bristol, United Kingdom) software were used to set up the protocol for the recordings. Every 10 sec a low-frequency stimulus (100 µs) was applied to the DG. To increase the signal-to-noise ratio, 8 acquisitions with 30 sec time-interval were averaged to one recording. Depending on the experimental setup, the recording times differed. The DG was stimulated continuously during the experiment to ensure a stable and continuous activation.

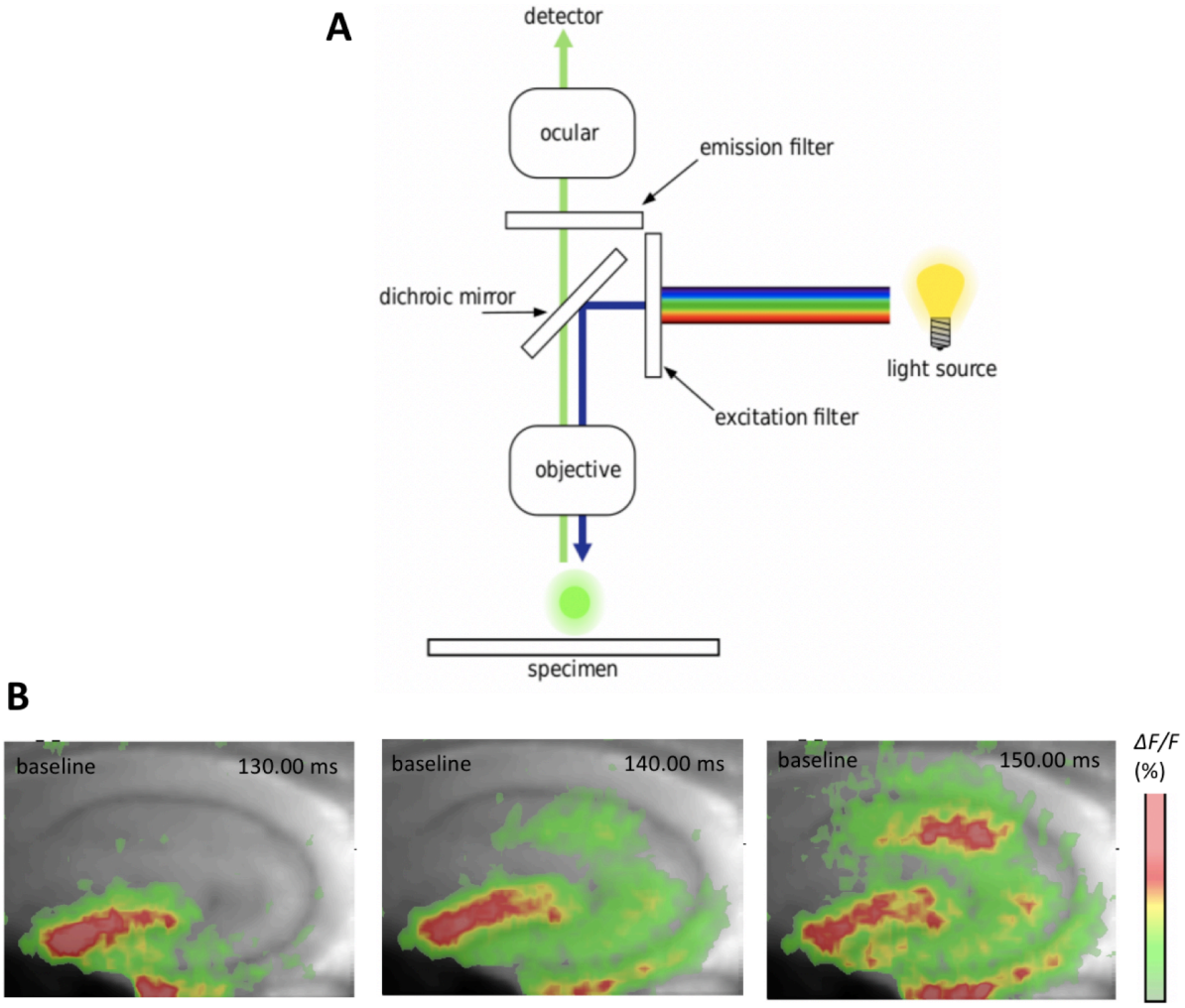

Fig. 25: VSDI setup and images of a processed stimulation signal. A: The light source emits light through an excitation filter onto a dichroic mirror that projects the light through the objective and onto the stained specimen (blue arrow). Fluorescence from the slice passes through the dichroic mirror, through the emission filter and to the CCD-sensor (detector; green arrow) (modified after Mühlpfordt and Bachnicki (2008)). **B:** Images taken from a filmstrip representing the propagation of a depolarization-mediated FDS signal through the trisynaptic circuit of the hippocampus at baseline conditions. A higher value of the fractional change in fluorescence (*ΔF/F*) are represented in warmer colors (red; see color bar), lower values in colder colors.

For control experiments, I recorded the baseline activity for at least 30 min until the neuronal activity remained stable. To mimic a healthy patient getting GA in a laboratory setting, I applied either 1%/0.6% isoflurane, 2%/1.4% sevoflurane or 65% xenon for 40 min and recorded the signal afterwards.

To assure a sufficient oxygen supply and to avoid a change in pH during the experiments, the maximum xenon concentration which can be applied is limited to 65%. For baseline and washout conditions, a nitrogen control gas (65% N_2, 30% O_2, 5% CO_2) admixture was applied together with carbogen to the aCSF and exchanged for the actual experiments with a pre-calibrated gas mixture containing 65% xenon, 30% O_2, 5% CO_2. With this procedure, the O_2 and CO_2 partial pressure were kept constant. The concentration of dissolved xenon in aCSF under these conditions was 1.9 ± 0.5

mM as determined by headspace gas chromatography (Mattusch, Kratzer et al. 2015). Applying a pure xenon anesthesia at normobaric conditions is not possible in rodents because the 'MAC immobility' is hyperbaric with 1.61 atm (standard atmosphere; ~160 Vol%) (Koblin, Fang et al. 1998). 65% xenon is close to 1 MAC xenon for humans (57-71%, volume is age-dependent (Nickalls and Mapleson 2003) and frequently used in previous studies (Haseneder, Kratzer et al. 2009).
To make the experiments with isoflurane and sevoflurane comparable to xenon, I also tested lower concentrations of these gases (0.6% isoflurane, 1.4% sevoflurane). The concentrations of sevoflurane and isoflurane are presented as volume percent (Vol%) and correlate with the applied vapor dial settings in a linear fashion (Haseneder, Kratzer et al. 2009). After application of the inhalational anesthetics, I closed the vaporizers/gas bottles and let the gas wash out for 60 min before the basal activity was measured again.

To mimic a patient with elevated amounts of Aβ in their brain in a laboratory setting, I applied different isoforms of Aβ at a concentration of 50 nm to aCSF and let it incubate for 90 min after baseline measurements. Isoflurane, sevoflurane and xenon were applied for 40 min and the activity was recorded. After a 60 min washout, the activity was recorded again.

3.3.5 VSDI-Analysis

The data from the VSDI experiments were analyzed using a special Macro in MATLAB (MATLABR2016b, The MathWorks, Natick, USA) that was named 'VSDI ROI Tool' and was kindly programmed by Dr. Sebastian Berger and Rami Eisawy of the TUM. With the help of this Macro, the color-coded fluorescence of the brain slices, represented as the 'fast depolarization signal (FDS)', was analyzed by certain parameters in defined ROI (region of interest) of the CA3 and CA1 region. The term *'area'* is a numeric value that counts all active pixel in a ROI. An active pixel can be described as a pixel whose change of fluorescence *(ΔF/F)* is at least 3x higher than the standard deviation of the background noise within a movie and its 512 frames. It is a parameter to determine the spread of the excitation upon stimulation (Fig. 25 B).

The value **FDS_{MaxInt}** describes the **mean** of the maximal change of fluorescence throughout all frames of every active pixel within a ROI.
The value **$FDS_{AreaInt}$** describes the **sum** of the intensities of each active pixel within a ROI for all 512 frames of a movie.
The value **FDS_{AUC}** is giving a somewhat overall effect. It includes the propagation of the signal (area), the intensity (Int) and the duration of excitation. It resembles the area under the curve (AUC) of the graph depicting the **$FDS_{AreaInt}$**.

3.4 Field excitatory postsynaptic potentials (fEPSPs) – LTP

3.4.1 Slice preparation and experimental setup

7-10 weeks old male mice (Black6, C57B161N) were used for LTP experiments. The animals were anesthetized with isoflurane and decapitated using a guillotine. The head was placed quickly into ice-cold ringer solution saturated with carbogen (95% O_2, 5% CO_2). After removing the brain from the skull, the cerebellum was cut off and the brain separated into its hemispheres using a sharp razor blade. The medial face was then glued to the tray of the microtome and the brain hemispheres cut into 350 µm thick slices. Slices recovered for at least 30 min at 34 °C and 1 h at RT before being transferred into the recording chamber of the extracellular setup, where they were continuously perfused with carbogen-saturated aCSF at a flow rate of about 5-8 ml/min at RT (20-22 °C) and fixated with a small platinum grid.

Two fine bipolar tungsten electrodes were used to alternately evoke field excitatory postsynaptic potentials (fEPSPs) in the striatum of the CA1 region of the hippocampus (every 15 sec; 20 µs; 4-5 V). I used a borosilicate glass micropipette (Clark Electromedical Instruments, Pangbourne Reading, United Kingdom) filled with aCSF (open resistance 1-2 MΩ) and placed it between the two electrodes to record the fEPSPs. The measurement of an internal control was possible because I stimulated non-overlapping neuron populations of the Schaffer collateral-associated commissural pathway through this special positioning (Fig. 26) (Kratzer, Mattusch et al. 2012, Rammes, Seeser et al. 2018).

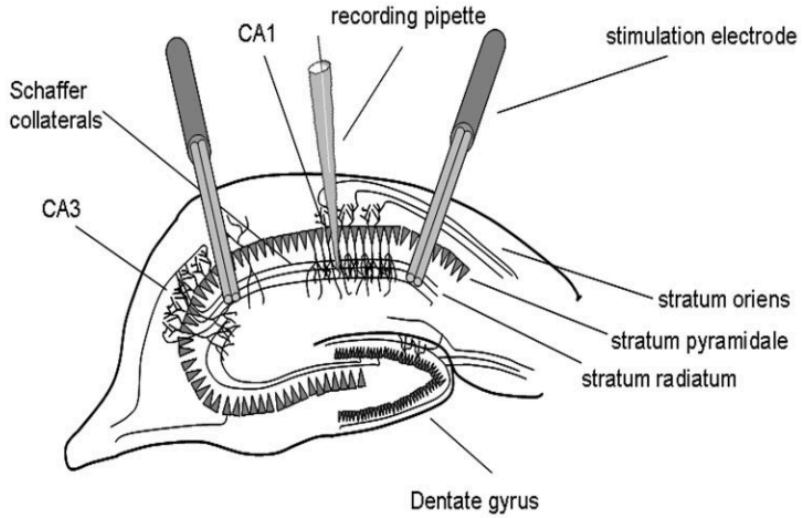

Fig. 26: Schematic drawing of the LTP setup. Two bipolar tungsten electrodes were placed onto the anterior and posterior stratum radiatum of the CA1 region of the hippocampus to excite the Schaffer collaterals. The recording pipette was placed in between these electrodes (modified after Kratzer, Mattusch et al. (2012)).

To start the experiments, baseline stimulations were recorded until a stable response of 30-40% of the maximal response could be measured (-0.5 mV). To evoke LTP in the control experiments, a high frequency stimulus (HFS; 100 pulses at 100 Hz) was applied through one of the stimulation

electrodes. LTP was recorded for 60 min with the same stimulation settings used for baseline recordings. Afterwards, I incubated Aβ at a concentration of 50 nM for 90 min, evoked LTP again and recorded for another 60 min. In experiments including xenon, I first applied Aβ before I triggered and measured LTP for the first time. After these 60 min, 30% xenon mixed with 30% O_2, 30% N_2, 5% CO_2 (pH 7.3 - 7.4) plus the gas admixture of 65% N_2, 30% O_2 and 5% CO_2 was applied for 20 min. Right after, LTP was evoked again in the other electrode. After LTP induction, xenon was applied for another 10 min (Fig. 27).

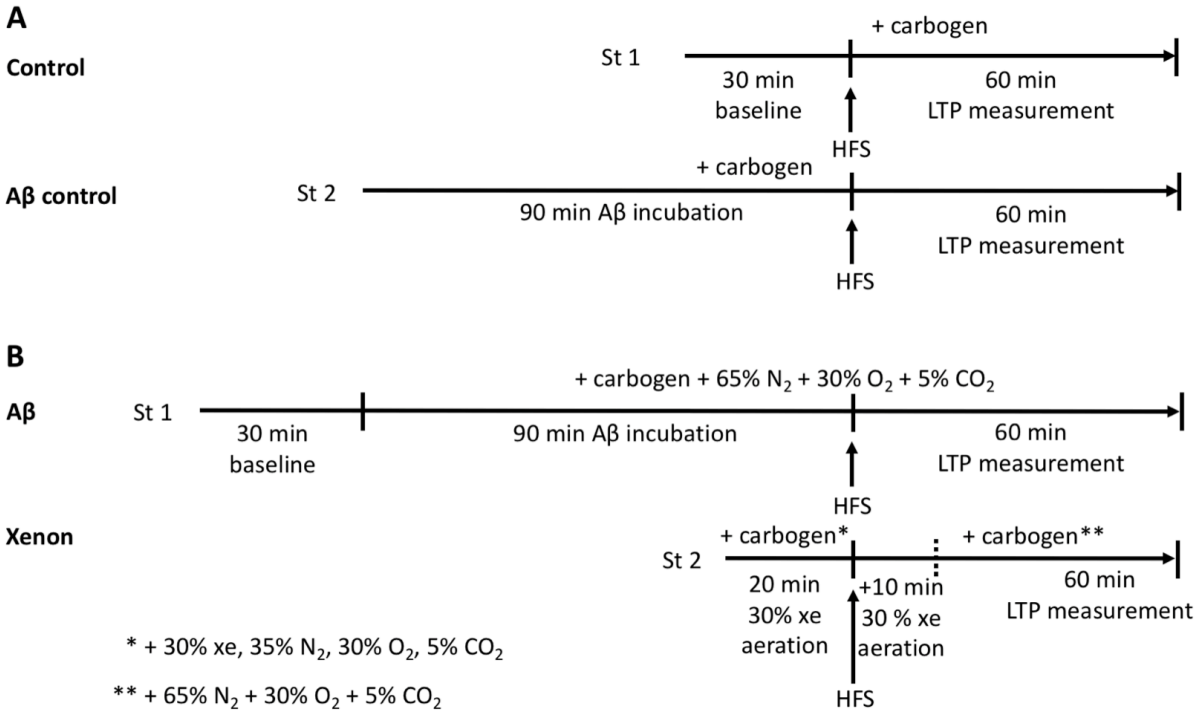

Fig. 27: Experimental time line of LTP experiments. A: Baseline recording was measured for 30 min before high frequency stimulation (HFS) was induced via St 1 and long-term potentiation (LTP) was recorded. HFS was induced in St 2 after incubation of Aβ. ACSF was saturated with carbogen. **B:** After baseline measurement and Aβ incubation, HFS was applied via St 1 and LTP was recorded. ACSF was saturated with carbogen + 65% N_2 + 30% O_2 + 5% CO_2. After aeration with 30% xe + 35% N_2 + 30% O_2 + 5% CO_2, for 20 min, St 2 induced HFS. Afterwards, the gas admixture was applied for an additional 10 min before replacement by carbogen + 65% N_2 + 30% O_2 + 5% CO_2. Stimulation electrode 1 and 2 = St 1, St 2.

3.4.2 LTP analysis

The electrodes 1 and 2 stimulated alternately every 15 seconds. Two fEPSPs of the corresponding input were averaged and the initial slope was analyzed between 20% and 80% of the amplitude. This value was subsequently normalized and plotted against time. The fEPSPs were recorded with the Synaptic Electrophysiology software WinLTP and analyzed offline with the Reanalysis WinLTP software.

All recorded values were normalized to the last 5 measurements (10 min) before HFS and the baseline was compared to the last 10 min of the experiment (50^{th}-60^{th} min HFS). 60 min after HFS, fEPSP slopes have to be increased at least 20% compared to the averaged fEPSPs of the baseline to be considered an LTP.

3.5 Western Blot

Western blotting, also called immunoblot, is a widely used biomolecular technique that separates extracted proteins according to their molecular masses through an electric field via gel electrophoresis. Afterwards, the proteins get blotted onto a membrane and the target protein gets detected and identified via a primary and a secondary antibody (Fig. 28). It is used as a general method to identify specific proteins within a mixture of proteins (Burnette 1981).

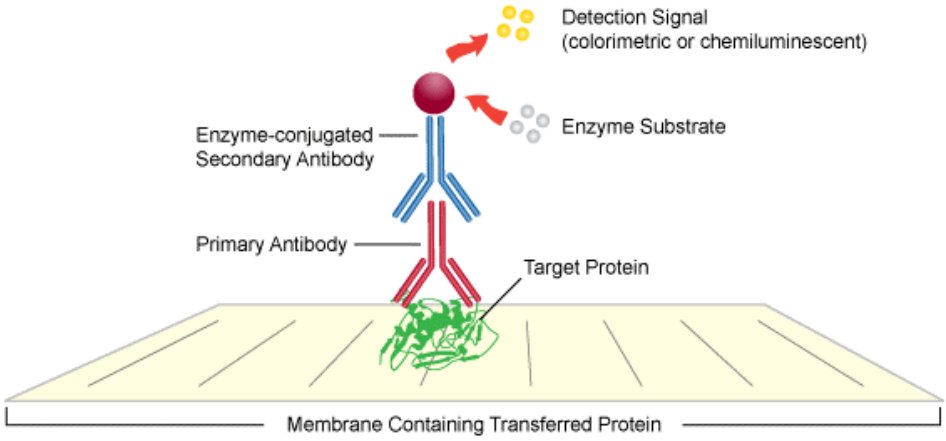

Fig. 28: Illustration of detection in Western Blots. The primary antibody binds to the target protein on the membrane. The membrane is then incubated with a chemiluminescence substrate. An enzymatic reaction occurs producing light which is detected by a CCD-camera (from: https://www.leinco.com/western-blotting-protocol/; last accessed February 2022).

3.5.1 Tissue preparation, protein extraction and quantification

For western blot experiments, 350 µm thick sagittal brain slices of WT mice (C57B161N) were cut and incubated according to the slices for LTP measurements. After incubation at RT for 1 h, the slices were divided into 4 groups. Group 1 was the control group and incubated for 2.5 h without any additional treatment. Group 2 incubated for 1.5 h with $A\beta_{1\text{-}42}$ (50 nM) before incubating another 60 min while being saturated by carbogen. Group 3 incubated for 1.5 h in carbogen, followed by 60 min aeration with either 65% xenon, 1% isoflurane or 2% sevoflurane. Group 4 incubated for 1.5 h with $A\beta_{1\text{-}42}$ before it was aerated with the anesthetics for 60 min. After incubation, slices were transferred onto a petri dish where the hippocampus was separated and collected in 1.5 ml Eppendorf-tubes

containing 300 µl radio-immunoprecipitation assay (RIPA) buffer (Sigma-Aldrich; 20 µl/ml 50X Complete, 1 mM PMSF und 1 µg/ml Pepstatin, Roche, Basel, Switzerland). The tissues were then homogenized on ice using the Amersham Sample Grinding Kit (GE Healthcare Europe GmbH, Freiburg). Centrifugation of the probes at 13000 G for 30 min at 4 °C (Biofuge fresco, Heraeus, Hanau) isolated the soluble protein. Solution containing the protein extract was transferred into a new tube.

I used the Bradford-assay for protein quantification (Bio-Rad Laboratories, Hercules, CA, USA). Triplets of the protein were applied onto a 96-well plate together with BSA-standard solutions (Bovine Serum Albumin Standard Pre-Diluted Set, Life Technologies GmbH, Darmstadt). With the help of the DC Protein Assay by Bio-Rad, the blue staining of the probes was quantified via photometry at 650 nm (sunrise^{TM} Reader, Tecan Trading AG, Männedorf, Switzerland) and the protein concentration determined through the generated standard curve.

The final concentration of the protein was adjusted to 2 µg/ml a using loading buffer containing NuPage LDS Sample Buffer, a reducing agent (Invitrogen AG, Carlsbad, CA, USA), Glycerol to increase the density of the solution and Blue to visualize the solvent front during electrophoresis. Proteins were then heated up to 95 °C for 5 min in a heating block (Eppendorf AG, Hamburg) to denature their structure.

3.5.2 Separation of the proteins through electrophoresis

3.5.2.1 Polyacrylamide gels

I prepared polyacrylamide-gels the day before an experiment according to the recipe in the appendix in a mold consisting of two sealed glass plates with spacers between the glass plates. The spacers had a thickness of 0.75 mm. A gel consists of the stacking gel and the separating gel. The lower gel (separating gel) was poured first and covered with several drops of isopropanol to ensure the elimination of bubbles from the meniscus and the protection from oxygen. After polymerization of the lower gel, isopropanol was discarded and the stacking gel was poured onto the solid separation gel. The combs that form the pockets into the gel which later contain the probes were inserted into the stacking gel without creating bubbles. The mesh of the stacking gel is lower than that of the separating gel to ensure a proper collection of the proteins at low voltage (100 V) before separation according to protein size at 200 V. Since I investigated proteins ranging from 14 to 150 kDa, I prepared 10% and 15% gels. The percentage shows the concentration of acrylamide in the gel. The lower the concentration, the better the resolution of higher molecular weight proteins.

3.5.2.2 Gel-electrophoresis and Blotting

For western blotting, I used sodium dodecyl sulfate-polyacrylamide gel electrophoresis (SDS-PAGE) to separate the proteins of interest between 5 and 250 kDa. It was developed by Ulrich K. Laemmli in 1970. SDS in the gels and running buffer denatures the complex structures of proteins through their

negative charges. The negatively charged proteins now migrate towards the positively charged anode through the mesh of the gel. Smaller proteins migrate faster through the mesh and the proteins get separated according to molecular size (Fig. 29).

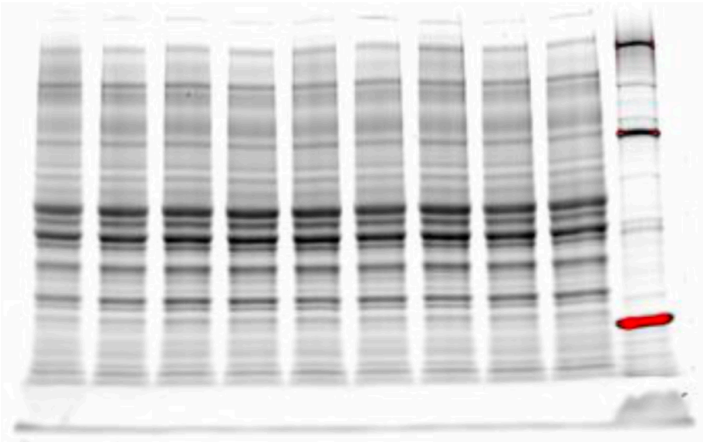

Fig. 29: Separated proteins on a 10% gel. Probes were activated on the gel through a UV-camera.

The Bio-Rad electrophoresis chamber was filled with running buffer before probes were loaded into the pockets of the gel. For comparison, pocket 1 always contained a standard probe, slot 10 a protein size marker (Novex Sharp Pre-Stained Protein Standard, Thermo Fisher Scientific Inc., Waltham, MA, USA). Electrophoresis was started and the negatively charged proteins were separated according to their size through an electrical field into protein bands (Fig. 29). For activation, gels were illuminated with a UV-camera (ChemiDoc™ XRS, Bio-Rad). Afterwards, the proteins were blotted/transferred onto a polyvinylidenfluoride-membrane (Amersham Hybond low fluorescence 0.2 µm PVDF, GE Healthcare) with the help of a tank-blot-system (Bio-Rad) in transfer/blotting buffer at 80 V for 60 min (Fig. 30).

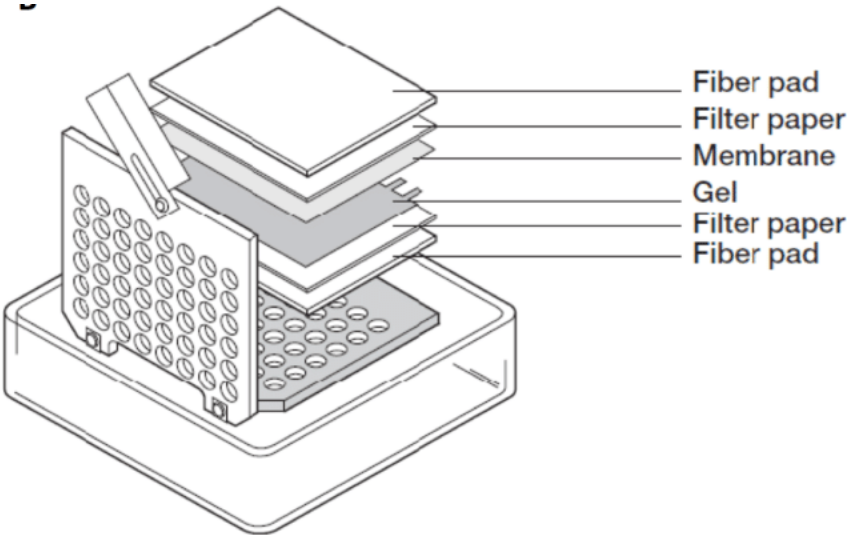

Fig. 30: Bio-Rad Western Blotting Sandwich arrangement. The setup of the electrophoresis chamber is always the following: Fiber pad – filter paper – membrane – gel – filter paper – fiber pad. (from: http://www.radio.cuci.udg.mx/bch/EN/Forschung/GelSandwich.gif; last accessed February 2022).

The membrane was then illuminated and recorded with the ChemiDoc™ camera to save it for analysis of the total protein. To prevent unspecific antibody bindings, the membranes were incubated and blocked for at least 1 h in 5% bovine serum albumin (BSA). After that, membranes were rinsed 3 x 10 min with Tris buffered saline (TBS) containing 0.1% Tween 20 before they were incubated ON with the first antibody (AB) at 4 °C on a shaker (see appendix for AB concentrations). The next day, after rinsing the membrane 3 x 5 min with TBS/T, it was incubated for 60 min at RT with the secondary AB (horseradish-peroxidase (HRP) anti-rabbit; 1:10000). To detect the protein of interest, the membrane was incubated for at least 1 min in Enhanced Chemiluminescence (ECL) solution (Luminol, P-Coumaric acid, H_2O_2) before being illuminated again with the ChemiDoc™ camera.

3.5.3 Western Blot Analysis

The evaluation of the Western blot data is carried out with the help of the program Image Lab from Bio-Rad. The amount of protein sought is determined by the intensity (gray values, Fig. 30) of the band and then normalized with the total protein of each sample. The different blots can be compared, based on the standard on each membrane, and were evaluated in an Excel file.

Fig. 31: Analysis of Western blot experiments with Image Lab™. The intensity of the protein bands represents the amount of proteins of interest (right). These get normalized through the total amount of protein of each probe on the membrane (left).

3.6 Spine Density

3.6.1 Brain slice preparation

With the help of a Microtome, I cut the brains of EGFP mice sagittally into 100 µm slices. Hippocampal slices were collected and recovered at 34 °C for 30 min before resting another 60 min at RT. For Aβ experiments, 50 nm of $A\beta_{1-42}$ was applied to the aCSF surrounding the slices and incubated for 90 min. For combinational experiments including Aβ plus the anesthetic, $A\beta_{1-42}$ was incubated first before volatile anesthetic was applied right after for 60 min. After these incubation steps, slices were transferred into a 6-well plate containing PBS. The slices were unfolded and fixed with nets and metal holders before they were incubated in fresh 4% PFA oN at RT.

3.6.2 Immunostaining

To further intensify the representation of the neurons and dendrites in the brain slices, immunostaining was performed. To wash off PFA, slices were rinsed with PBS (1X). Afterwards, the slices were incubated for 2 h on a shaker in a solution containing PBS (1X), 0.5 % Triton X-100 and 10% Normal Goat Serum (NGS) to block unspecific binding of antibodies.

To intensify the GFP fluorescence signal, slices were then stained with a α-GFP rabbit IgG antibody. The conjugate was diluted with PBS (1X) to a concentration of 1:200 and incubated with the slices for another 2 h at RT on a shaker (dark). After that, slices were washed again with PBS and were finally mounted onto a glass slide with Dako Fluorescence Mounting Medium and covered with coverslips.

They were then stored at 4 °C in darkness before further usage. In general, the slices can be stored like that for 2-3 months.

3.6.3 Microscopy and analysis of dendritic spines

Dendritic spines labeled by EGFP were detected by confocal microscopy (40x/60x oil objective). 8-10 dendrites were analyzed per animal. I used the ZEN software (Carl Zeiss Microscopy GmbH) for acquisition and detected all 13 layers in a Z-stack interval of 0.61 mm. Figures in this study show maximum intensity projections of the dendrites (Fig. 59), while the analysis was performed in 3D images. A constant frame size of 512 x 256 pixels was used to build the final images.

4. Statistical analysis

4.1 TR-FRET

A Kruskal-Wallis-test accompanied by the Dunn-Sidak post-hoc analysis was conducted using MATLAB R2017b (The Mathworks, Natick, MA, USA). The median is presented as the central mark in boxplots as well as the 1st and 3rd quartile (bottom and top edges of boxplot). Outliers are indicated by '+'. Whiskers indicate extreme values that are not considered outliers.

4.2 Silver Staining

To ascertain a statistical significance between the groups 'control' and '+ iso/sevo/xenon', the Mann-Whitney-U-test was performed in GraphPad Prism 9 (Graph Pad Software, La Lolla, CA, USA). The Kruskal-Wallis test, followed by the Dunn-Sidak post-hoc analysis, was used to test weather incubation times differ significantly. Graphs represent the mean ± SEM. Asterisks (*) represent a statistical significance ($p < 0.05$).

4.3 VSDI

To test for significance between neuronal activity at baseline level and activity after Aβ incubation, a paired t-test was performed in GraphPad Prism 9. To test for statistical differences between all groups (baseline – anesthetic – washout; baseline/Aβ – anesthetic - washout), an Ordinary one-way ANOVA was carried out. Significance was tested via Bonferroni's post-hoc multiple comparisons test between different states of neuronal activity: baseline, anesthetics and washout. Asterisks (*) represent a statistical significance ($p < 0.05$).

4.4 LTP

To test for significant differences between control and experimental conditions, I performed a Wilcoxon signed rank test in MATLAB R2017b. The strength of the effects was determined by Cohen's U31 (MATLAB-based MES toolbox (REF: PMID: PMID: 22082031)). This test quantifies the fraction of the difference in % between experimental groups that are below a certain comparison value. In my case, the difference was set to 0%. Additionally, I calculated 95% confidence intervals using 10k-fold bootstrapping. The median is presented as the central mark in boxplots as well as the 1st and 3rd quartile (bottom and top edges of boxplot). Outliers are indicated by '+'. Whiskers indicate extreme values that are not considered outliers. Asterisks (*) represent a statistical significance ($p < 0.05$).

4.5 Spine Density

The Mann-Whitney-U-test in GraphPad Prism 9 was used to statistically compare the groups pairwise. Asterisks (*) represent a statistical significance ($p < 0.05$).

4.6 Western Blot

The Kruskal-Wallis test was used to test for differences between the different experimental conditions. Analysis was done with Graph Pad Prism 9. Asterisks (*) represent a statistical significance ($p < 0.05$).

5. Results

5.1 TR-FRET: Effect of xenon, isoflurane and sevoflurane on aggregation of Aβ

In my TR-FRET assays, 2% isoflurane and 4% sevoflurane (resembling the concentration of 1 MAC each) did not show any significant influence on the aggregation properties of the Aβ solution (Fig. 32). Also, a low concentration of 30% xenon, which is used in my LTP experiments, had no effect (data not shown).

65% xenon instead reduced the aggregation of Aβ to synaptotoxic oligomers significantly (p= > 0.05) when compared to control, isoflurane or sevoflurane (Fig. 32). To show that an inhibition of Aβ aggregation was possible in this assay in general, I applied the Aβ aggregation inhibitor MRZ13646 developed by MERZ Pharma (Frankfurt am Main, Germany) (Parsons and Rammes 2017) at a concentration of 3 µM to the Aβ solution and showed that it decreased the aggregation of Aβ proteins significantly (Fig. 32). Also, an increasement of Aβ aggregation compared to control was possible through the addition of $MgCl^{2+}$ to the Aβ solution during incubation (data not shown).

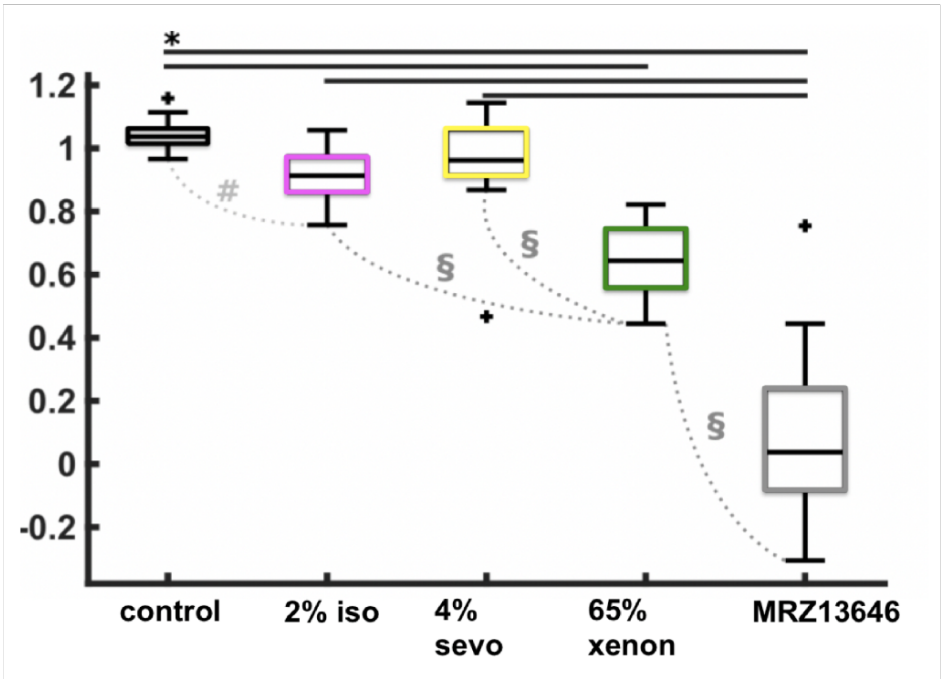

Fig. 32: Isoflurane and Sevoflurane do not influence Aβ aggregation, Xenon decreased Aβ aggregation. 2% isoflurane (iso)- and 4% sevoflurane (sevo) do not reduce of Aβ aggregation compared to control (cont) (cont: 1.04 ± 0.002, n= 9; 2% iso: 0.91 ± 0.04, n= 6; 4% sevo: 0.96 ± 0.07, n= 8). In contrast, application of 65% xenon reduces aggregation significantly (0.64 ± 0.03, n= 13). As an internal aggregation inhibitor control, the substance MRZ13646 was tested and reduced aggregation (0.04 ± 0.09, n= 10). Dotted lines show strong (AUC > 0.8, #) and very strong (AUC > 0.9, §) effects. Outliers are shown by +.

5.2 Silver Staining: Effect of anesthetics on Aβ aggregation

Aβ proteins (100 µM) separated as bands of monomers (4 kDa), trimers (15 kDa), tetramers (20 kDa) after gel electrophoresis and staining of the slices with silver nitrate. Higher oligomers (25 kDa+) appeared as ‘smears´instead of bands.
The relative staining intensity of the protein bands did not differ significantly from each other after an incubation time of 0 min (control), 90 min and 6 h. The longer the incubation time, the more the staining intensity decreased compared to control. After 3 d and 7 d, intensity of the protein bands seem to decrease significantly (Fig. 33-35).

The application of 65% xenon, 2% sevoflurane or 1% isoflurane to Aβ proteins before electrophoresis did not have any influence on the aggregation properties of monomers, trimers, tetramers and oligomers independent on the incubation time (Fig. 33-35).

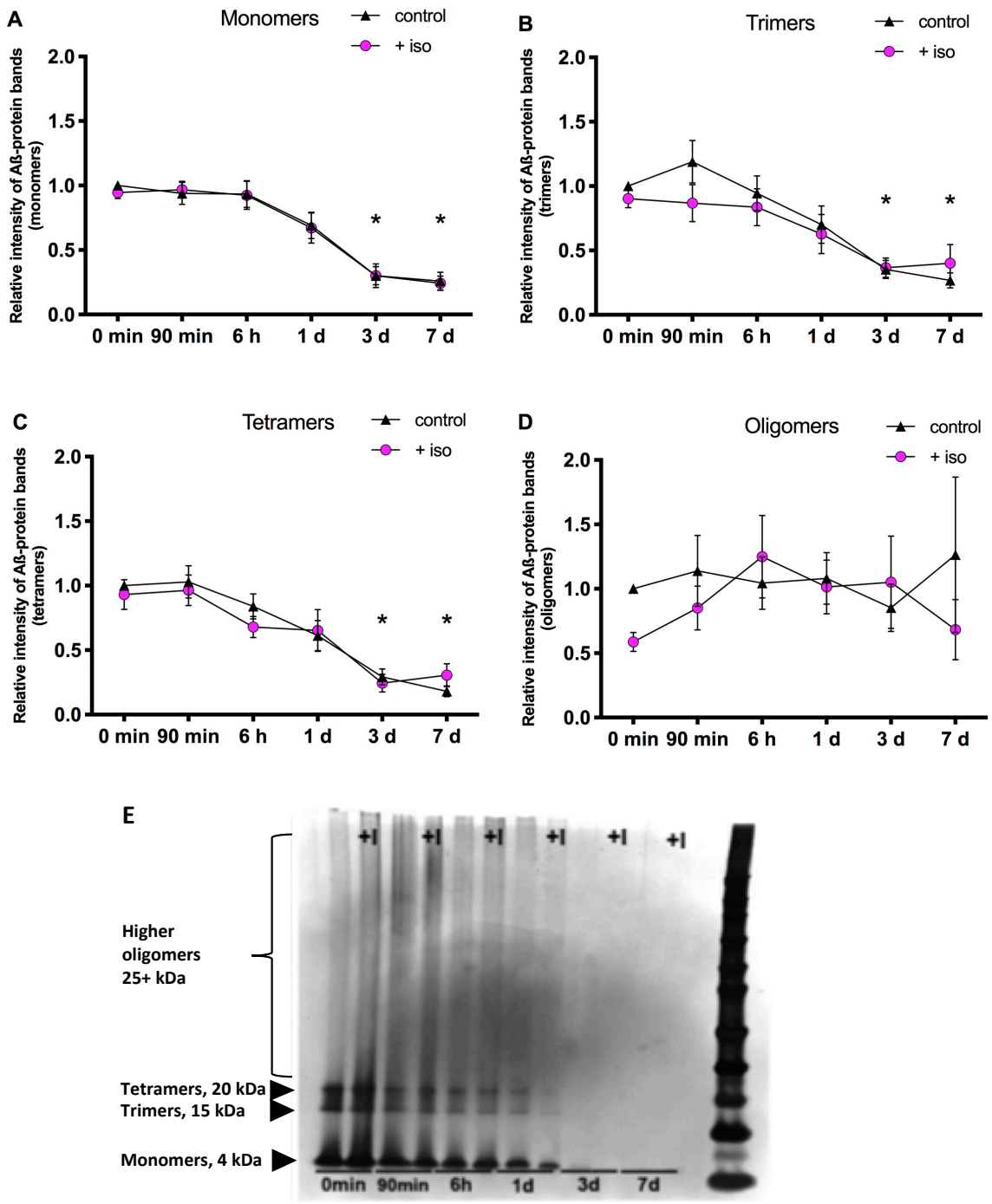

Fig. 33: No influence of isoflurane on aggregation properties of $A\beta_{1-42}$. A: Isoflurane did not influence aggregation of Aβ. 3 d (cont: p= 0.0020, iso: p= 0.0059) and 7 d (cont: p= 0.0009, iso: p= 0.0037) after start of incubation, the amount of protein decreased significantly when compared to control. **B:** 3 d (cont: p= 0.0072, iso: p= 0.0216) and 7 d (cont: p= 0.0028, iso: p= 0.0303) after start of incubation, the amount of trimers reduced significantly. **C:** Amount of tetramers was significantly reduced after 3 d (cont: p= 0.0024, iso: p= 0.0068) and 7 d (cont: p= 0.0002, iso: p= 0.0188). **D:** Amount of oligomers did not change. Asterisks (*) indicate a significant difference compared to control (0 min incubation). Abbreviation: +I= plus isoflurane. n= 7.

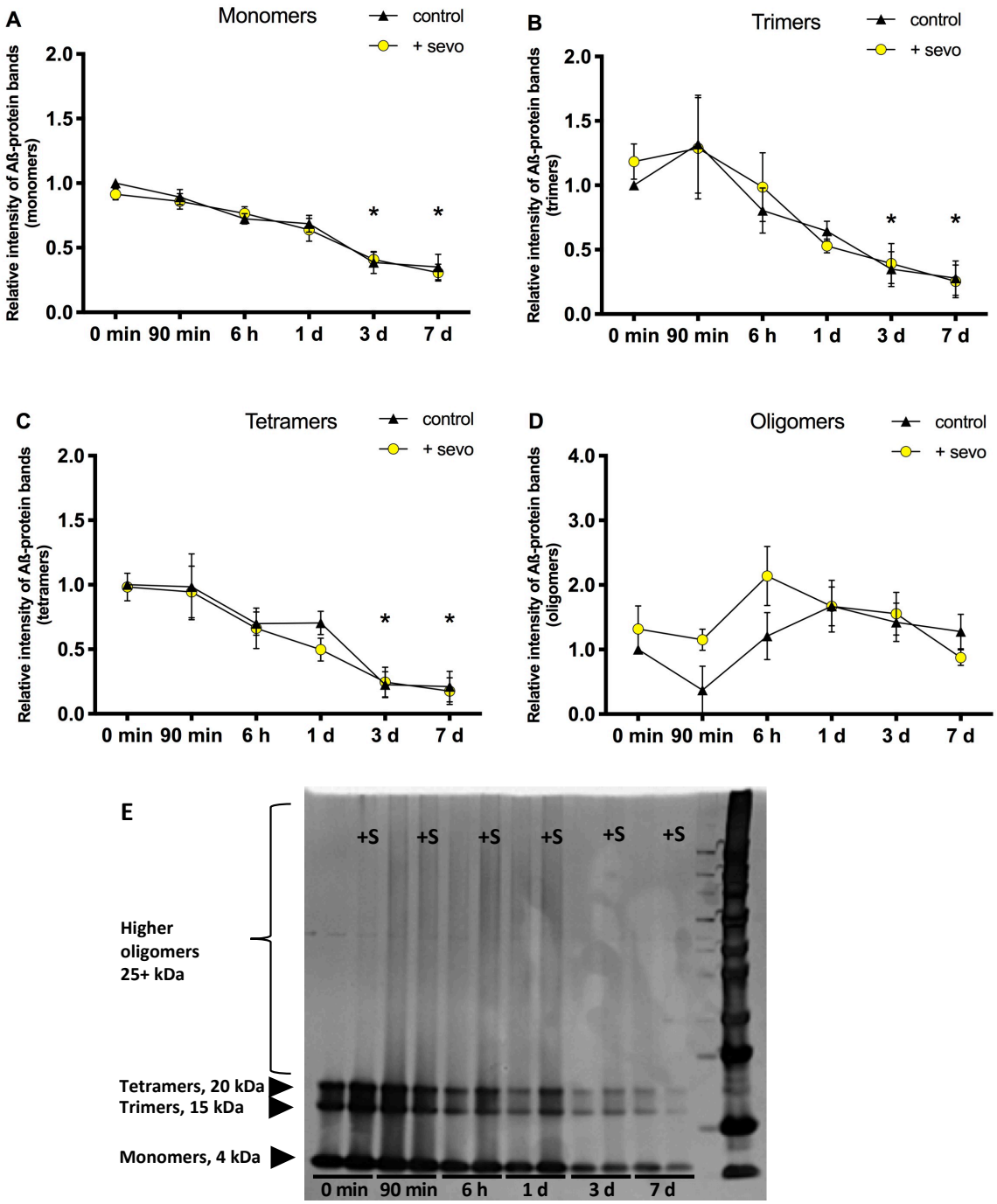

Fig. 34: No influence of sevoflurane on aggregation properties of $A\beta_{1-42}$. A: Sevoflurane did not influence aggregation of Aβ. 3 d (cont: p= < 0.0001, sevo: p= 0.0040) and 7 d (cont: p= < 0.0001, sevo: p= 0.0007) after start of incubation, the amount of trimers was significantly reduced compared to control. **B:** 3 d (cont: p= 0.0045, sevo: p= 0.0247) and 7 d (cont: p= 0.0013, sevo: p= 0.0018) after start of incubation, the trimers were significantly reduced. **C:** Amount of tetramers was significantly reduced 3 d (cont: p= 0.0118) and 7 d (cont: p= 0.0297, sevo: p= 0.0036) after start of incubation. **D:** Oligomers did not change significantly over time. Asterisks (*) indicate a significant difference compared to control (0 min incubation). Abbreviation: +S= plus sevoflurane.

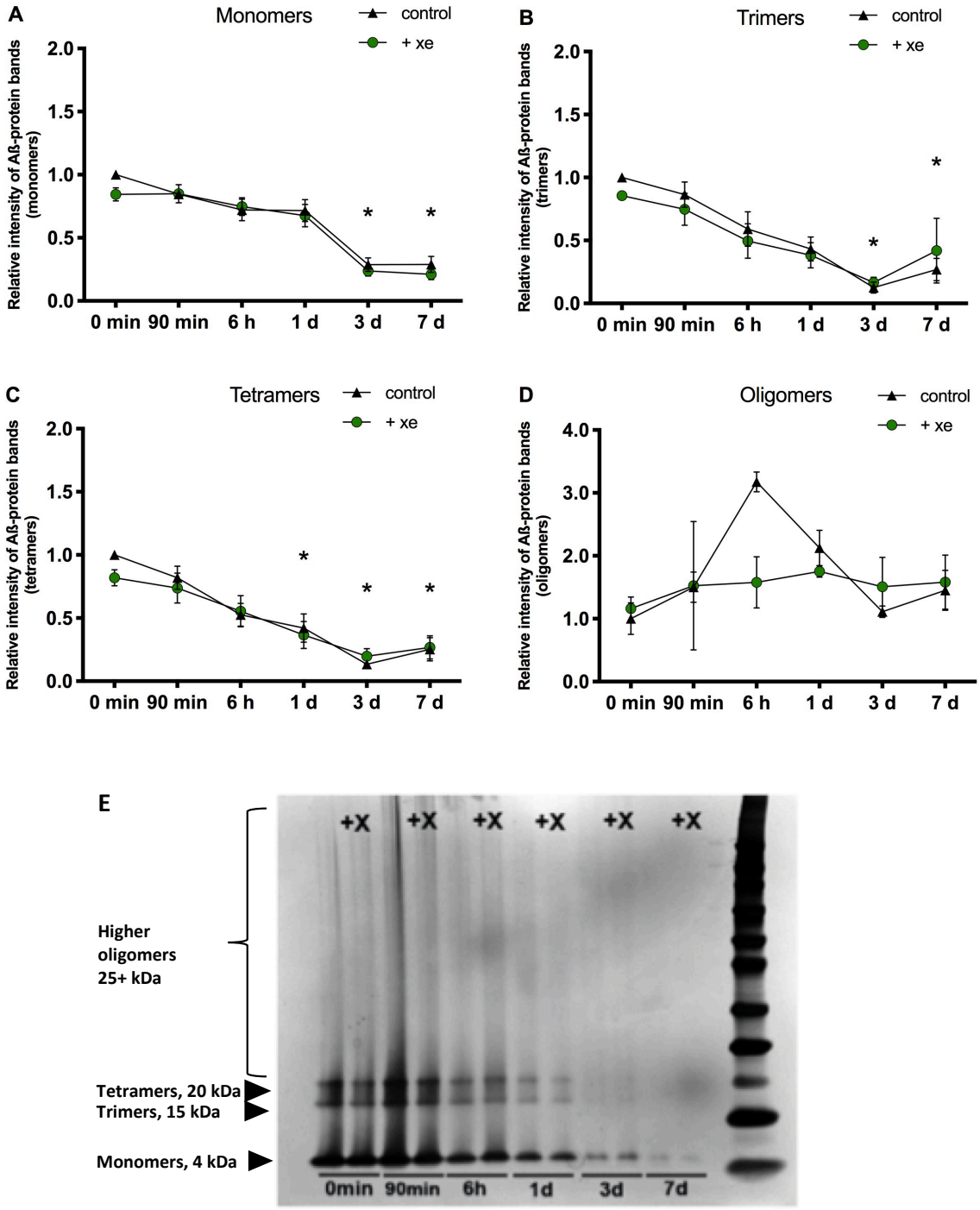

Fig. 35: No influence of xenon on aggregation properties of $A\beta_1$-42. A: Xenon did not influence aggregation of Aβ. The amount of trimers were significantly reduced 3 d (cont: p= < 0.0001, xe: p= 0.0008) and 7 d (cont: p= < 0.0001, xe: p= 0.0006) after start of incubation when compared to control. **B:** 3 d (cont: p= 0.0117, xe: p= 0.0027) and 7 d (cont: p= 0.0028, xe: p= 0.0152) after start of incubation, the amount of trimers decreased significantly. **C:** 1 d (cont: p= 0.0139), 3 d (cont: p= < 0.0001, xe: p= 0.0018) and 7 d (cont: p= 0.0001, xe: p= 0.0063) after incubation start, the amount of oligomers decreased significantly. **D:** Oligomers did not change significantly over time. Asterisks (*) indicate a significant difference compared to control (0 min incubation). Abbreviation: +X= plus xenon. n= 7.

5.3 Voltage-Sensitive Dye Imaging

5.3.1 Basal activity in the murine hippocampus

I measured and recorded the basal activity of the hippocampal trisynaptic formation without the application of any substance. I found no significant differences of the FDS (*ΔF/F*), representing basal neuronal activity, between the CA3 and the CA1 region.

Figure 36 compares three different parameters I used to analyze my VSDI results (FDS_{AUC}, $FDS_{AreaInt}$ and FDS_{MaxInt}) via the 'VSDI ROI Tool'. Because FDS_{AUC} includes three important parameters (area, time and intensity) instead of only two, it was further used to analyze my VSDI data.

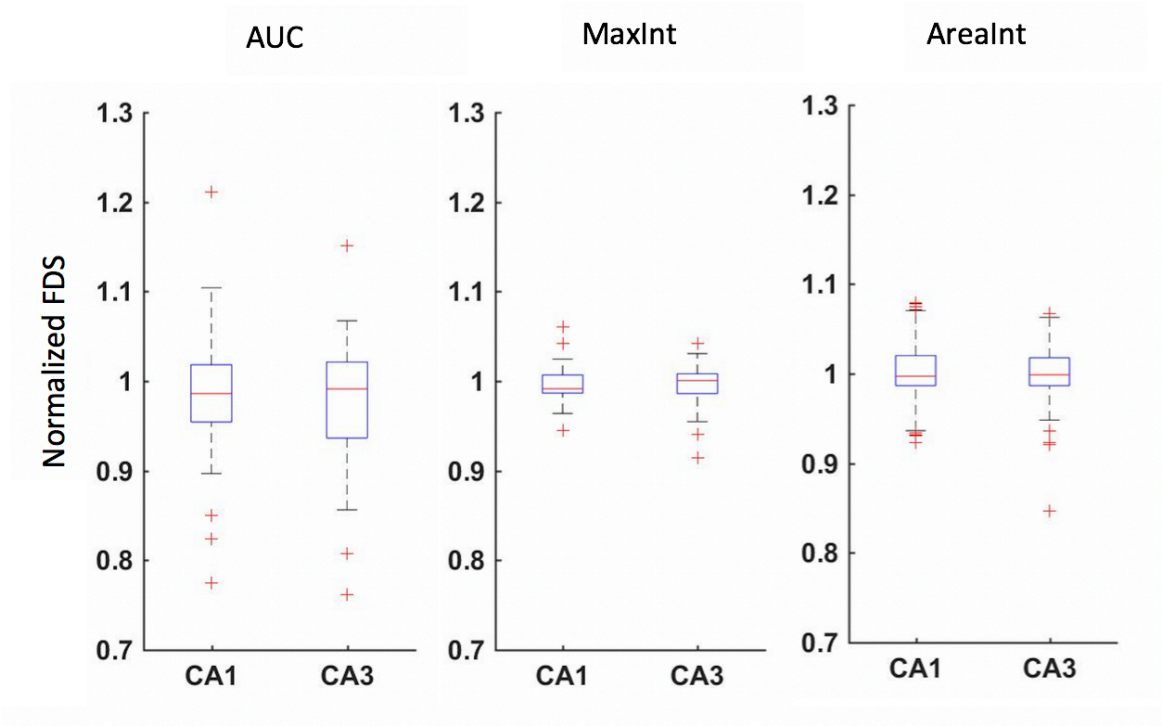

Fig. 36: Basal activity of the CA1 and CA3 region in the hippocampus. The analysis of the basal activity in the CA1 and CA3 region of all 3 analysis parameters (FDS_{AUC}, FDS_{MaxInt}, $FDS_{AreaInt}$) revealed no significant differences between the regions. In each boxplot, the central mark indicates the median, and the bottom and top edges the 25th and 75th percentiles, respectively. The whiskers extend to the most extreme data points not considered outliers. Outliers are plotted individually using the '+' symbol.

5.3.2 Effect of different Aβ isoforms on neuronal activity

Control experiments showed that monitoring the neuronal activity in the VSDI setup for 4-6 h did not influence the quality of neuronal signal propagation in the trisynaptic circuit of the hippocampus and VSDI was therefore supposedly not accompanied by a run-down. The activity was stable and I therefore propose, that the slices stayed vital throughout my experiments (Fig. 37).

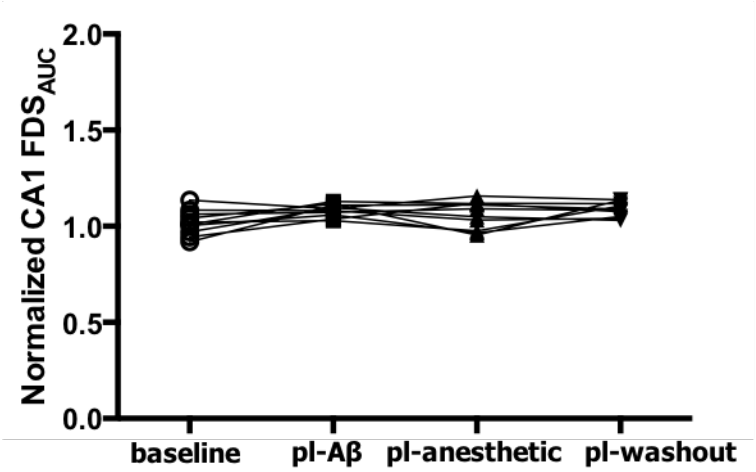

Fig. 37: Basal neuronal activity did not change over time. In my control experiments (n= 4) there was no significant change in FDS_{AUC} (*ΔF/F*), representing a change in neuronal activity, over a time course of 4 h (comparable to the length of experiments). Abbreviations: pl= placebo.

Three of four different isoforms of Aβ I investigated ($Aβ_{1-42}$, $Aβ_{1-40}$, AβpE3, 3NTyrAβ) did not change the neuronal activity (change in FDS_{AUC} (*ΔF/F)*) in the CA3 and CA1 region of the hippocampus significantly when applied at 50 nM for 90 min when compared to baseline activity. In several slices, the activity increased numerically, but it is not clear whether this effect occurred because of Aβ or because of other factors that were not determined. The activity of both the CA1 and CA3 region increased significantly (CA1: p= 0.0049; CA3: p= 0.0100, n= 21) after incubation of $Aβ_{1-40}$ for 90 min (Fig. 38).

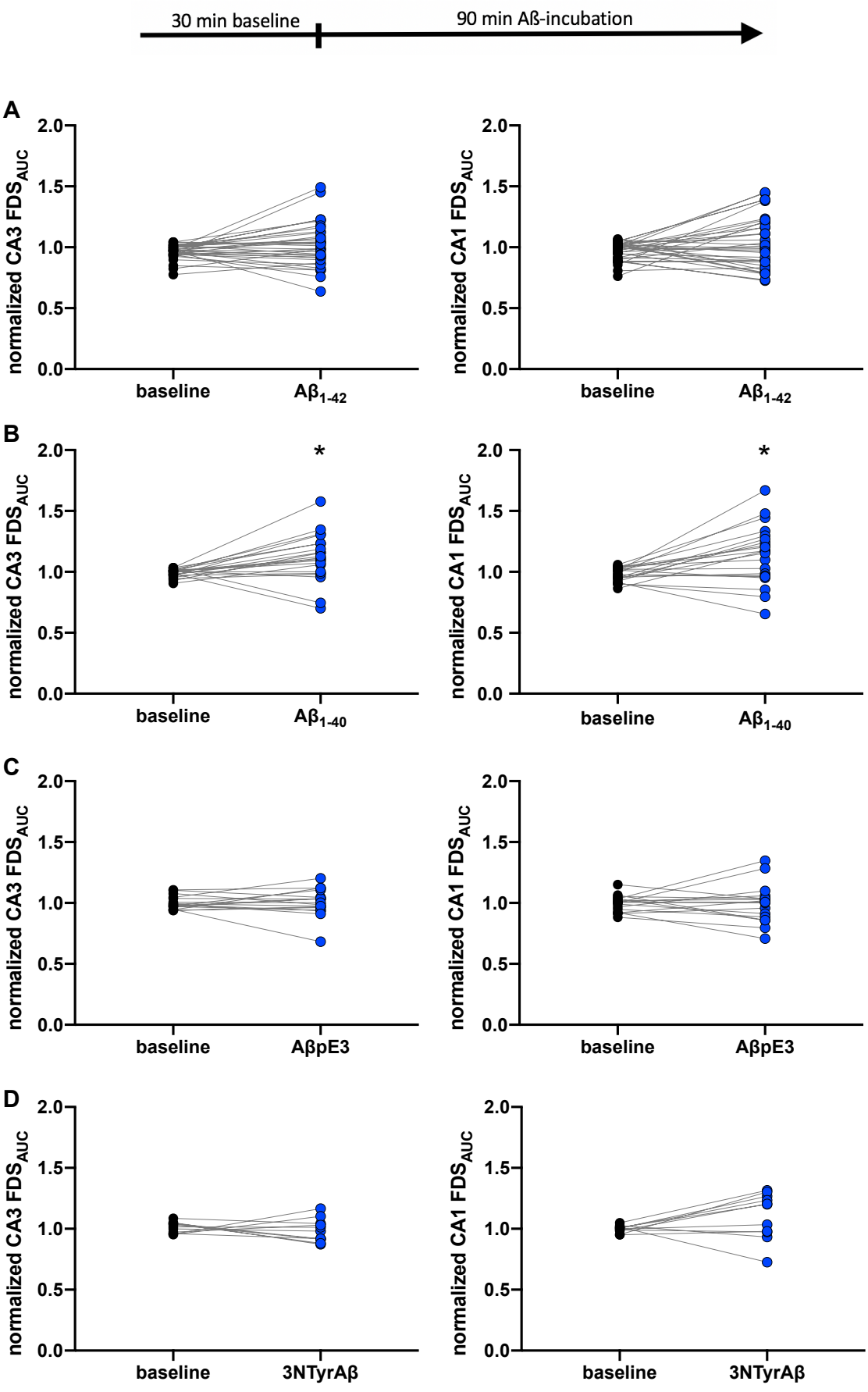
30 min baseline
90 min Aß-incubation
A
B
C
D
normalized CA3 FDS$_{AUC}$
normalized CA1 FDS$_{AUC}$
2.0
1.5
1.0
0.5
0.0
baseline
Aβ$_{1-42}$
Aβ$_{1-40}$
AβpE3
3NTyrAβ
*

Fig. 38: Only $A\beta_{1\text{-}40}$ changed neuronal activity in the hippocampus. A: Baseline measurements show control conditions (black circles). The incubation of $A\beta_{1\text{-}42}$ did not change the FDS_{AUC} (*ΔF/F)* significantly (mean ± SEM): CA3: baseline: 0.97 ± 0.01, $A\beta_{1\text{-}42}$: 1.00 ± 0.03, p= 0.07; CA1: baseline: 0.99 ± 0.01, $A\beta_{1\text{-}42}$: 1.00 ± 0.04, p= 0.19). n= 34. **B:** The incubation of $A\beta_{1\text{-}40}$ increased neuronal activity in the CA3 and CA1 region significantly. CA3: baseline: 0.97 ± 0.01, $A\beta_{1\text{-}40}$: 1.17 ± 0.05; p= 0.0049, n= 21). **C + D:** No change of FDS_{AUC} after incubation with AβpE3 (baseline: 1.00 ± 0.01, AβpE3: 1.00 ± 0.03; p= 0.75, n= 17) and 3NTyrAβ (baseline: 1.00 ± 0.01, 3NTyrAβ: 1.20 ± 0.06; p= 0.12, n= 11).

5.3.3 Effect of inhalational anesthetics on neuronal activity of the hippocampus

In order to simulate a healthy patient receiving anesthesia in a laboratory setting, I applied isoflurane, sevoflurane and xenon to the brain slices after recording the baseline activity without the addition of Aβ.

After washing either 0.6% or 1% isoflurane for 40 min into the aCSF surrounding the slice with a vaporizer, the neuronal activity, indicated by the change in FDS_{AUC} (*ΔF/F)*, of the mouse hippocampus decreased significantly in the CA3 and CA1 region when compared to baseline recordings (Fig. 39). I saw the same effect in slices treated with either 1.4% or 2% sevoflurane (Fig. 40). The differences between the applied concentrations were only significant between 1.4% sevoflurane and 65% xenon (Fig. 41).

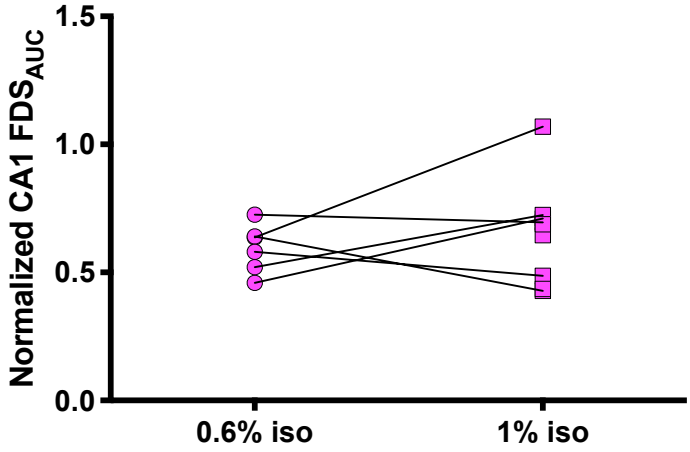

Fig. 39: Comparison of different isoflurane concentrations. The application of either 0.6% isoflurane (iso) or 1% iso for 40 min, did not show a significant difference in the effect on the neuronal activity of the CA1 region of the hippocampus (p= 0.5031).

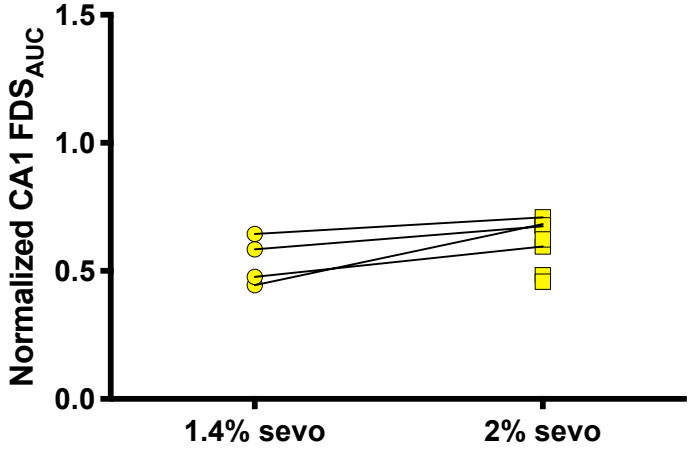

Fig. 40: Comparison of different sevoflurane concentrations. The application of either 1.4% sevoflurane (sevo) or 2% sevo for 40 min, did not show a significant difference in the effect on the neuronal activity of the CA1 region of the hippocampus (p= 0.2216).

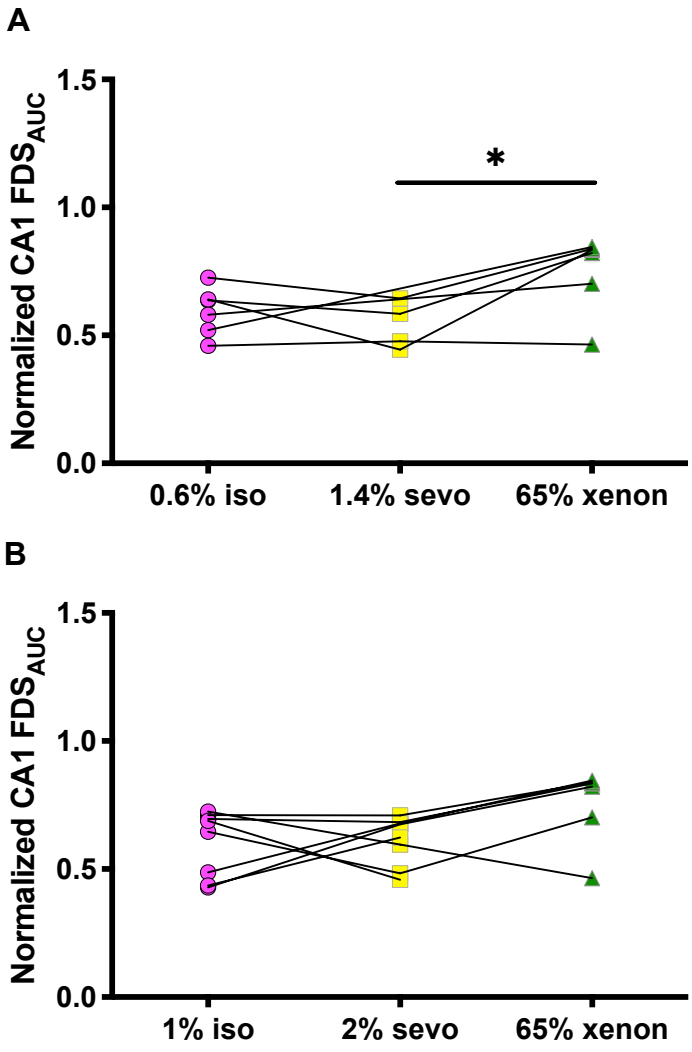

Fig. 41: Comparison of different gas concentrations. The effect on neuronal activity after application of 0.6% isoflurane (iso) compared to 1.4% sevoflurane for 40 min showed no significance (p= > 0.9999). 0.6% isoflurane compared to the effect of 65% xenon did not show a significant difference (p= 0.1199). There was a significant difference between 1.4% sevoflurane and 65% xenon (p= 0.0472).

After baseline recording of at least 30 min to get a stable signal, I aerated the aCSF for 40 min with the three different anesthetics. The activity of both the CA1 and CA3 region decreased quickly and significantly independent of the gas concentrations. 65% xenon did not decrease the CA3 region significantly as the only compound (Fig. 42). 30% xenon did not alter the activity in the hippocampus (data not shown).

After a washout of 60 min, the activity of the CA1 region recovered in all groups back to the baseline activity niveau after a washout of 60 min (Fig. 42). The CA3 region did not recover completely back to baseline levels after application of 0.6% isoflurane.

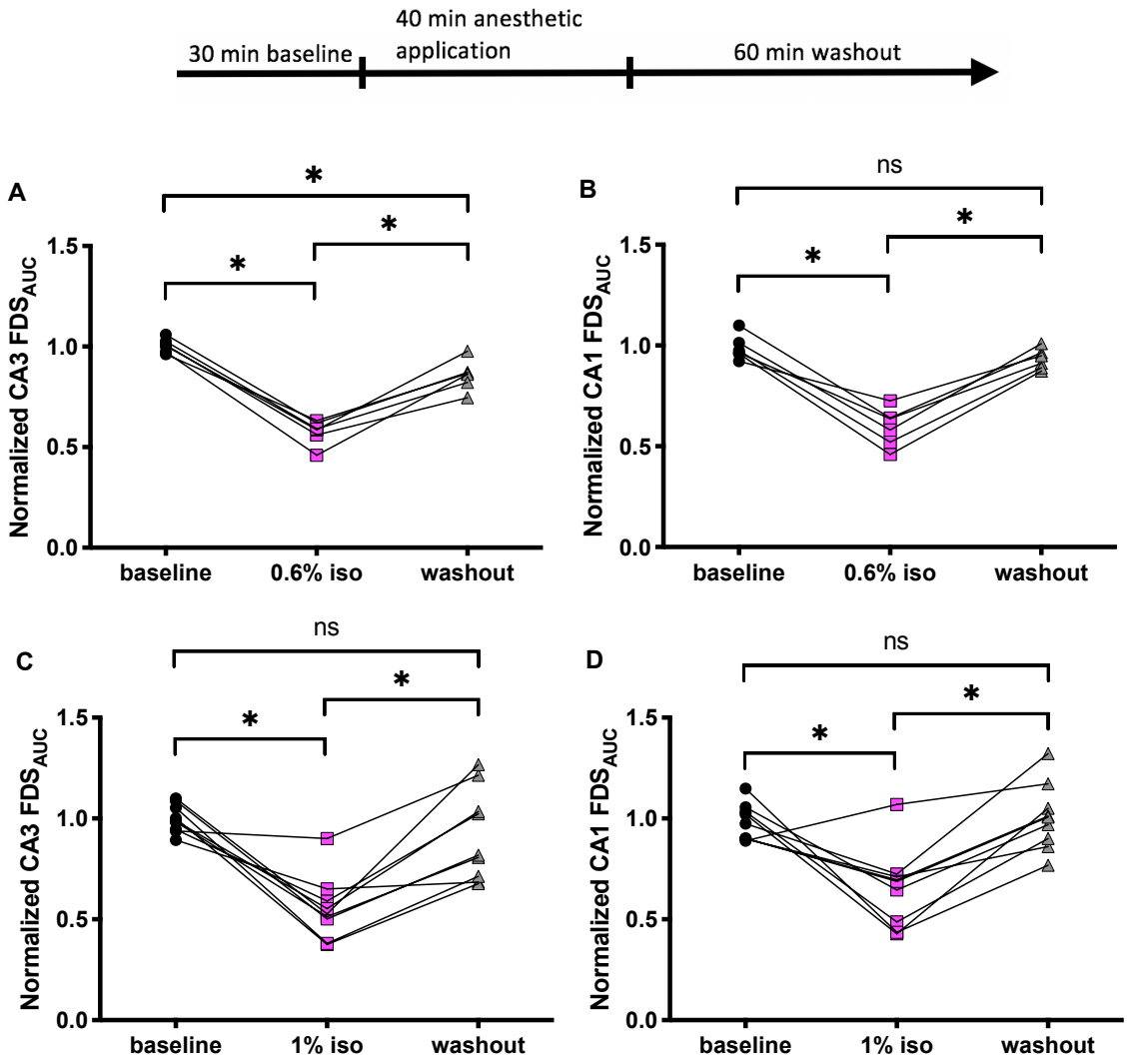

Fig. 42: Effect on neuronal activity and washout of 0.6% and 1% isoflurane. A + B: 0.6% isoflurane (iso) decreased the neuronal activity in the CA3 (A: p= < 0.0001, n= 6) and CA1 region (B: p= 0.0011, n= 6) significantly. The activity recovered in the CA1 region (B: p= 0.2071), but not in the CA3 region (A: p= 0.0020, n= 6) back to baseline levels after a washout of 60 min. **C + D:** 1% iso decreased the neuronal activity in the CA3 (p= < 0.0001, n= 9) and CA1 region (p= 0.0006, n= 9) significantly. The activity recovered in the CA1 region (B; p= > 0.9999) and in the CA3 region (A; p= 0.8779, n= 8) back to baseline levels after a washout of 60 min.

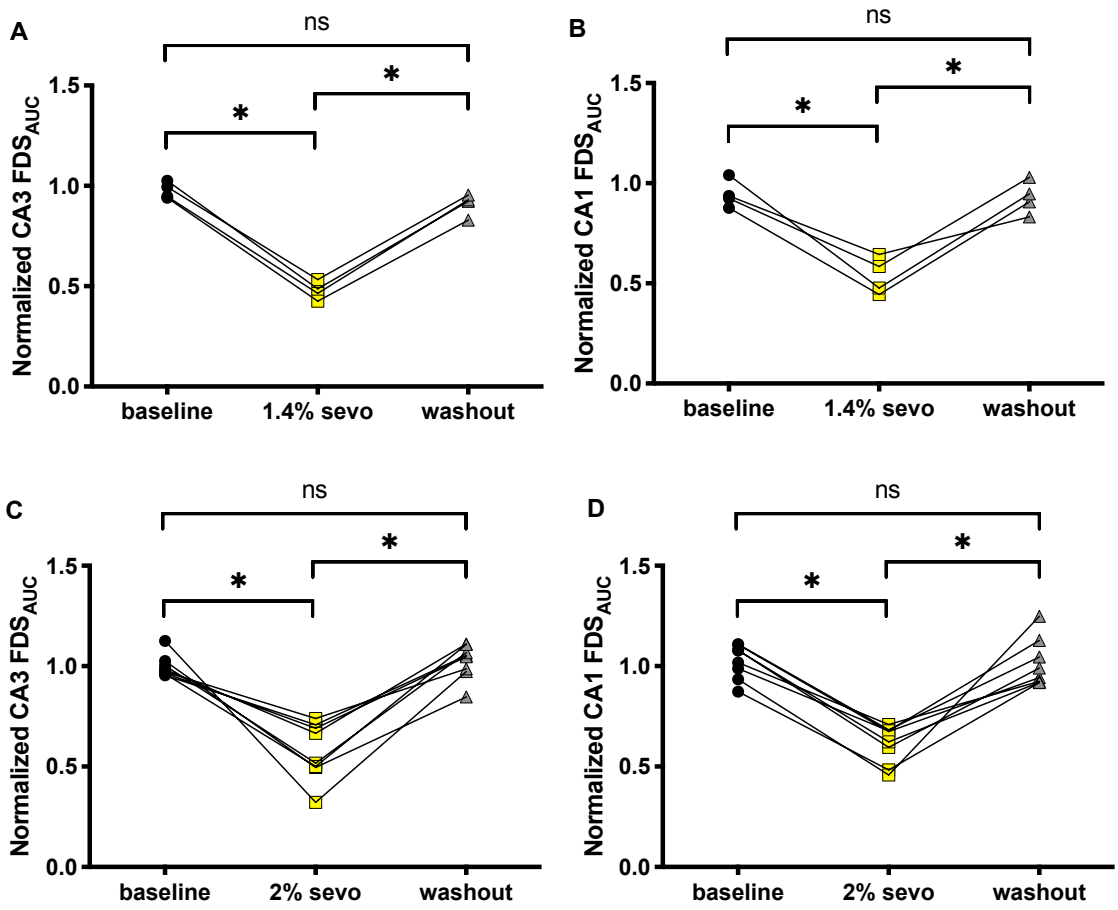

Fig. 43: Effect on neuronal activity and washout of 1.4% and 2% sevoflurane. A + B: 1.4% sevoflurane (sevo) decreased the neuronal activity in the CA3 (p= < 0.0001, n= 4) and CA1 region (p= 0.0002, n= 4) significantly. The activity recovered in the CA1 region (B; p= > 0.9999) and in the CA3 region (p= 0.2262) back to baseline levels after a washout of 60 min. **C + D:** 2% sevo decreased the neuronal activity in the CA3 (p= < 0.0001, n= 8) and CA1 region (p= 0.0002) significantly. The activity recovered in the CA1 region (p= > 0.9999) and in the CA3 region (p= > 0.9999) back to baseline levels after a washout of 60 min.

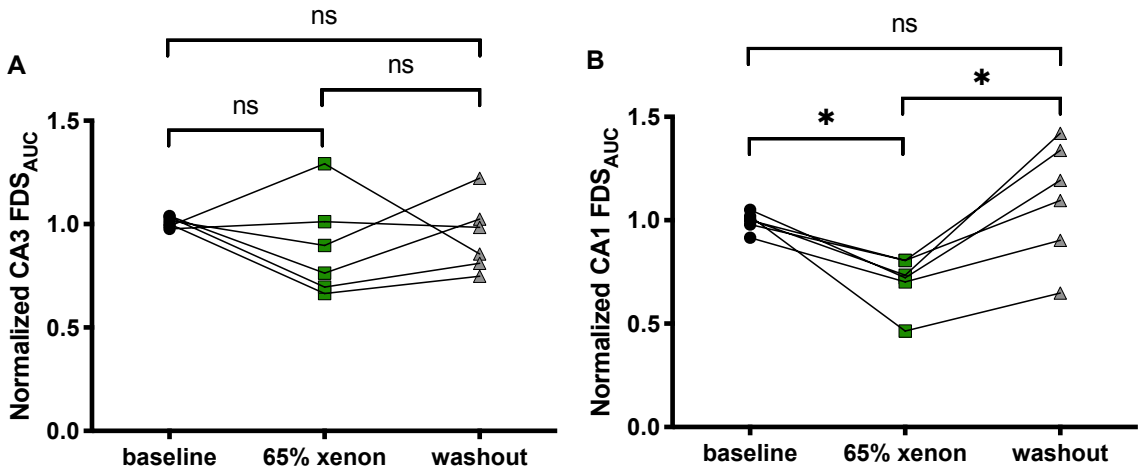

Fig. 44: Effect on neuronal activity and washout of 65% xenon. 65% xenon decreased the neuronal activity in the CA1 (p= 0.0457, n= 6), but not in the CA3 region (p= 0.6935) significantly. The activity recovered in the CA1 region (p= 0.9990) and in the CA3 region (p= > 0.9999) back to baseline levels after a washout of 60 min.

5.3.4 The combination of Aβ and anesthetics

To mimic a patient with elevated amounts of Aβ in the brain undergoing anesthesia (due to age, AD or other diseases) in a laboratory setting, I incubated the hippocampal brain slice with 50 nM Aβ before aeration with anesthetics.

The application of 1% isoflurane for 40 min prevented the recovery of both the CA1 and CA3 region after a washout of the gas for 60 min when compared to Aβ levels Aβ levels represent the 'baseline activity' in these experiments (Fig. 45). Also, a washout of 2-3 h did not recover the neuronal activity completely (data not shown). The same phenomenon occurred after incubation of $A\beta_{1-40}$ and AβpE3 with 1% isoflurane.

I lowered the concentration of isoflurane to 0.6% and applied it to slices treated with $A\beta_{1-42}$ and found the neuronal activity to recover completely in the CA1, but not in the CA3 region after washout of this sub-anesthetic concentration of isoflurane.

The treatment of the slices with 2% sevoflurane combined with 50 nM $A\beta_{1-42}$, $A\beta_{1-40}$ and AβpE3 failed to regain neuronal activity states of Aβ baseline levels. The activity of the CA3 and CA1 region recovered completely after washout when 3NTyrAβ and 2% sevoflurane were combined. The application of a subanesthetic concentration of 1.4% sevoflurane to slices incubated with $A\beta_{1-42}$ resulted in a complete recovery of the hippocampal activity in the CA1, but not in the CA3 region.

The application of AβpE3 and 3NTyrAβ and the aeration with 65% xenon lead to a recovery of hippocampal activity in both regions. The combination of $A\beta_{1-40}$ and 65 % xenon resulted in no complete washout and recovery of neuronal activity in the CA3 region ($A\beta_{1-40}$) and the CA1 region ($A\beta_{1-42}$).

5.3.4.1 $A\beta_{1-42}$

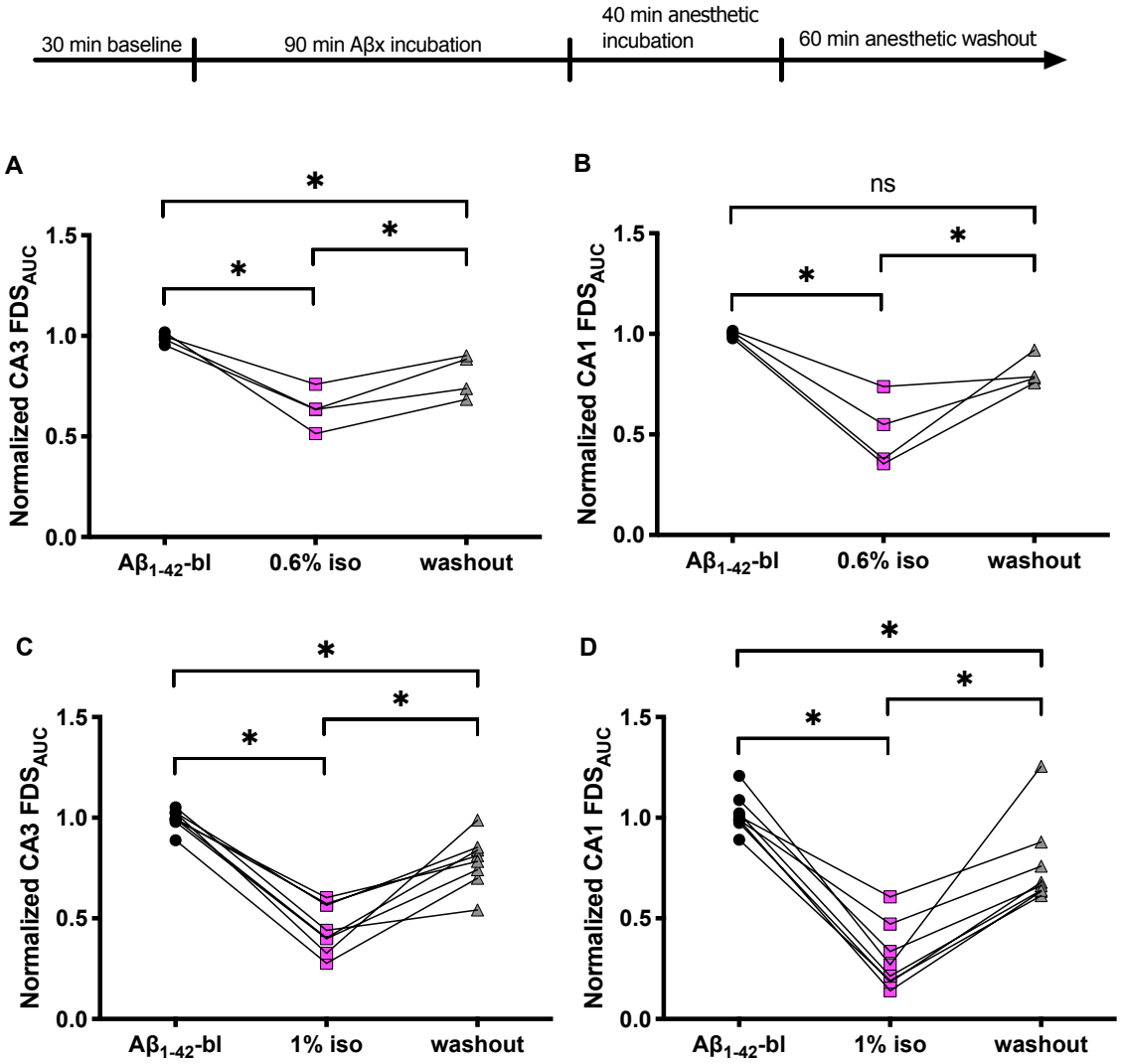

Fig. 45: Effect on neuronal activity and washout of 0.6% and 1% isoflurane in the presence of $A\beta_{1-42}$. A + B: 0.6% isoflurane (iso) decreased the neuronal activity in the CA1 (p= 0.0008, n= 4) and in the CA3 region (p= 0.0005, n= 4) significantly. The activity recovered in the CA1 region (p= 0.1253) back to baseline levels after a washout of 60 min, but not in the CA3 region (p= 0.0409). **C + D:** 1% iso decreased the neuronal activity in the CA1 (p= < 0.0001, n= 8) and in the CA3 region (p= < 0.0001) significantly. The activity did not recover in the CA1 (p= 0.0165) and CA3 region (p= 0.0021) after a washout of 60 min.

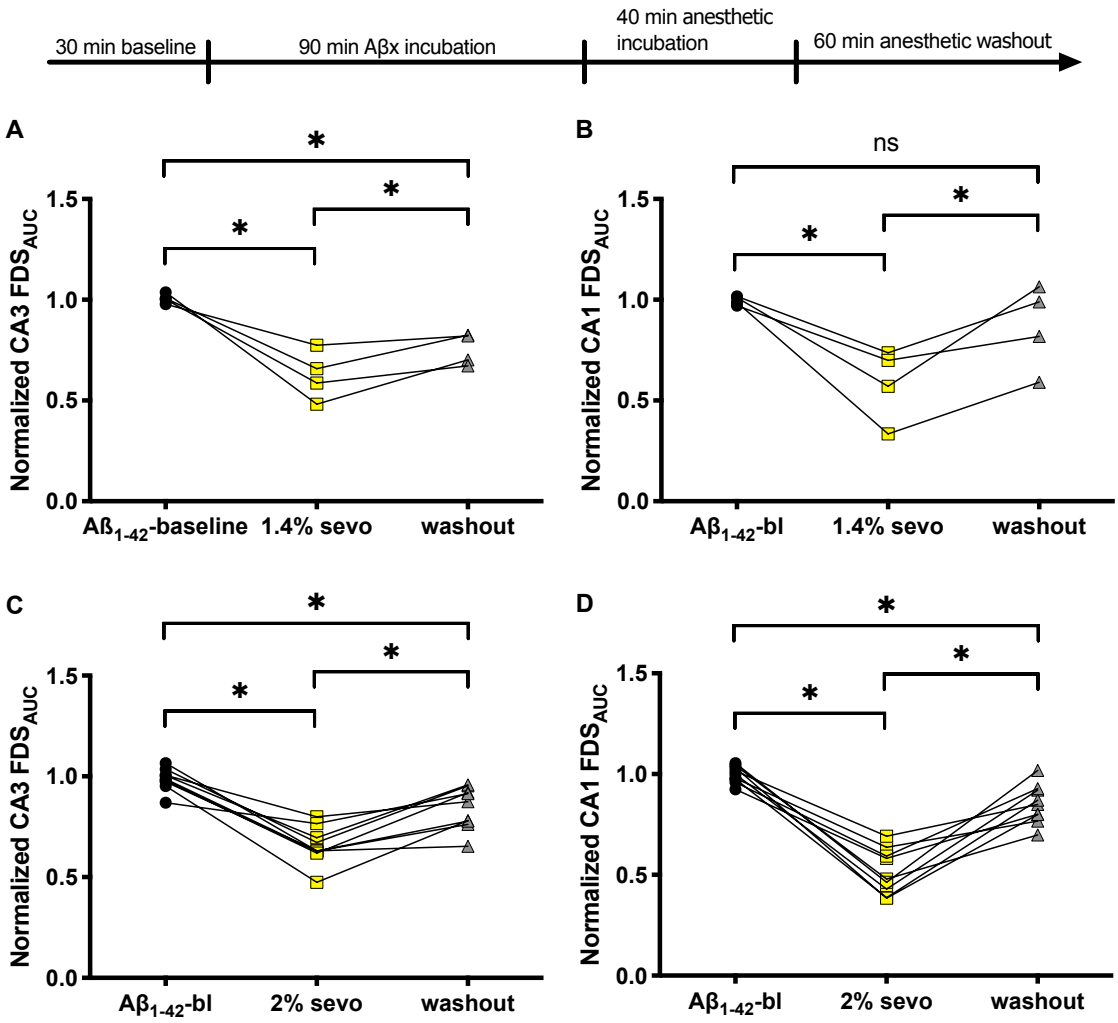

Fig. 46: Effect on neuronal activity and washout of 2% sevoflurane in the presence of $A\beta_{1-42}$. A + B: 1.4% sevoflurane decreased the neuronal activity in the CA1 (p= 0.0169, n= 4) and in the CA3 region (p= 0.0004) significantly. The activity did not recover in the CA3 region (p= 0.0075) but only in the CA1 region (p= 0.8414) after a washout of 60 min. **C + D:** 2% sevoflurane decreased the neuronal activity in the CA1 (p= < 0.0001, n= 9) and in the CA3 region (p= < 0.0001) significantly. The activity did not recover in the CA1 region (p= 0.0054) and in the CA3 region (p= 0.0063) after a washout of 60 min.

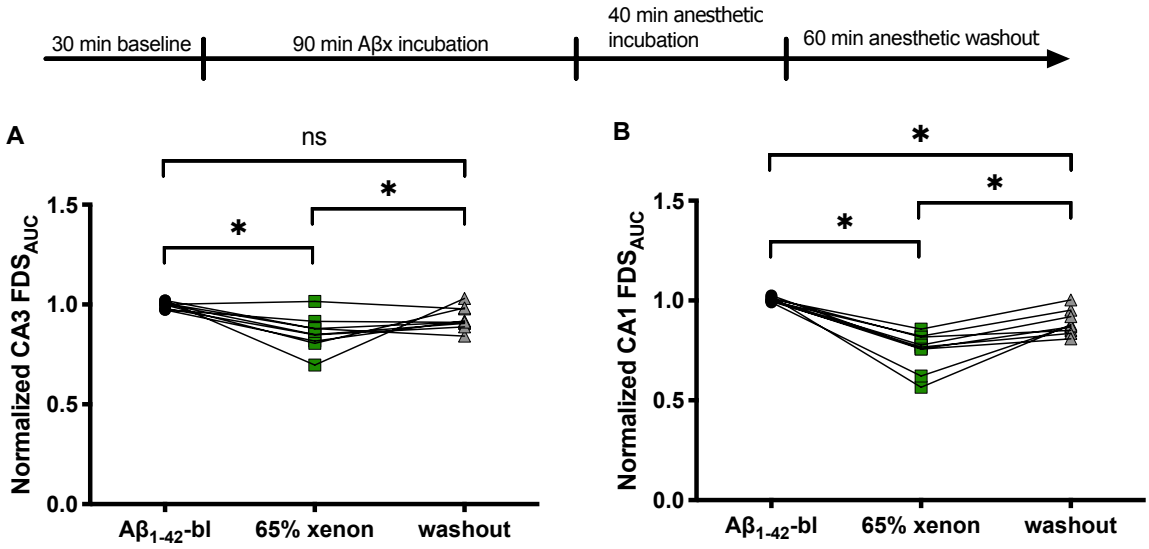

Fig. 47: Effect on neuronal activity and washout of 65% xenon in the presence of Aβ$_{1-42}$. 65% xenon decreased the neuronal activity in the CA1 (p= < 0.0001, n= 9) and in the CA3 region (p= < 0.0001, n= 9) significantly. The activity did not recover in the CA1 region (B; p= 0.0025), but only in the CA3 region (A; p= 0.0800) back to baseline levels after a washout of 60 min.

5.3.4.2 Aβ$_{1-40}$

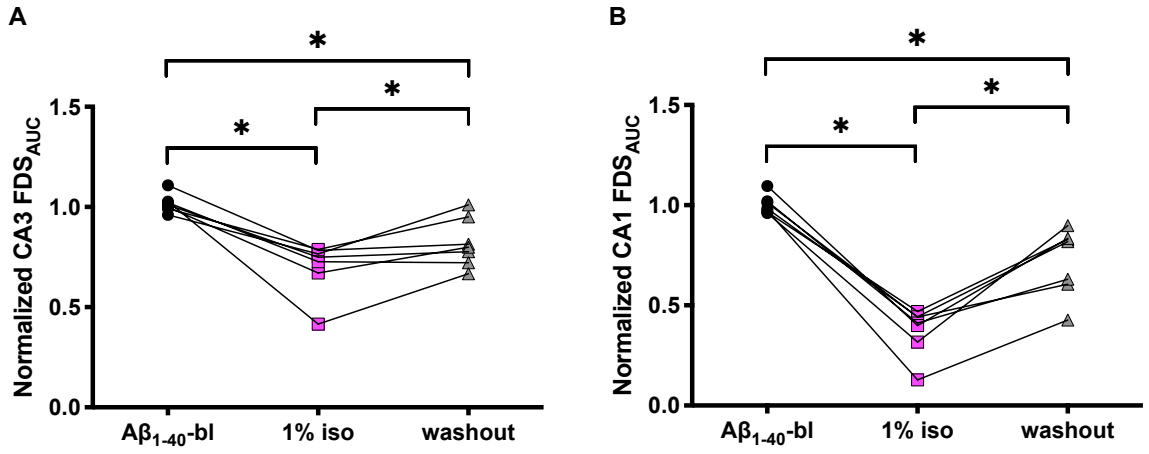

Fig. 48: Effect on neuronal activity and washout of 1% isoflurane in the presence of Aβ$_{1-40}$. A + B: 1% isoflurane decreased the neuronal activity in the CA1 (p= < 0.0001, n= 7) and in the CA3 region (p= < 0.0001) significantly. The activity did not recover in the CA1 region (p= 0.0014) and in the CA3 region (p= 0.0086) back to baseline levels after a washout of 60 min.

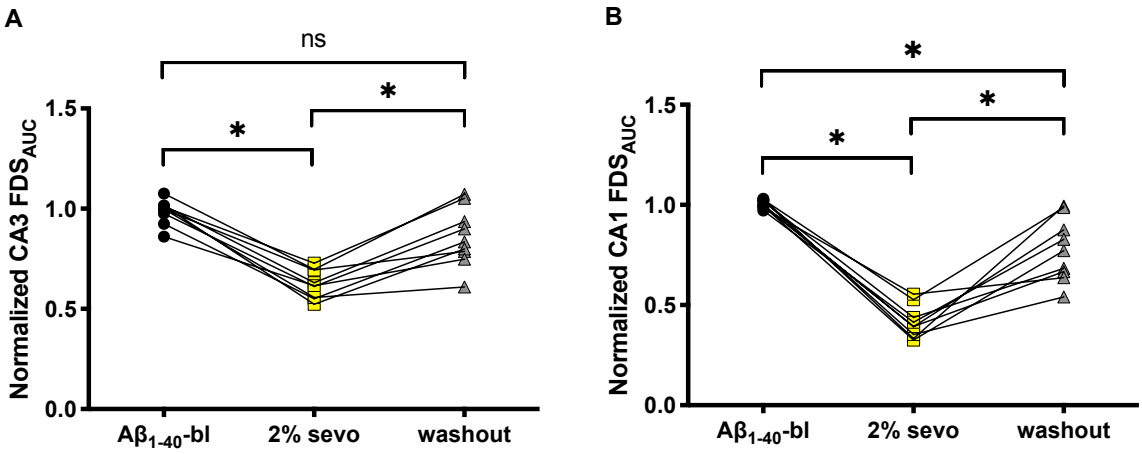

Fig. 49: Effect on neuronal activity and washout of 2% sevoflurane in the presence of Aβ$_{1-40}$. A + B: 2% sevoflurane decreased the neuronal activity in the CA1 (p= < 0.0001, n= 9) and in the CA3 region (p= 0.0002) significantly. The activity did not recover in the CA1 region (p= 0.0003), but only in the CA3 region (p= 0.0895) back to baseline levels after a washout of 60 min.

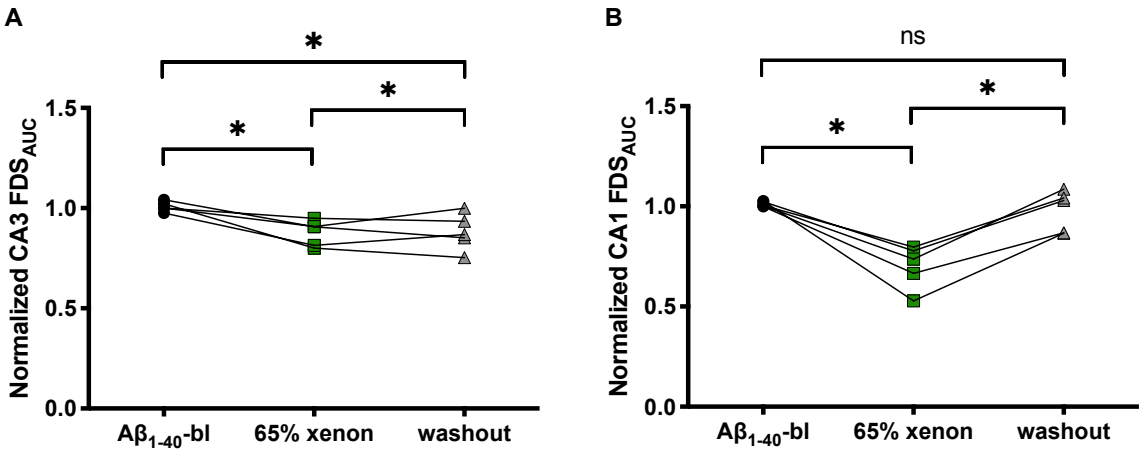

Fig. 50: Effect on neuronal activity and washout of 65% xenon in the presence of Aβ$_{1-40}$. A + B: 65% xenon decreased the neuronal activity in the CA1 (p= 0.0003, n= 5) and in the CA3 region (p= 0.0261) significantly). The activity did not recover in the CA3 region (p= 0.0330), but only in the CA1 region (p= > 0.9999) back to baseline levels after a washout of 60 min.

5.3.4.3 AβpE3

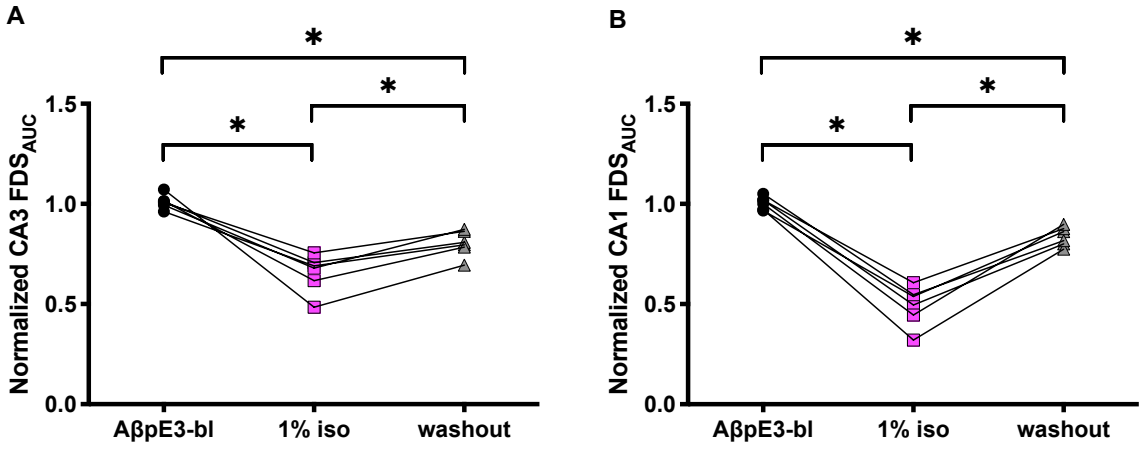

Fig. 51: Effect on neuronal activity and washout of 1% isoflurane in the presence of AβpE3. A + B: 1% isoflurane decreased the neuronal activity in the CA1 (p= < 0.0001, n= 6) and in the CA3 region (p= < 0.0001) significantly. The activity did not recover in the CA1 region (p= 0.0017) and in the CA3 region (p= 0.0004) back to baseline levels after a washout of 60 min.

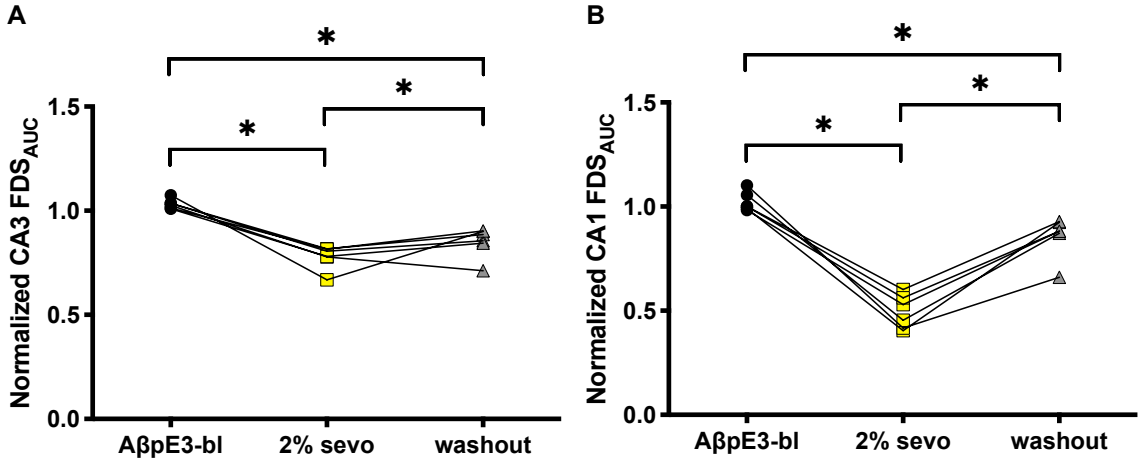

Fig. 52: Effect on neuronal activity and washout of 2% sevoflurane in the presence of AβpE3. A + B: 2% sevoflurane decreased the neuronal activity in the CA1 (p= < 0.0001, n= 6) and in the CA3 region (p= < 0.0001) significantly. The activity did not recover in the CA1 region (p= 0.0079) and in the CA3 region (p= 0.0001) back to baseline levels after a washout of 60 min.

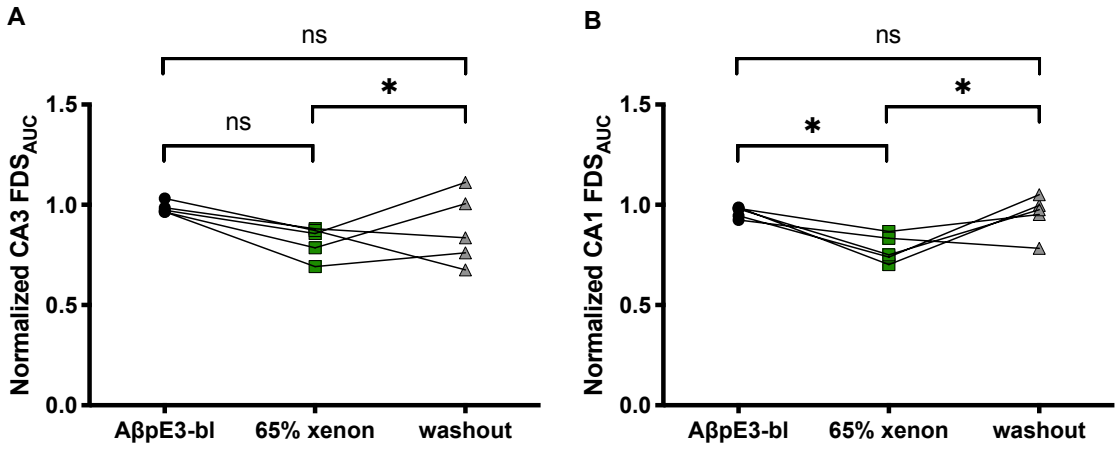

Fig. 53: Effect on neuronal activity and washout of 65% xenon in the presence of AβpE3. A + B: 65% xenon decreased the neuronal activity in the CA1 (p= 0.0048, n= 5) but not in the CA3 region (p= 0.1172) significantly. The activity in the CA3 (p= 0.4941) and in the CA1 region (p= >0.9999) recovered back to baseline levels after a washout of 60 min.

5.3.4.2 3NTyrAβ

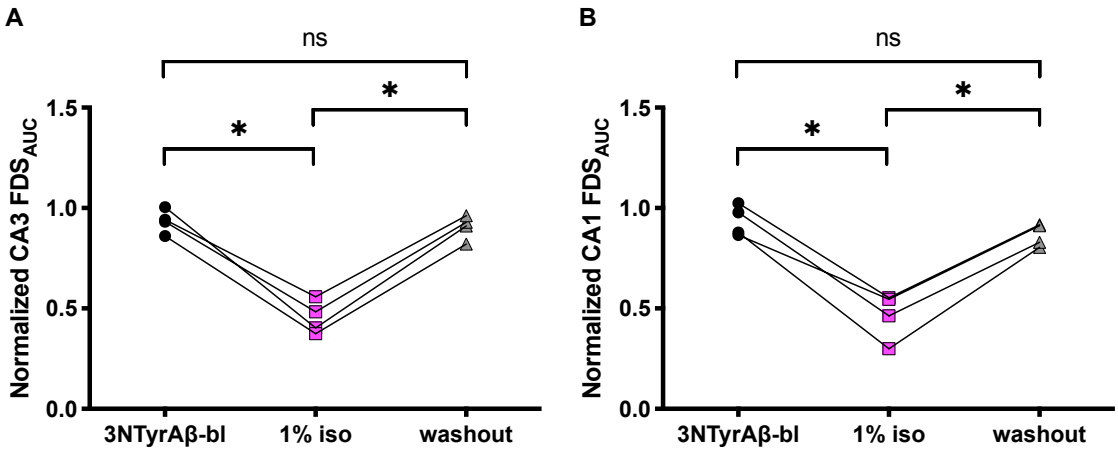

Fig. 54: Effect on neuronal activity and washout of 1% isoflurane in the presence of 3NTyrAβ. 1% isoflurane decreased the neuronal activity in the CA1 (p= 0.0001, n= 4) and in the CA3 region (p= < 0.0001) significantly. The activity in the CA1 region (p= 0.8437) and in the CA3 region (p= > 0.9999) recovered back to baseline levels after a washout of 60 min.

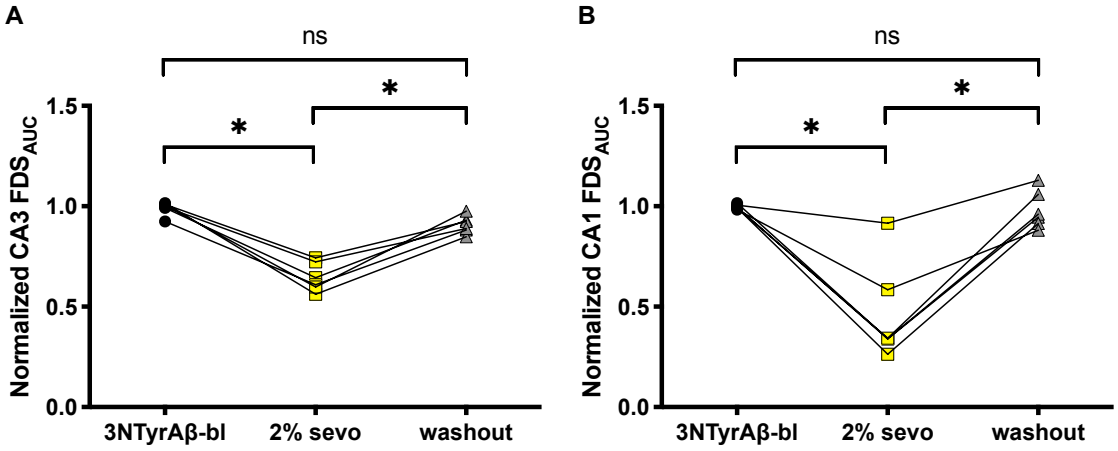

Fig. 55: Effect on neuronal activity and washout of 2% sevoflurane in the presence of 3NTyrAβ. 2% sevoflurane decreased the neuronal activity in the CA1 (p= < 0.0001, n= 6) and in the CA3 region (p= < 0.0001) significantly. The activity in the CA1 region (p= > 0.9999) and in the CA3 region (p= 0.0507) recovered back to baseline levels after a washout of 60 min.

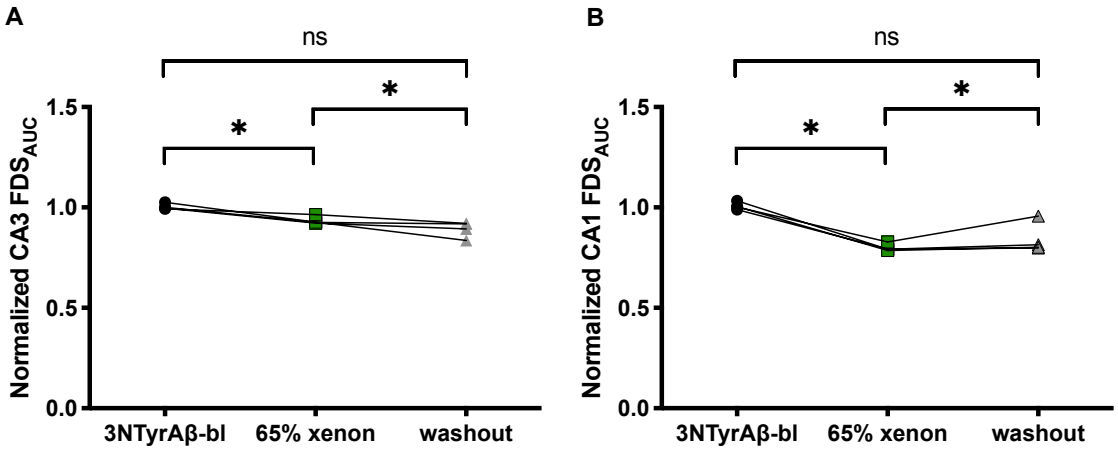

Fig. 56: Effect on neuronal activity and washout of 65% xenon in the presence of 3NTyrAβ. 65% sevoflurane decreased the neuronal activity in the CA1 (p= 0.0004, n= 4) and in the CA3 region (p= 0.0158) significantly. The activity in the CA1 region (p= 0.0023) and in the CA3 region (p= 0.0007) recovered back to baseline levels after a washout of 60 min.

5.4 Field excitatory postsynaptic potentials (fEPSPs)

5.4.1 AβpE3 and 3NTyrAβ prevent CA1-LTP

In my experiments, fEPSPs in the CA1 were significantly potentiated after HFS to 134% [121% 173%] and 125% [119% 190%] under control conditions, respectively. A physiological concentration of 50 nM AβpE3 significantly (p= 0.0312, n= 6), reduced CA1 LTP to 109% [66% 131%] after an oligomerization period of 90 min. Also, the incubation of 3NTyrAβ significantly (p= 0.0156, n= 7) reduced LTP to 106% [79% 112%] (Fig. 57 A + B).

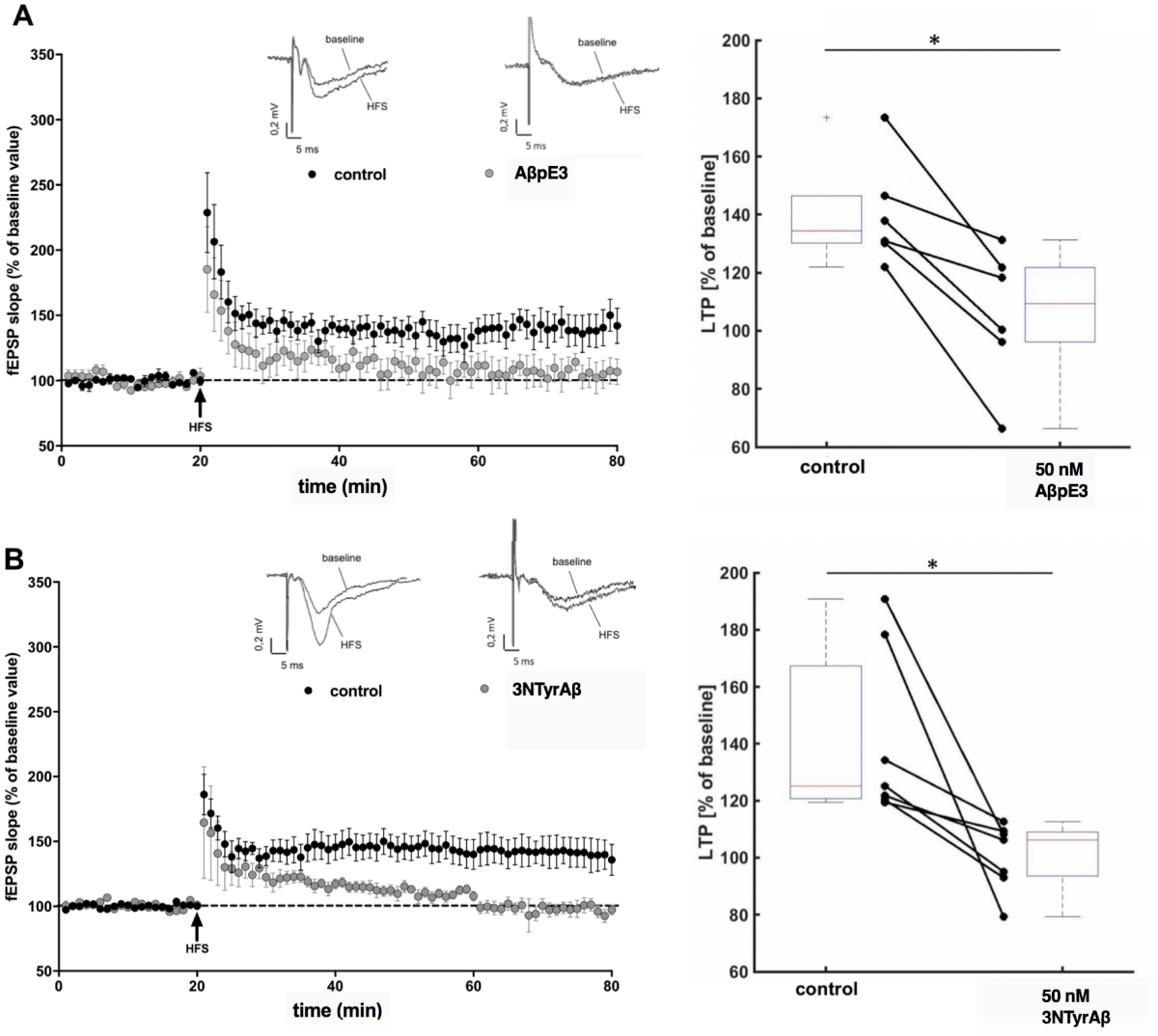

Fig. 57: AβpE3 and 3NTyrAβ prevent CA1-LTP. A: High frequency stimulation (HFS) triggered LTP (n= 6) as control (black circels). Incubation of AβpE3 (grey circles, n= 6) or **B:** 3NTyrAβ (grey circles, n= 7) before induction of HFS significantly reduced CA1-LTP. Circles represent the average field excitatory postsynaptic potential (fEPSP) slopes (mean ± SEM) that were normalized to the 10 min baseline period right before LTP stimulation at every minute. Representative fEPSP traces are indicated by insets above graph. **C:** CA1 LTP was significantly reduced by AβpE3 (p= 0.0312) from 134% [121% 173%] to 109% [66% 131%]. CA1 LTP was significantly reduced by 3NTyrAβ (p= 0.0156) from 125% [120% 190%] to 106% [79% 112%].

5.4.2 Xenon restores only pyroglutamate-Aβ-induced blockade of LTP

Previously, Bürge, Kratzer et al. (2019) showed that the blockage of hippocampal CA1-LTP after incubation with 100 nM $A\beta_{1-42}$, but not $A\beta_{1-40}$, could be reversed by the application of 30% xenon. They also showed that 30% *per se* does not interfere with the formation of CA1-LTP after HFS. To expand this study, I chose the same experimental setup and tested the effects of the physiological concentration 50 nM AβpE3 and 3NTyrAβ and their combination with 30% xenon mixed with 35% N_2, 30% O_2, 5% CO_2 plus a gas mix of 65% N_2, 30% O_2 and 5% CO_2. To ensure a stable pH, I measured the pH regularly. It stayed between 7.3-7.4 throughout the experiments.

After incubation of both Aβ species for 90 min, hippocampal CA1-LTP was significantly reduced (AβpE3: 104% [94% 108%], 3NTyrAβ: 107% [90% 115%]. The application of 30% xenon for 30 min directly after 90 min incubation of Aβ reversed the synaptotoxic effects on LTP of AβpE3 to 124 % [111 % 139 %]. The blockage of CA1-LTP by 3NTyrAβ could not be reversed (96 % [72 % 139 %] (Fig. 58 A + B).

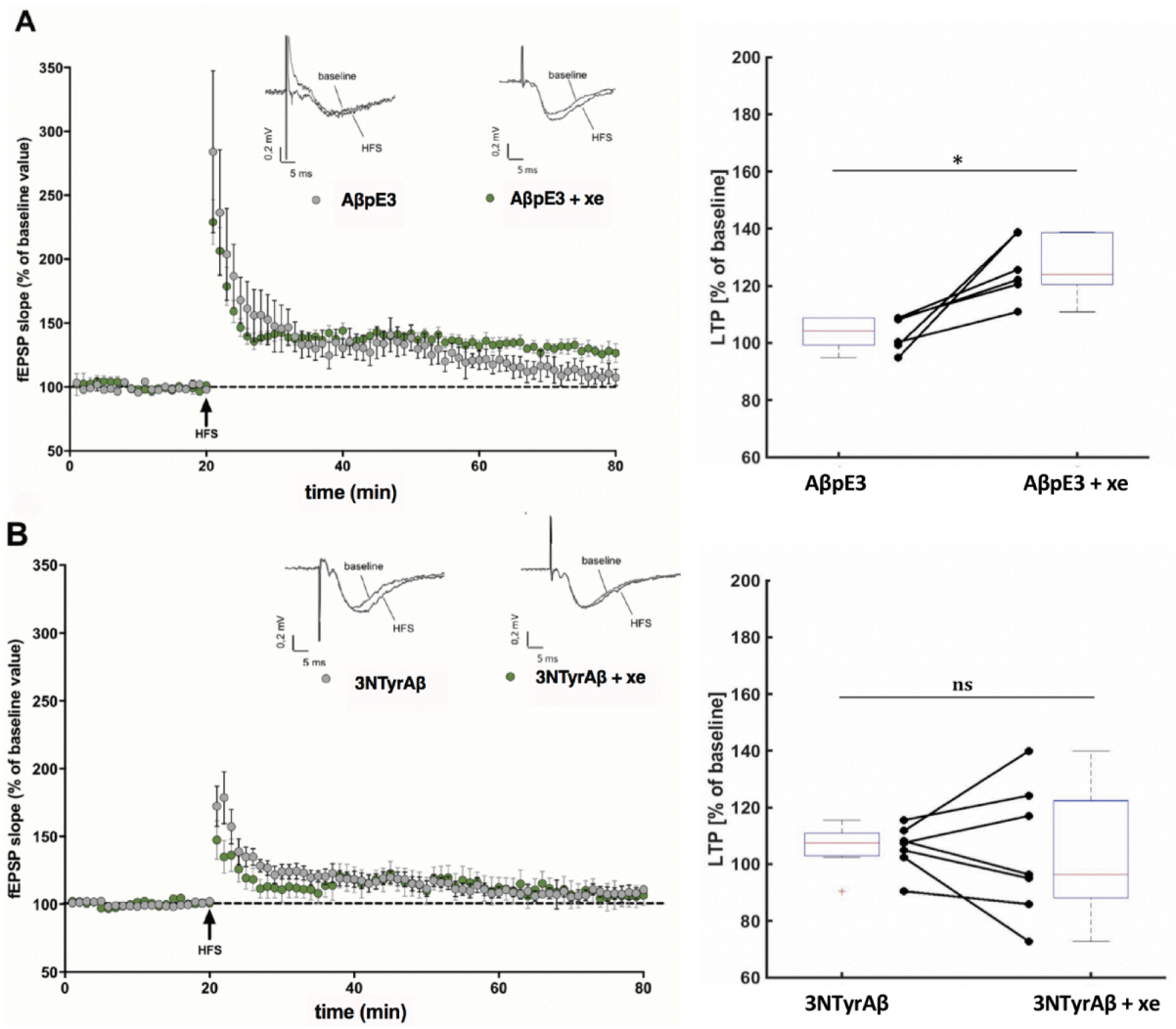

Fig. 58: 30% xenon restores only AβpE3-induced LTP blockade. A: Inbucation of AβpE3 (grey circles, n= 7, 104% [94% 108%]) and **B:** 3NTyrAβ (grey circles, n= 7, 107 % [90% 115%]) before HFS induction significantly reduced LTP. Circles represent the average field excitatory postsynaptic potential (fEPSP) slopes (mean ± SEM) that were normalized to the 10 min baseline period right before LTP stimulation at every minute. Representative fEPSP traces are indicated by insets above graph. **C:** 30% xenon significantly restored the LTP blockage by AβpE3 (p= 0.0312) to 124% [111% 139%], whereas the LTP in slices treated with 3NTyrAβ could not be restored (p= 0.4285, 96% [72% 139%]).

5.5 Dendritic Spine density

The application of 50 nM $A\beta_{1-42}$, in combination with or without N_2, significantly decreased spine density in the CA1 region of the murine hippocampus (Fig. 59 A-C, p= 0.0275). The addition of 1% isoflurane did not influence this neurotoxic effect of $A\beta_{1-42}$ (p= 0.0125), whereas 2% sevoflurane restored the decrease in spine density significantly, resulting in no significant difference to the number of spines in control experiments (p= 0.1888) (Fig. 59 A + B).

The application of 65% xenon + N_2 lead to a significant increase in dendritic spines in the presence of $A\beta_{1-42}$ compared to control experiments (p= 0.035) (Fig. 59 A + B).

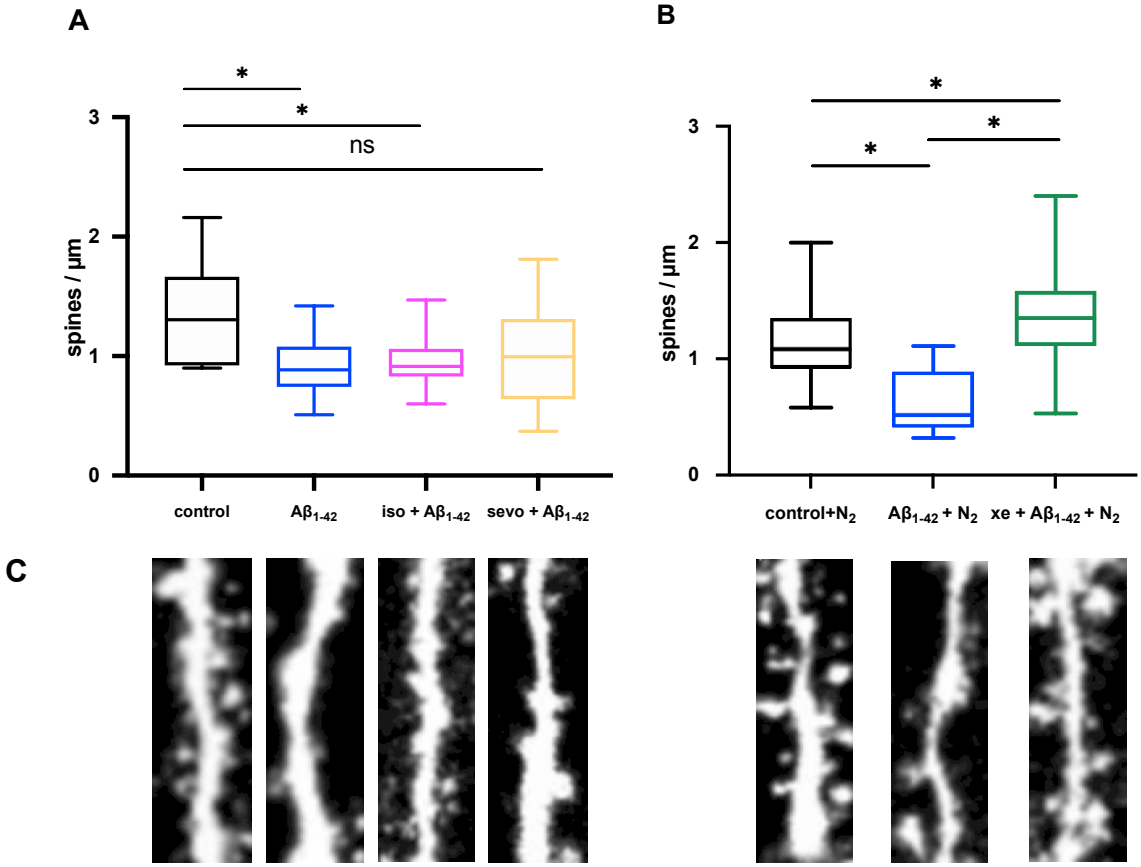

Fig. 59: Xenon and sevoflurane restore $A\beta_{1-42}$-induced spine density attenuation. A: Incubation of $A\beta_{1-42}$ reduced spine density significantly (control: 1.30 ± 0.5 spines/µm, n= 6, $A\beta_{1-42}$: 0.89 ± 0.3 spines/µm, n= 22, p= 0.0275). The number of spines decreased numerically in the presence of 2% sevo plus $A\beta_{1-42}$ (sevo + $A\beta_{1-42}$: 0.92 ± 0.21 spines/µm, n= 10, p= 0.1888) but the mean was not statistically different when compared to control. The application of 1% iso did not change the toxic effect of $A\beta_{1-42}$ on spines (iso + $A\beta_{1-42}$: 0.99 ± 0.44 spines/µm, n= 60, p= 0.0125). **B:** Reduction of spines by synaptic toxicity through $A\beta_{1-42}$ was significantly restored by application of 65% xe (control: 1.08 ± 0.31, n = 35, $A\beta_{1-42}$: 0.51 ± 0.21 spines/µm, n= 4, $A\beta_{1-42}$ + xe: 1.35 ± 0.35 spines/µm, n= 42, p= 0.035). Whiskers show minimum and maximum values. **C:** Exemplary microscopic representation of dendrites.

5.6 Autophagy protein expression is not changed by inhalational anesthetics

I investigated the expression of several different proteins that are important for the normal function of autophagy by Western Blotting. The results are presented as the mean ± SEM and represent the relative intensity of the protein bands as the expression of the different proteins.

5.6.1 ULK1 and pULK1

In my experiments, I did not find any significant changes in the expression levels of ULK1 in the hippocampus of WT mice treated with $A\beta_{1-42}$ and 1% isoflurane (p= 0.1147), 2% sevoflurane (p= 0.5060) and 65% xenon (p= 0.8925) alone or in combination (Fig. 60-62). Also, the expression of phosphorylated ULK1 (pULK1) did not change (iso: p= 0.0661; sevo: p= 0.2905; xenon: p= 0.4528).

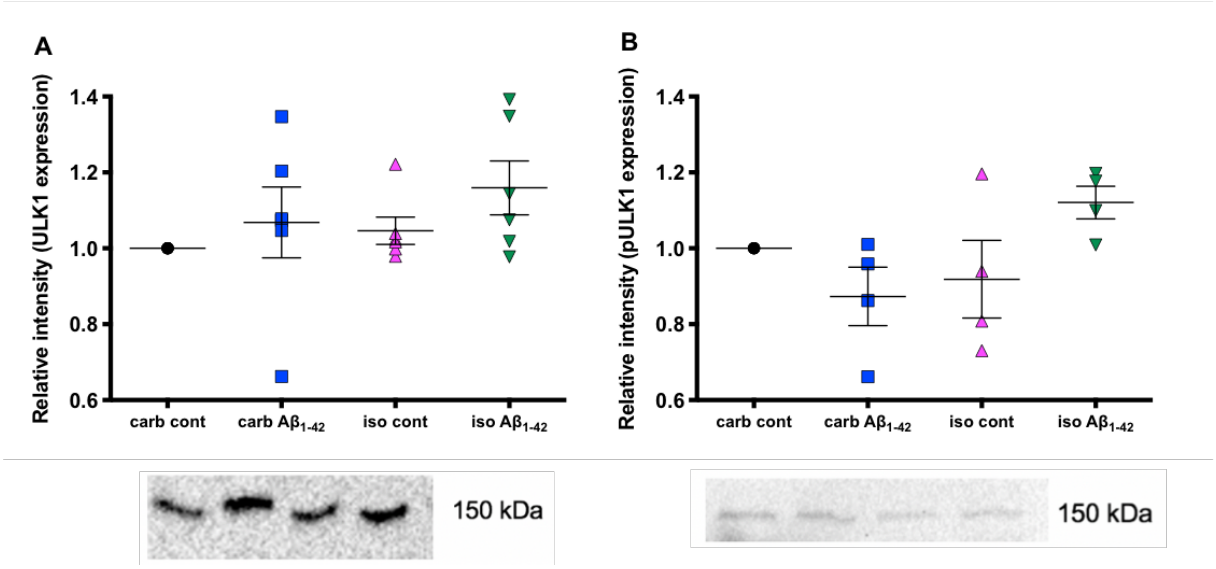

Fig. 60: Isoflurane did not change ULK1 and pULK1 expression. A + B: Intensities of the protein bands were normalized to the median of the control group (carb cont= carbogen control). The application of $A\beta_{1-42}$, 1% isoflurane (iso) and the combination of both did not change the expression of ULK1 (p= 0.1147, n= 6). **B:** The application of $A\beta_{1-42}$, 1% iso and the combination of both did not change the expression of pULK1 (p= 0.0661, n= 6). Lines represent the mean ± SEM. Bottom: Exemplary presentation of ULK1 protein bands**.** ULK1 shows a protein band at 150 kDa.

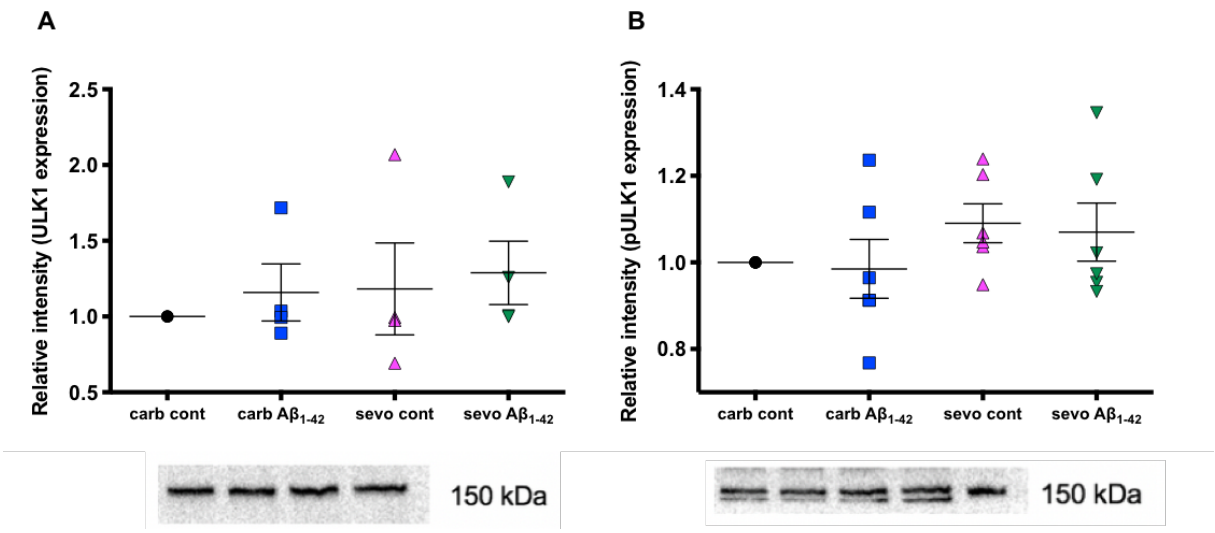

Fig. 61: Sevoflurane did not change ULK1 and pULK1 expression. A + B: Intensities of the protein bands were normalized to the median of the control group (carb cont= carbogen control). The application of $A\beta_{1-42}$, 2% sevoflurane (sevo) and the combination of both did not change the expression of ULK1 (p= 0.5060, n= 6). **B:** The application of $A\beta_{1-42}$, 2% sevo and the combination of both did not change the expression of pULK1 (p= 0.2905, n= 6). Lines represent the mean ± SEM. Bottom: Exemplary presentation of pULK1 protein bands**.** pULK1 shows a protein band at 150 kDa.

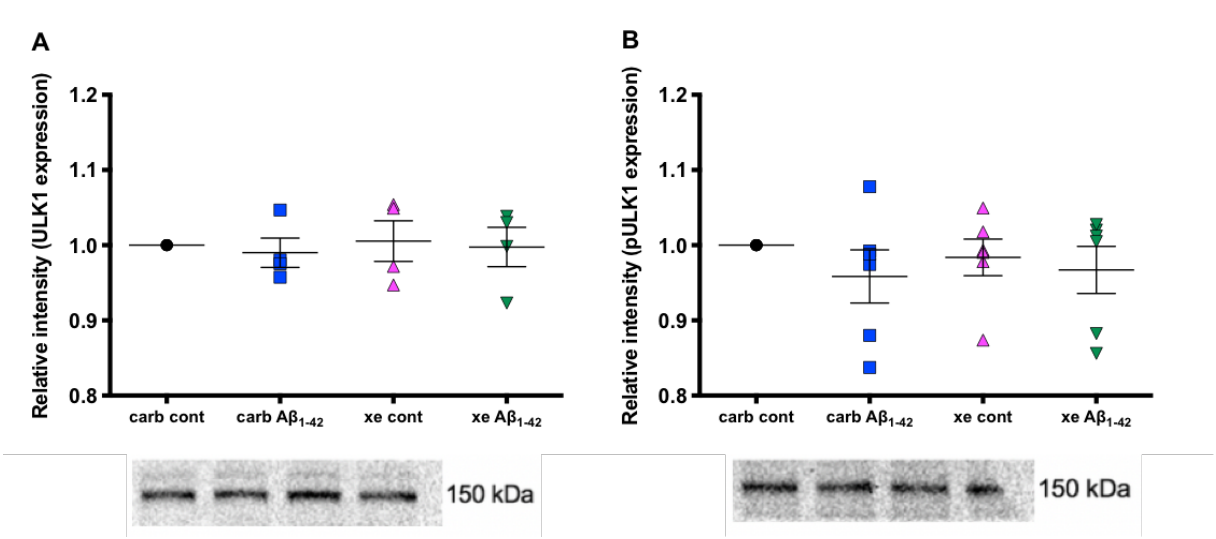

Fig. 62: Xenon did not change ULK1 and pULK1 expression. A + B: Intensities of the protein bands were normalized to the median of the control group (carb cont= carbogen control). The application of $A\beta_{1-42}$, 65% xenon (xe) and the combination of both did not change the expression of ULK1 (p= 0.8925, n= 6) and pULK1 (p= 0.4528, n= 6). Lines represent the mean ± SEM. Bottom: Exemplary presentation of pULK1 protein bands at 150 kDa.

5.6.2 p62/SQSTM1

I did not find any significant changes in the expression levels of p62 in the hippocampus of WT mice treated with $A\beta_{1-42}$ and anesthetics (65% xenon (p= 0.6618), 2% sevoflurane (p= 0.4400), 1% isoflurane (p= 0.7616)) alone or in combination (Fig. 63).

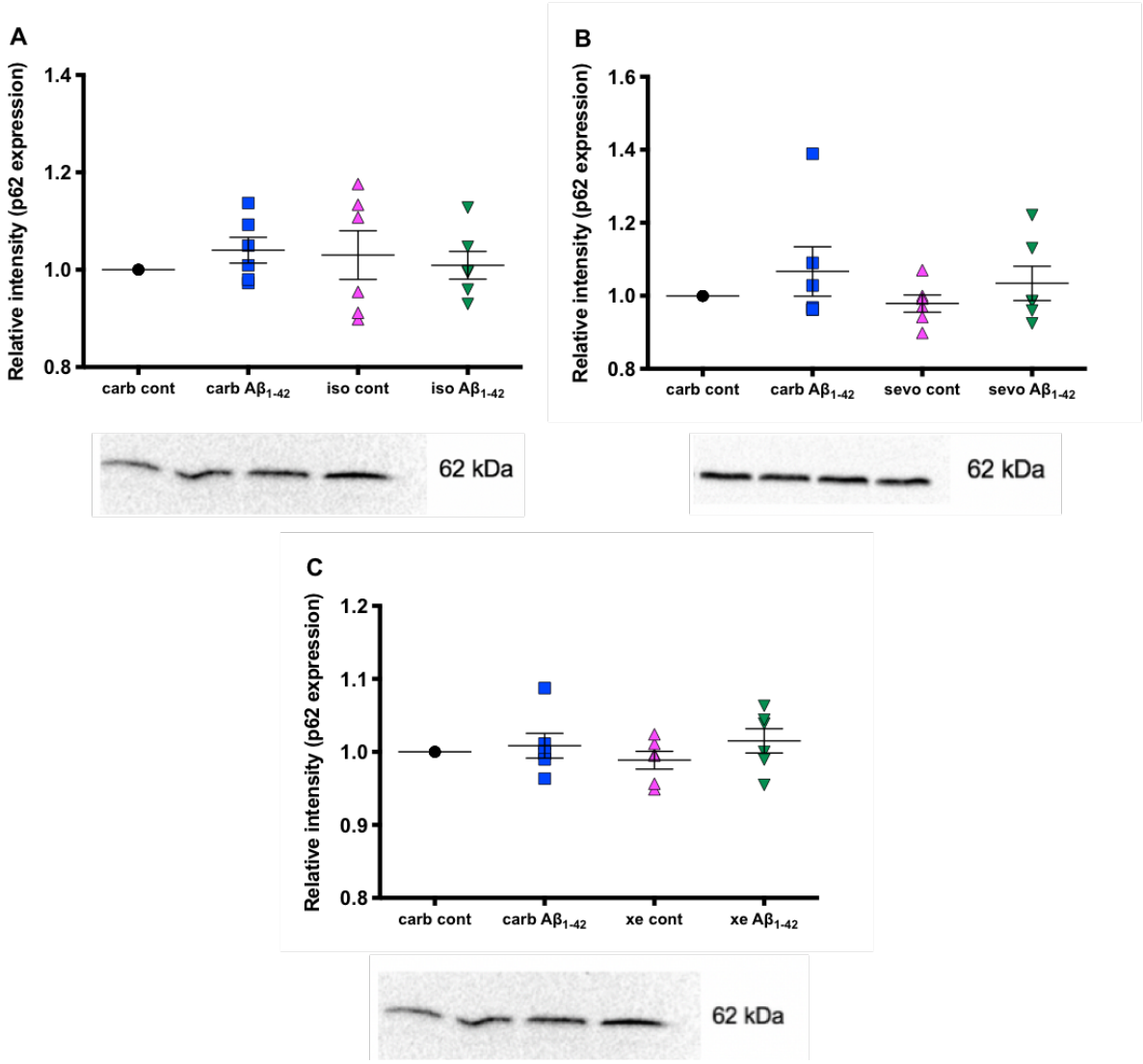

Fig. 63: Isoflurane, sevoflurane and xenon did not change p62 expression. A-C: Intensities of the protein bands were normalized to the median of the control group (carb cont= carbogen control). The application of $A\beta_{1-42}$, 1% isoflurane (iso), 2% sevoflurane (sevo) and 65% xenon (xe) and the combinations did not change the expression of p62 (iso: p= 0.7616, n= 6; sevo: p= 0.4400, n= 6; xe: p= 0.6618, n= 6). Lines represent the mean ± SEM. Bottom: Exemplary presentation of p62 protein bands at 62 kDa.

5.6.3 Beclin-1

I did not find any significant changes in the expression levels of Beclin-1 in the hippocampus of WT mice treated with $A\beta_{1-42}$ and anesthetics (65% xenon (p= 0.7486), 2% sevoflurane (p= 0.8833), 1% isoflurane (p=0.1493)) alone or in combination (Fig. 64).

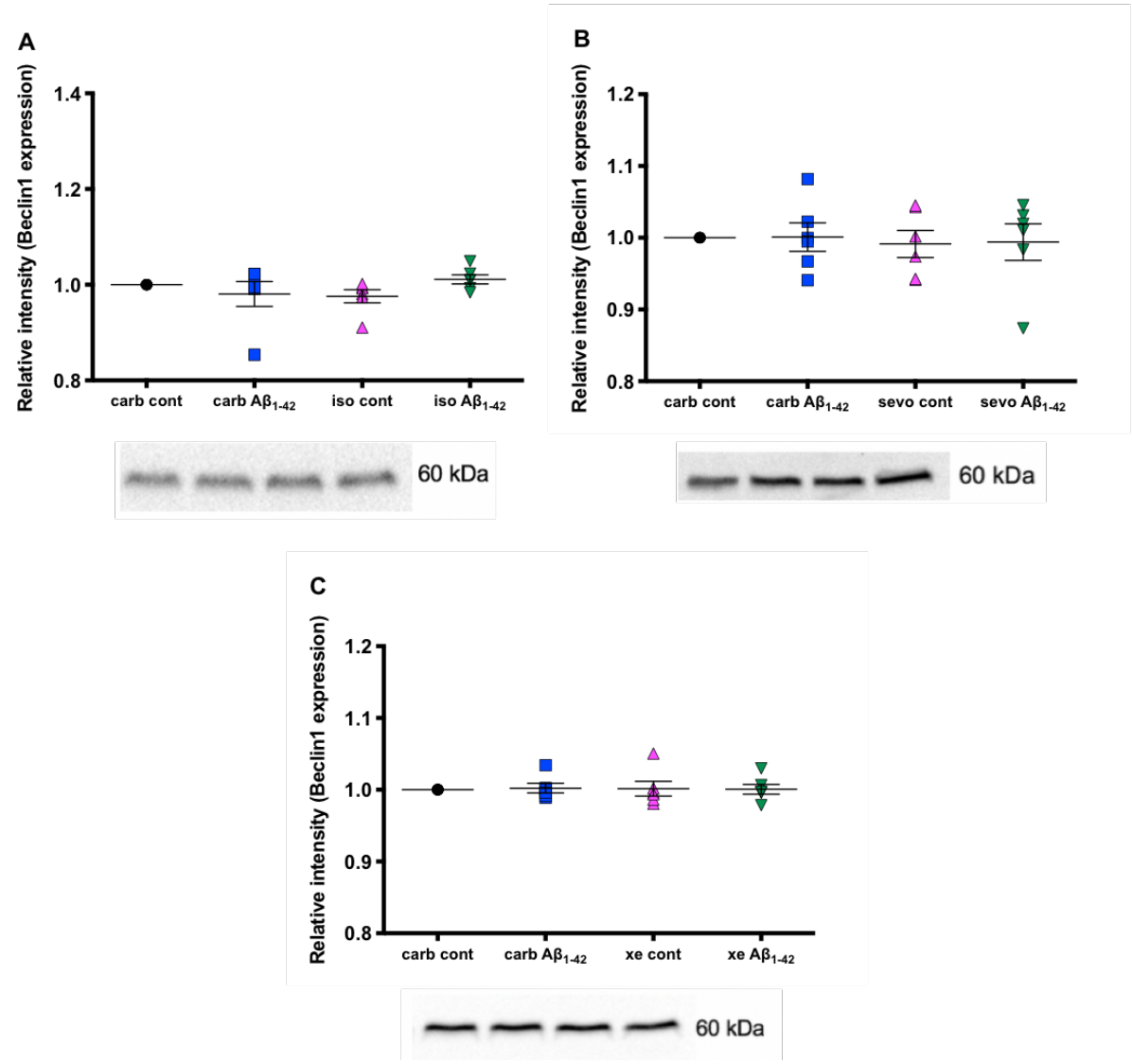

Fig. 64: Isoflurane, sevoflurane and xenon did not change Beclin1 expression. A-C: Intensities of the protein bands were normalized to the median of the control group (carb cont= carbogen control). The application of $A\beta_{1-42}$, 1% isoflurane (iso), 2% sevoflurane (sevo) and 65% xenon (xe) and the combination of both did not change the expression of Beclin-1 (iso: p= 0.1493, n= 6; sevo: p= 0.8833, n= 6; xe: p= 0.7486, n= 6). Lines represent the mean ± SEM. Bottom: Exemplary presentation of Beclin-1 protein bands at 60 kDa.

5.6.4 Atg12

I did not find any significant changes in the expression levels of Atg12 in the hippocampus of WT mice treated with $A\beta_{1-42}$ and anesthetics (65% xenon (p= 0.9500), 2% sevoflurane (p= 0.6800), 1% isoflurane (p= 0.1178)) alone or in combination (Fig. 65).

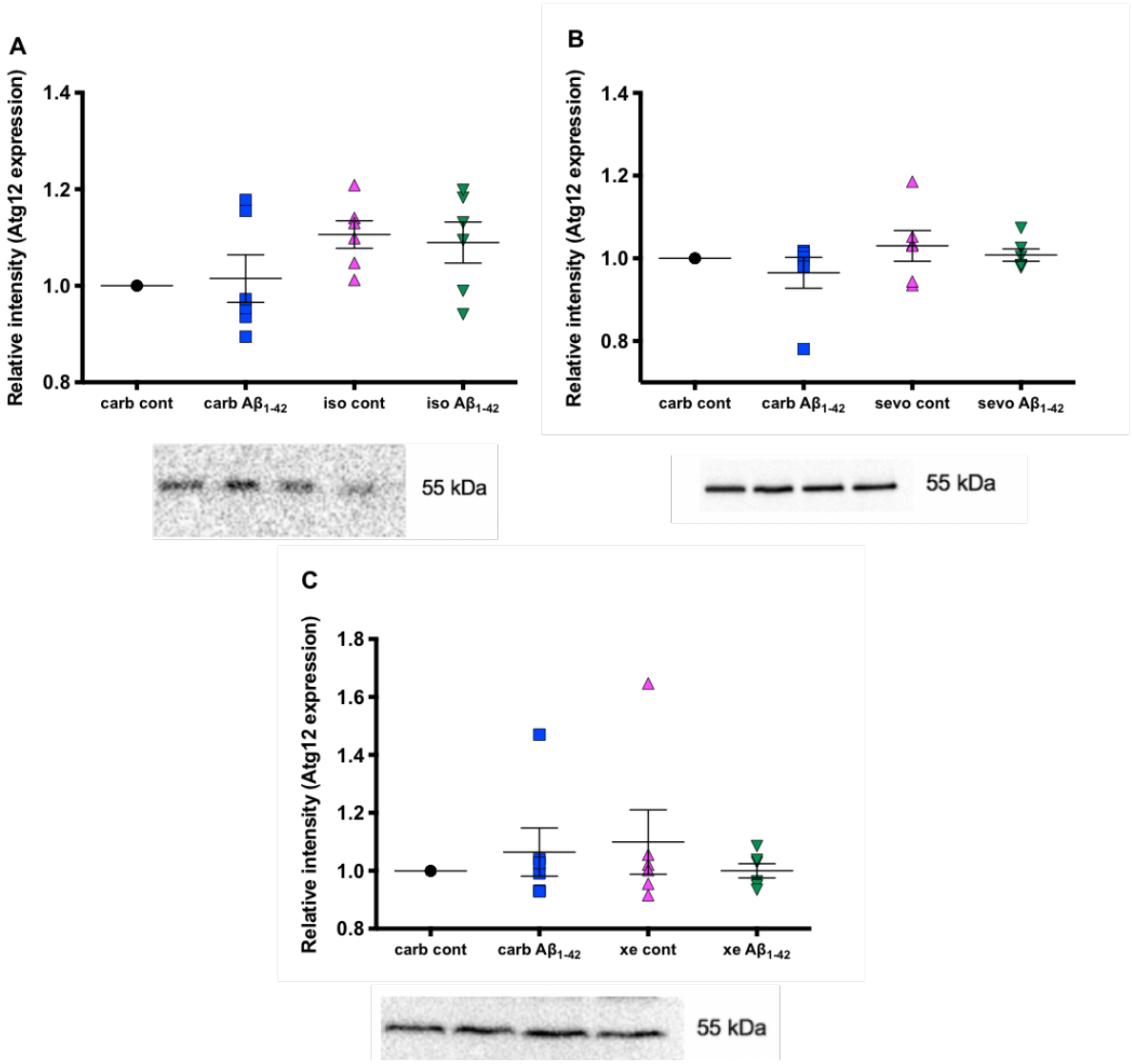

Fig. 65: Isoflurane, sevoflurane and xenon did not change Atg12 expression. A-C: Intensities of the protein bands were normalized to the median of the control group (carb cont= carbogen control). The application of $A\beta_{1-42}$, 1% isoflurane (iso), 2% sevoflurane (sevo) and 65% xenon (xe) and the combination of both did not change the expression of Atg12 (iso: p= 0.1178, n= 6; sevo: p= 0.6800, n= 6; xe: p= 0.9500, n= 6). Lines represent the mean ± SEM. Bottom: Exemplary presentation of Atg12 protein bands at 55 kDa.

5.6.5 PI3K Class III

I did not find any significant changes in the expression levels of PI3K Class III in the hippocampus of WT mice treated with $A\beta_{1-42}$ and anesthetics (65% xenon (p= 0.3155), 2% sevoflurane (p= 0.0734), 1% isoflurane (p=0.1360)) alone or in combination (Fig. 66).

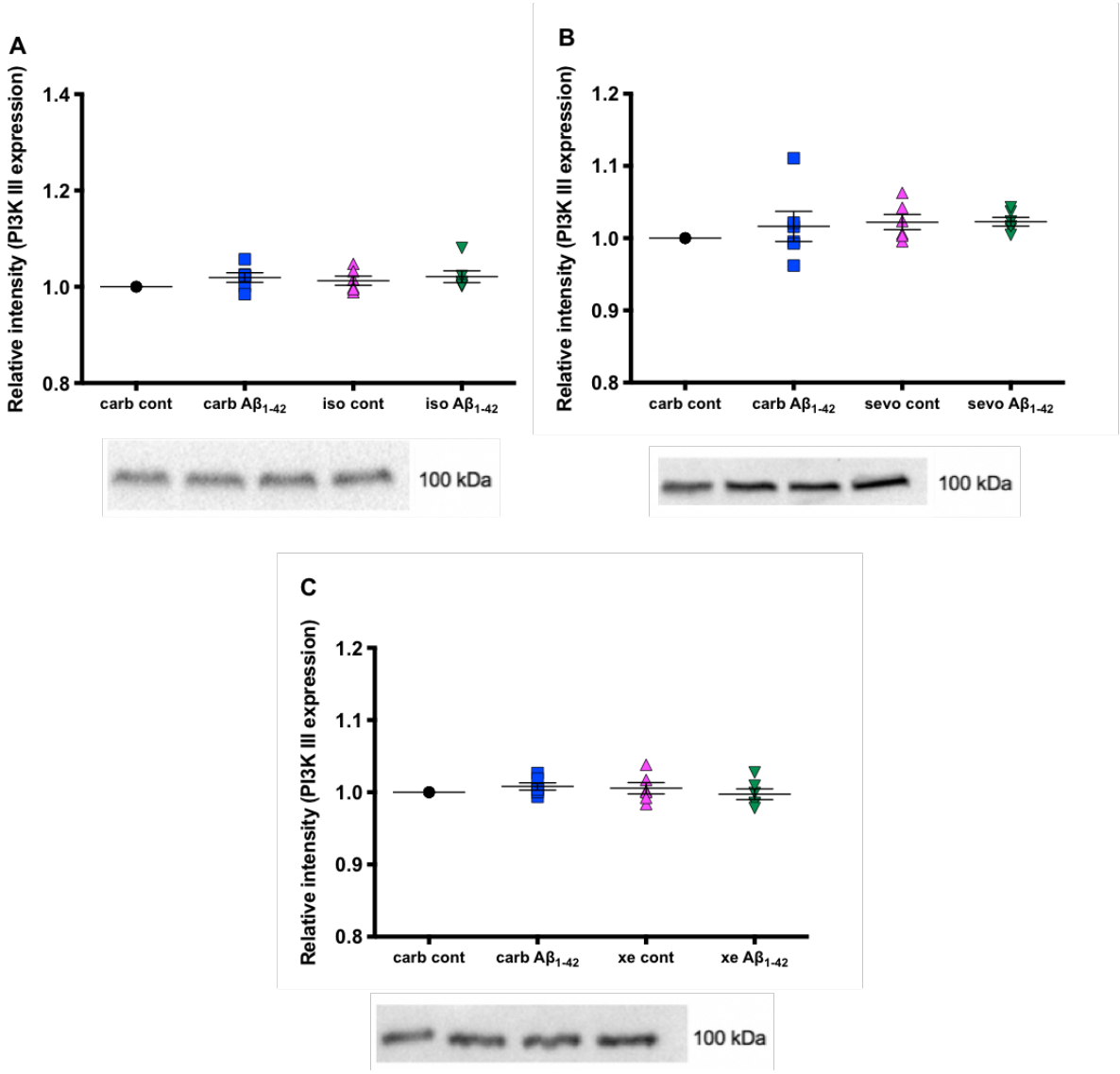

Fig. 66: Isoflurane, sevoflurane and xenon did not change PI3K III expression. A-C: Intensities of the protein bands were normalized to the median of the control group (carb cont= carbogen control). The application of $A\beta_{1-42}$, 1% isoflurane (iso), 2% sevoflurane (sevo) and 65% xenon (xe) and the combination of both did not change the expression of PI3K III (iso: p= 0.1360, n= 6; sevo: p= 0.0737, n= 6; xe: p= 0.3155, n= 6). Lines represent the mean ± SEM. Bottom: Exemplary presentation of PI3K III protein bands band at 100 kDa.

5.6.6 LC3B

I did not find any significant changes in the expression levels of LC3B in the hippocampus of WT mice treated with $A\beta_{1-42}$ and anesthetics (65% xenon (p= 0.4781), 2% sevoflurane (p= 0.2279), 1% isoflurane (p=0.1797)) alone or in combination (Fig. 67).

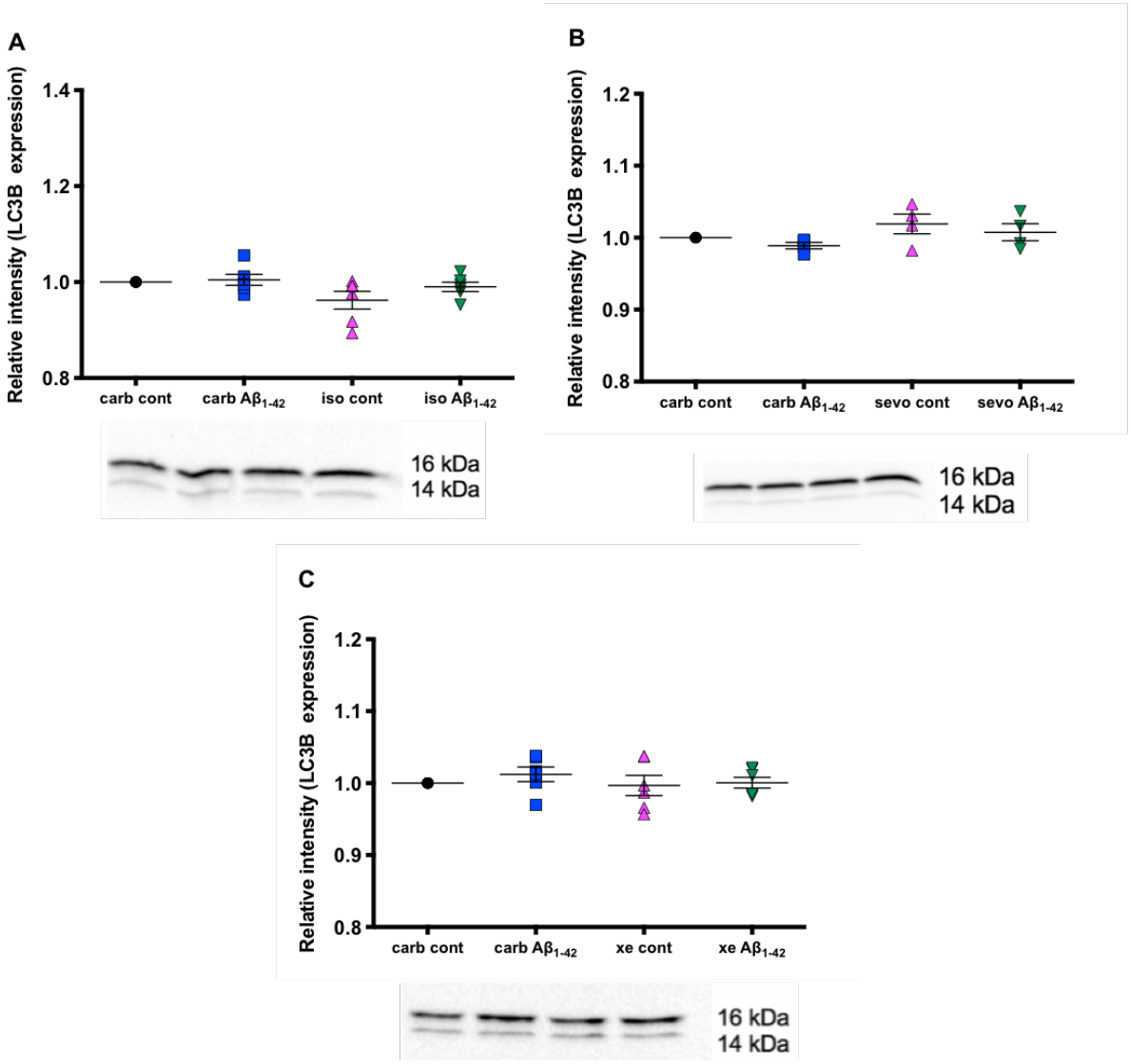

Fig. 67: Isoflurane, sevoflurane and xenon did not change LC3B expression. A-C: Intensities of the protein bands were normalized to the median of the control group (carb cont= carbogen control). The application of $A\beta_{1-42}$, 1% isoflurane (iso), 2% sevoflurane (sevo) and 65% xenon (xe) and the combination of both did not change the expression of LC3B (iso: p= 0.1797, n= 6; sevo: p= 0.2279, n= 6; xe: p= 0.4781, n= 6). Lines represent the mean ± SEM. Bottom: Exemplary presentation of LC3B protein bands at 16 and at 14 kDa.

5.6.7 Akt and pAkt

I did not find any significant changes in the expression levels of Akt in the hippocampus of WT mice treated with $A\beta_{1-42}$ and anesthetics (65% xenon (p= 0.9459); 2% sevoflurane (p= 0.2756); 1% isoflurane (p=0.1629)) alone or in combination. Also, the expression of pAkt did not change (iso: p= 0.5057; sevo: p= 0.8284; xenon: p= 0.2038) (Fig. 68-70).

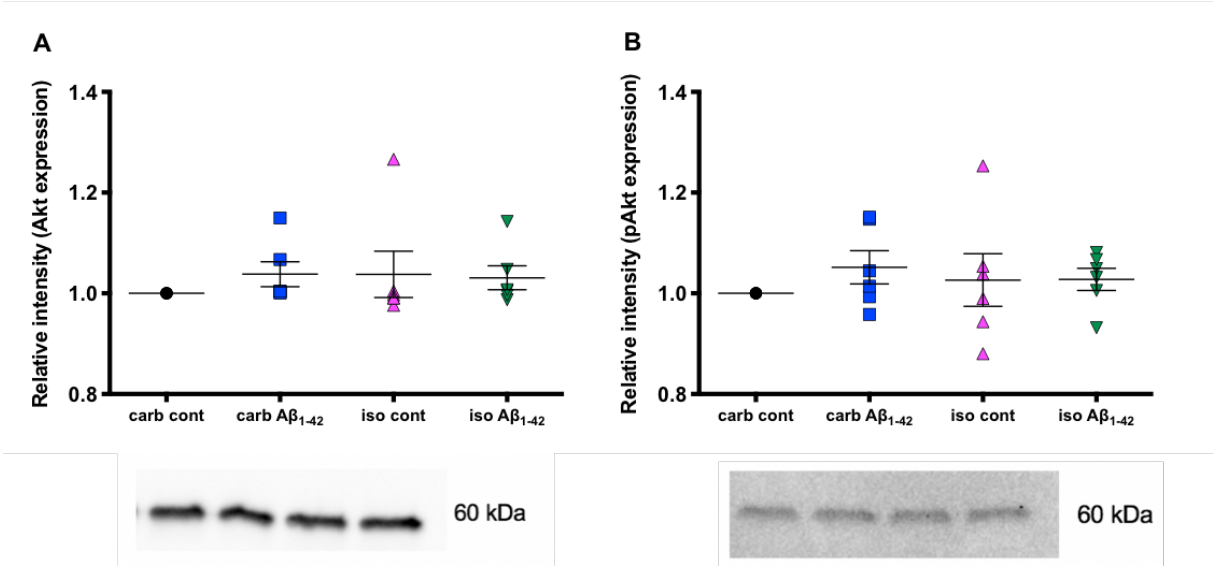

Fig. 68: Isoflurane did not change Akt and pAkt expression. A + B: Intensities of the protein bands were normalized to the median of the control group (carb cont= carbogen control). The application of $A\beta_{1-42}$, 1% isoflurane (iso) and the combination of both did not change the expression of Akt (p= 0.1629, n= 6) and pAkt (p= 0.5057, n= 6). Lines represent the mean ± SEM. Bottom: Exemplary presentation of pAkt protein bands at 60 kDa.

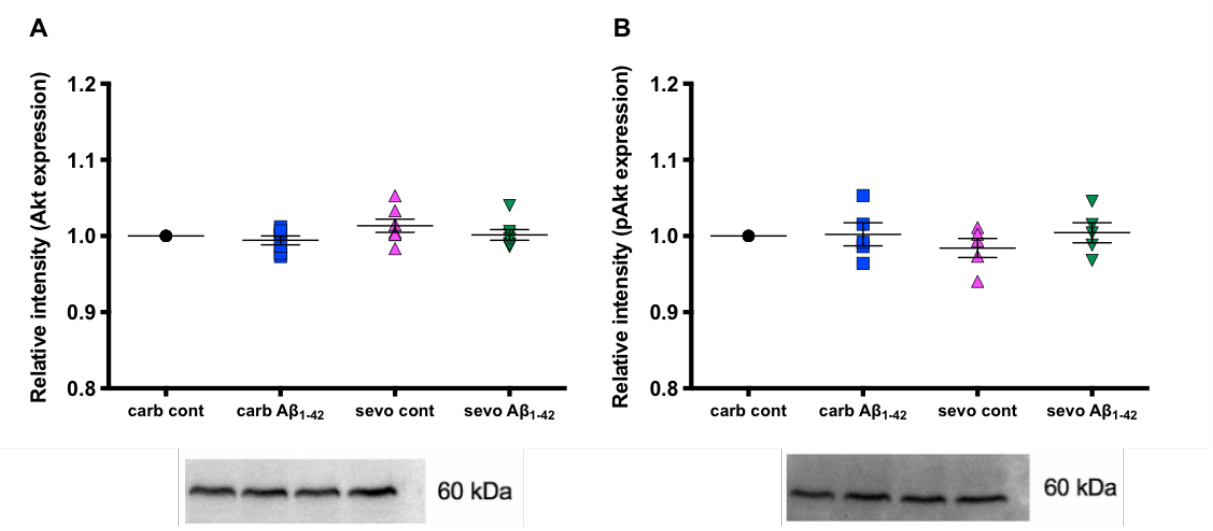

Fig. 69: Sevoflurane did not change Akt and pAkt expression. A + B: Intensities of the protein bands were normalized to the median of the control group (carb cont= carbogen control). The application of $A\beta_{1-42}$, 2% sevoflurane (sevo) and the combination of both did not change the expression of Akt (A: p= 0.2756, n= 6) and pAkt (B: p= 0.8284, n= 6). Lines represent the mean ± SEM. Bottom: Exemplary presentation of Akt and pAkt protein bands at 60 kDa.

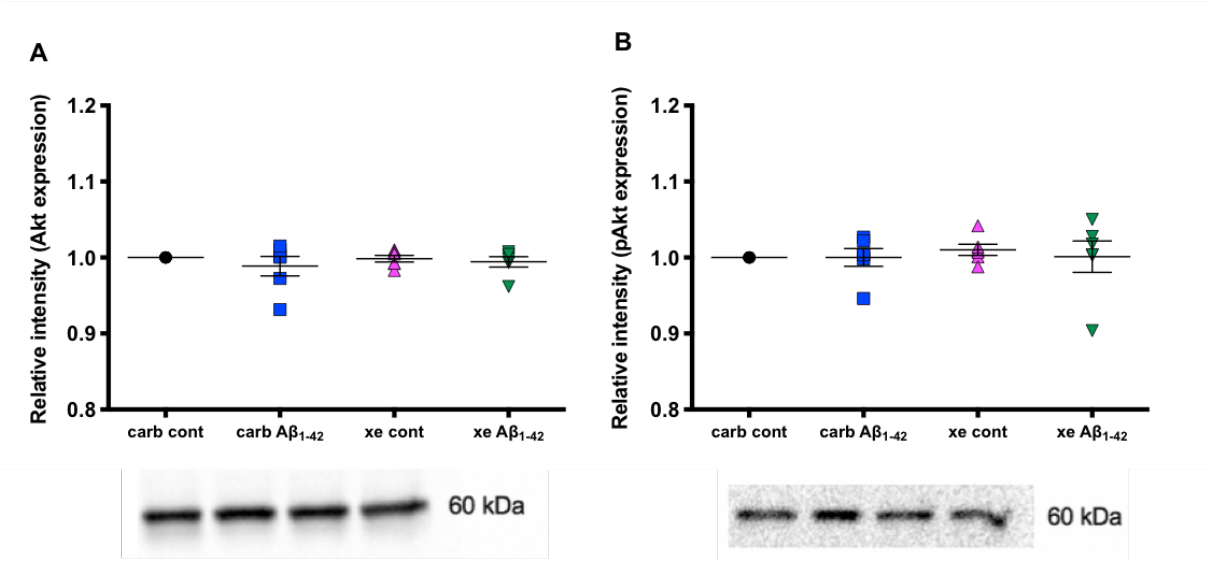

Fig. 70: Xenon did not change Akt and pAkt expression. A + B: Intensities of the protein bands were normalized to the median of the control group (carb cont= carbogen control). The application of $A\beta_{1-42}$, 65% xenon (xe) and the combination of both did not change the expression of Akt (A: p= 0.9459, n= 6) and pAkt (B: p= 0.2038, n= 6). Lines represent the mean ± SEM. Bottom: Exemplary presentation of Akt and pAkt protein bands at 60 kDa.

5.6.8 p53

I did not find any significant changes in the expression levels of p53 in the hippocampus of WT mice treated with $A\beta_{1-42}$ and anesthetics (65% xenon (p= 0.2056), 2% sevoflurane (p= 0.9023), 1% isoflurane (p=0.2937)) alone or in combination (Fig. 71).

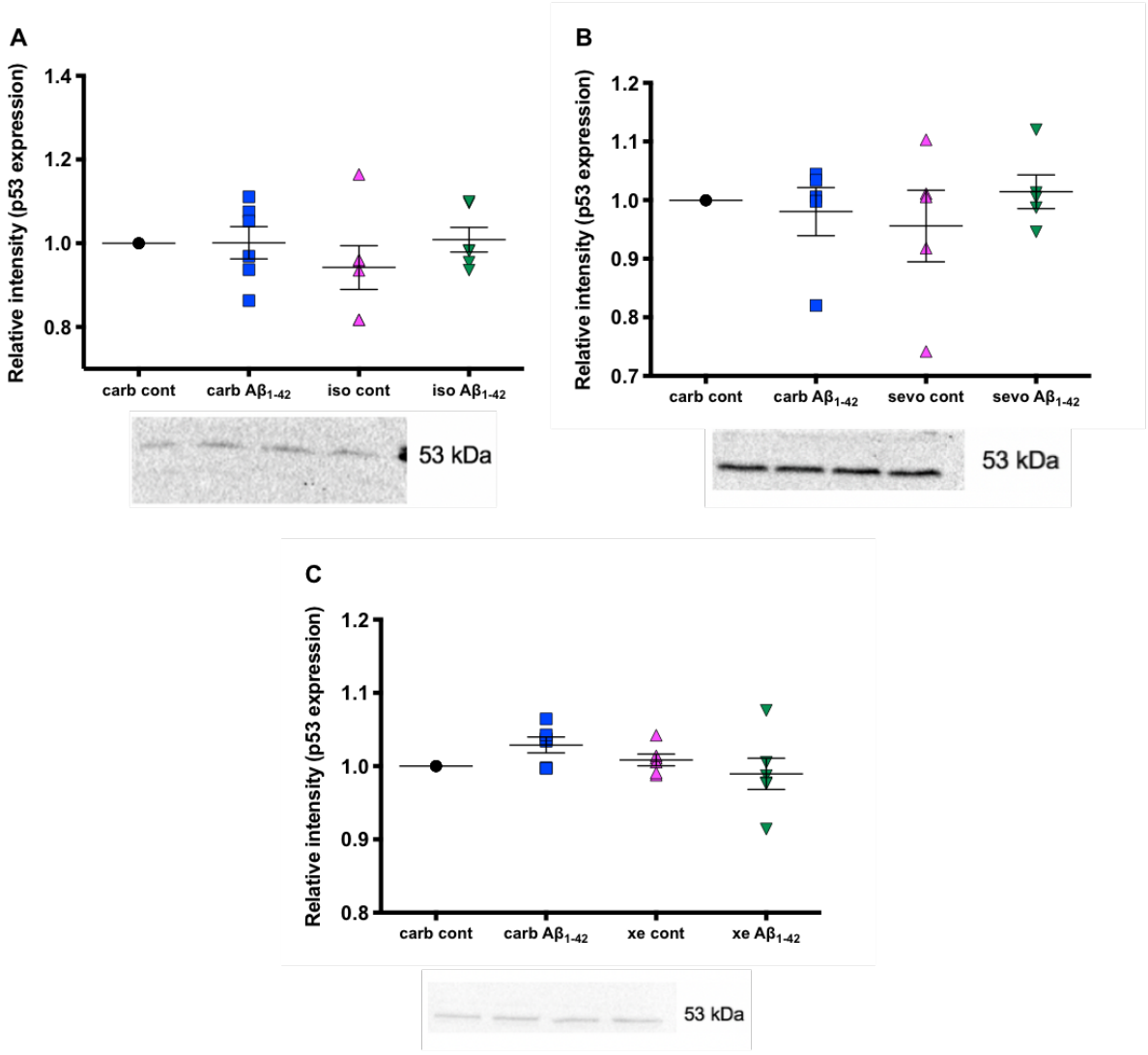

Fig. 71: Isoflurane, sevoflurane and xenon did not change p53 expression. A-C: Intensities of the protein bands were normalized to the median of the control group (carb cont= carbogen control). The application of $A\beta_{1-42}$, 1% isoflurane (iso), 2% sevoflurane (sevo), 65% xenon (xe) and the combination of both did not change the expression of p53 (iso: p= 0.2937, n= 6; sevo: p= 0.9023, n= 6; xe: p= 0.2056, n= 6). Lines represent the mean ± SEM. Bottom: Exemplary presentation of p53 protein bands at 53 kDa.

6. Discussion

Every day, thousands of patients receive general anesthesia during surgeries with frequently used inhalational anesthetics such as isoflurane and sevoflurane. Among these patients, the elderly and patients with different stages of AD and other morbidities are at risk of suffering from cognitive deterioration due to these substances. Pre-clinical studies indicate a relation between exposure to anesthetics and the risk of advancing or even inducing the development of AD (Jungwirth, Zieglgansberger et al. 2009, Seitz, Shah et al. 2011, Haseneder, Kochs et al. 2012, Liu, Pan et al. 2013, Kapila, Watts et al. 2014).

Thus far, the few clinical studies show contradictory results (Bohnen, Warner et al. 1994, Gasparini 2002, Seitz, Shah et al. 2011, Yang and Fuh 2015) and the pathological mechanisms behind this phenomenon are unclear. An increase of Aβ production and oligomerization due to the application of substances such as sevoflurane and isoflurane are under investigation (Eckenhoff, Johansson et al. 2004, Xie, Dong et al. 2007, Dong, Zhang et al. 2009, Mandal and Fodale 2009, Zhang, Tian et al. 2013).

In pre-clinical studies, widely divergent experimental conditions are used regarding anesthesia and incubation of Aβ. There is a strong need for conditions that are agreed-upon when working with Aβ to assure a valid interpretation and comparison of data, as well as a comparison to physiological conditions in AD patients.

The results of this dissertation are discussed in the following chapters.

6.1 Investigation of Aβ aggregation through TR-FRET

TR-FRET assays demonstrated that clinically relevant concentrations of isoflurane or sevoflurane did not affect aggregation, while using close to physiological Aβ levels (200 nM). Interestingly, xenon (at 1 MAC_{human}) even attenuated the formation of Aβ oligomers.

As described in chapter 3.1, I had to adjust the assay protocol developed by Merz Pharma to the conditions fitting my experimental setup. I needed to find a way to saturate the solutions of the assay with inhalative compounds. There were different factors that lead to problems in the adjustment of the protocol: In the assay by Merz Pharma, the probes were pipetted onto the well-plates with an automated pipetting robot. In my assay, I had to pipette manually by hand. That alone can lead to inaccuracies in the final concentrations. Another big difference compared to the original protocol is that I had to mix the buffer and Aβ solutions in protein low-binding tubes instead of putting them directly onto well-plates for incubation and measurement. This step might lead to a loss of solution although the tubes' surfaces are low binding. Loss of liquid through evaporation may also have occurred during gassing of the solutions.

The assays were developed and performed over a course of about 2 years. During several experiments, there were difficulties in finding the right ratio between the different Aβ isoforms to be able to distinguish between solutions that contained $MgCl^{2+}$ and that did not. After trying out different ratios, I ended up using the original ratio provided by the Merz protocol again. Possible reasons for

variations could be different Aβ stocks/batches, temperature changes in the lab or simply pipetting inaccuracies.
Despite other studies that showed sevoflurane and isoflurane to promote aggregation of Aβ (Xie, Dong et al. 2006, Xie, Dong et al. 2007, Dong, Zhang et al. 2009, Lu, Wu et al. 2010, Perucho, Rubio et al. 2010, Jiang and Jiang 2015), I could not detect any aggregation-promoting effects in my study. Increasing the concentrations of sevoflurane and isoflurane might result in a detectable effect on Aβ aggregation.

Surprisingly, exposure to 65% xenon significantly decreased aggregation of Aβ, suggesting that xenon might be able to counteract Aβ aggregation to oligomers. Applying xenon for longer or at a higher concentration might result in an even stronger decrease of aggregation.

One has to consider that TR-FRET assays cannot completely resemble the effect the gases might have on Aβ aggregates in the living brain of patients. The brain is a very complex organ and the proteins and gases tested might have different effects than in an artificial setup like the TR-FRET assay. However, developing simplified experimental designs allows the observation of isolated mechanistical processes such as Aβ aggregation. By using and modifying the TR-FRET assay, I was able to focus on the pure interaction of Aβ with anesthetics mainly disregarding the influence of another functional parameter.

6.2 Investigation of Aβ aggregation through Silver Staining

To investigate aggregation properties of Aβ in the presence of anesthetics, I performed a longitudinal analysis of $A\beta_{1-42}$ aggregation levels via Silver Staining. Shortly after application to the gel, the control sample showed Aβ aggregates up to 260 kDa. This is in agreement with findings by Economou, Giammona et al. (2016), who investigated Aβ oligomerization via atomic force microscopy. I could see monomers and low molecular weight oligomers such as trimers and tetramers as clearly separated bands on my gels. Larger oligomeric forms of Aβ presented as 'traces of stain'. Other scientists described the oligomers appearing on the gel as a 'smear' and assumed, that the gel has a resolution limitation or the smearing could be due to continuous associations and disassociations during electrophoresis analysis (Pryor, Moss et al. 2012).

Long-term Aβ incubation (1 d – 7 d) reduced the appearance of protein in my studies. Long incubation times may promote 'mass balance deficits' and the formation of high n oligomers/polymers. Very large, aggregated proteins could therefore no longer enter the gels through the start wells (Parsons, Ruitenberg et al. 2015). Another explanation for the 'loss' of protein would be precipitation over the course of 7 d like Parsons, Ruitenberg et al. (2015) suggested. Nevertheless, I securely closed the lids in my experiments and there was no obvious decrease in amount of solution in the tubes compared to other freshly prepared tubes.

Surprisingly, the appearance of higher oligomers did not change over time, but in some gels even showed a tendency to increase, possibly indicating a stabilization of these proteins over time. Another explanation could be an aggregation of lower proteins to higher oligomers over the time course of 7 d.

Isoflurane, sevoflurane and xenon did not show any significant effect on aggregation properties of Aβ monomers, trimers, tetramers and oligomers when compared to control bands.
The concentration of Aβ seems to play a central role when comparing the results of TR-FRET assays and silver staining experiments. When applied at a more physiological concentration of 200 nM, xenon reduces protein aggregation in TR-FRET assays. When I had to apply the protein at a concentration of 100 µM in silver staining experiments, xenon had no influence on aggregation properties.
The proportion of Aβ and xenon was – compared to the proportion in TR-FRET assays - unfavorable in the silver staining experiments. Higher concentration of xenon (e.g. > 65%) would have possibly been necessary to reduce the strong aggregation of Aβ. LTP data showed, that a stoichiometric excess of ~2 x 10^3 xenon over Aβ would be necessary to change the neurotoxic impact of $Aβ_{1-42}$.

Investigating oligomeric forms of Aβ proteins has always been challenging, because scientists have to use very high and therefore non-physiologic concentrations of the protein. Still, for the investigation of the direct effects of compounds such as anesthetics, it is important to perform such experiments.

6.3 Investigation of hippocampal activity in the presence of Aβ and anesthetics through VSDI

By using VSDI it is possible to investigate the electrical activity of complex neuronal circuits in tissues like the brain in real-time with high spatial-temporal resolution. I studied the change of neuronal activity in the hippocampus of WT mice in the presence of different Aβ isoforms and inhalational anesthetics. My goal was to mimic a healthy patient versus a patient with increased amounts of Aβ undergoing GA in a laboratory setting.
Baseline activity resembled the healthy and awake patient in all groups. In the Aβ group, I determined the effect of $Aβ_{1-42}$, $Aβ_{1-40}$, AβpE3 and 3NTyrAβ on neuronal activity. Previous studies on LTP of the hippocampus showed that treatment with Aβ oligomers resulted in epileptiform activity of the hippocampus through an imbalance of glutamatergic and GABAergic signaling (Lei, Xu et al. 2016). This strong and continuous activation can lead to neurodegeneration as it appears in AD. The risk to develop this so called 'nonconvulsive epileptiform activity' is increased in familial AD and early stages of sporadic AD. Mendez, Catanzaro et al. (1994) and Amatniek, Hauser et al. (2006) confirmed these findings in the cortex and hippocampus of transgenic AD mice. Based on these findings, I hypothesized that Aβ would increase neuronal activity in the hippocampus. Surprisingly, I only found $Aβ_{1-40}$ to increase neuronal activity significantly. In slices treated with other isoforms I could see a numeric, but not significant increase in activity. An explanation for this finding might be the incubation time of Aβ for only 90 min.

In the anesthetic group, I determined the change of neuronal activity after application of anesthetics alone. To assure monitoring of viable neuronal activity, I used 65% xenon because higher concentrations are difficult to achieve (see detailed explanation in chapter 3.3.4) (Haseneder, Kratzer et al. 2009). To ensure the application of equipotent concentrations of xenon, isoflurane and sevoflurane I used 0.6% isoflurane and 1.4% sevoflurane. Additionally, I applied iso and sevo at 1% and 2%, respectively.
The activity of the hippocampus decreased significantly and quickly after application of all gases for 40 min. The FDS signal decreased less after application of only 0.6% isoflurane and 1.4% sevoflurane, but not significantly different to higher concentrations. This phenomenon shows that isoflurane and sevoflurane, even at concentrations well below 1 MAC of mice and humans, seem to be very potent anesthetics leading to a rapid reduction in activity of the hippocampus – mainly through strong activation of $GABA_A$ receptors (Simon, Hapfelmeier et al. 2001, Ishizeki, Nishikawa et al. 2008).
The current experiments show a complete recovery of neuronal activity after washout of isoflurane and sevoflurane and do therefore not indicate a negative effect of these commonly used anesthetics alone on the hippocampus and its activity.

The focus of my VSDI experiments was the determination of neuronal activity changes in the presence of Aβ plus inhalational anesthetic – representing a patient with elevated Aβ amounts undergoing general anesthesia (Aβ + anesthetic group) in a laboratory setting.

My findings show a very diverse picture: The higher concentrations of sevoflurane (2%) and isoflurane (1%), as well as xenon in combination with $Aβ_{1-42}$ somehow lead to a prevention of full recovery from the reduced activity level back to baseline levels in the CA1 region. In contrast, lower concentrations lead to a near complete recovery, indicating that higher concentrations of these inhalational anesthetics somehow interfere with $Aβ_{1-42}$ to change activity levels. In the CA3 region, slices treated with 65% xenon were the only to regain baseline activity levels.
Surprisingly, experiments with AβpE3 and $Aβ_{1-40}$ lead to a different picture: Slices treated with xenon regained baseline activity levels after washout also in the CA1 region, implying that xenon might not interfere with these Aβ isoforms.
Through the excessive overactivation of NMDARs through Aβ (Li, Sun et al. 2016) in combination with the strong synaptic depression caused by anesthetics, NMDARs might desensitize and internalize – causing this lasting synaptic depression in my VSDI experiments.

$Aβ_{1-42}$ affects the glutamatergic system, mainly the NMDAR function (Martinez-Coria, Green et al. 2010, Wilcox, Lacor et al. 2011, Rammes, Gravius et al. 2015), as well as AMPA receptor function (Tu, Okamoto et al. 2014, Guntupalli, Widago et al. 2016, Jurado 2018). NMDARs are crucial for the induction of LTP (Texido, Martin-Satue et al. 2011) and are therefore key mediators of synaptic transmission. Elevated resting Ca^{2+} has been observed previously in neuronal culture and in AD mouse

models (Kuchibhotla, Goldman et al. 2008, Um, Kaufman et al. 2013) and, moreover, is also a hallmark of AD pathophysiology (Yu, Chang et al. 2009, Woods and Padmanabhan 2012).
The increased Ca^{2+}-influx can have pathological effects such as blockage of LTP and a loss of normal neuronal function through dysfunction of mitochondria, leading to cell death, neurodegeneration and cognitive dysfunction over time (Lambert, Barlow et al. 1998, Selkoe 2001, Parsons, Stoffler et al. 2007, Liu, Chang et al. 2019).
The strong activation of GABARs plus an increased release of GABA by isoflurane and sevoflurane combined with the effect of Aβ – an indirect activation of GABARs through the excessive activation of NMDARs – strongly inhibit neuronal activation (Zhao, De Felice et al. 2008). To a certain extent, also sevoflurane and isoflurane may inhibit NMDARs and presumably AMPARs, leading to an additional neuronal depression (Parsons, Stoffler et al. 2007).

Taken together, treatment of murine hippocampal slices with certain oligomeric Aβ species plus inhaled anesthetics may lead to a potentiated, strong and lasting depression of synaptic activity in the hippocampus, possibly leading to blockade of LTP and cognitive deficits after GA.
Post-translationally modified Aβ proteins such as AβpE3 and 3NTyrAβ may produce their toxicity through different membrane receptors/proteins (e.g. NMDARs, AMPARs, calcium channels, insulin receptors (Serra-Batiste, Ninot-Pedrosa et al. 2016)). This might explain the heterogenous results in my VSDI and LTP experiments. These modified Aβ proteins may even be capable of forming their own ion channels, leading to abnormal intracellular responses and downstream changes (Bürge, Kratzer et al. 2019) (e.g. Ca^{2+}-influx, synaptic excitation/depression) (Luscher and Malenka 2012). Results from TR-FRET assays and silver staining experiments did not indicate a direct influence of sevoflurane and isoflurane on Aβ aggregation. I therefore propose that the lasting neuronal depression is not caused by increased oligomerization by neither anesthetic used in this study.

6.4 Recovery of synaptic plasticity after blockade through Aβ

There is growing evidence that soluble Aβ oligomers cause early memory problems in AD patients by disrupting LTP before Aβ plaques or and hyperphosphorylated tau proteins are detectable in the patient's brain (Luscher and Malenka 2012; Walsh et al. 2002; Rammes et al. 2011).
Many studies have shown that physiological concentrations of different Aβ species inhibit LTP *in vivo* and *ex vivo* in the CA1 layer of the murine hippocampus, resulting in inhibition of normal cognition and induction of neurotoxic downstream changes (Walsh, Klyubin et al. 2002, Rammes, Hasenjager et al. 2011, Cline, Bicca et al. 2018, Rammes, Seeser et al. 2018, Bürge, Kratzer et al. 2019).
NMDARs are important for the formation of LTP and antagonists of NMDAR delivered at concentrations that do not interfere with physiological functions *in vitro* are able to prevent neuronal toxicity by Aβ proteins (Rammes, Hasenjager et al. 2011, Rammes, Seeser et al. 2018, Bürge, Kratzer et al. 2019). Especially the NMDAR subunit 2B (GluN2B) has been shown to be highly involved in mediating Aβ-induced synaptotoxic effects (Rammes, Seeser et al. 2018).

Researchers in my workgroup showed that xenon, a low affinity NMDAR antagonist (Kratzer, Mattusch et al. 2012), administered at a subanesthetic concentration of 30% partially restored $A\beta_{1-42}$-, but not $A\beta_{1-40}$-induced blockage of LTP. These results suggest a neuroprotective characteristic of xenon in these experimental conditions (Bürge, Kratzer et al. 2019).
The results of my LTP experiments build on these findings. I tested possible neuroprotective effects of 30% xenon against AβpE3- and 3NTyrAβ-induced LTP blockade.
I found 30% xenon to restore LTP blockade caused by AβpE3 but not 3NTyrAβ. This finding indicates that different Aβ isoforms may act via different receptors or subunits to produce their neurotoxicity. Researchers of my workgroup also found radiprodil, an NMDA antagonist, to have beneficial effects against neurotoxicity of $A\beta_{1-42}$, $A\beta_{1-40}$ and 3NTyrAβ, but not AβpE3 (Rammes, Seeser et al. 2018, Bürge, Kratzer et al. 2019). These results further support my thesis and might also explain the heterogenous results between different Aβ species in my VSDI experiments. Another explanation could simply be a higher potency of 3NTyrAβ on LTP than AβpE3.
I had to apply xenon at a concentration of 30% which does not inhibit LTP (Bürge, Kratzer et al. 2019). Kratzer, Mattusch et al. 2012 showed that even though 65% xenon inhibited LTP, this effect was reversible after washout of xenon. Taking this fact into account, increasing the concentration of xenon to 1 MAC_{human} might even be more neuroprotective against Aβ during anesthesia (Bürge, Kratzer et al. 2019). A combination of a NMDAR antagonism by xenon and its inhibitory effect on Aβ aggregation may be beneficial in patients undergoing GA.

6.5 Spine Density

To further analyze the effect of frequently used inhalational anesthetics on synaptic plasticity in the presence of Aβ, I investigated the dendritic spine density of the CA1 region of the murine hippocampus. Dendritic spines are membrane protrusions and resemble postsynapses on the cellular level. Their structure and formation are highly dynamic and their function is critical for neural circuits (Alvarez and Sabatini 2007) and synaptic plasticity (Engert and Bonhoeffer 1999, Maletic-Savatic, Malinow et al. 1999, McCann and Ross 2017). Studies have shown that spine density is abnormally increased or decreased in morbidities such as AD leading to dysfunction of normal neuronal mechanisms (Takashima, Ieshima et al. 1989, el Hachimi and Foncin 1990). An explanation could be the neurotoxic effect of certain Aβ oligomers on spines. Oligomers decrease spine density through an NMDAR-dependent signaling pathway (Selkoe 2005) in EGFP-M mice and acute hippocampal slices treated with Aβ (Shankar, Bloodgood et al. 2007, Head, Patel et al. 2009, Smith, Pozueta et al. 2009, Rammes, Seeser et al. 2018).
Isoflurane and sevoflurane seem to also influence spine density, although studies show somewhat contradictory results thus far. Researchers suggest that this effect might be dependent on the concentration of the anesthetic and the developmental stage of the animal during application (De Roo, Klauser et al. 2009, Tan, Ren et al. 2009, Briner, De Roo et al. 2010). Many studies either use cell cultures (Papa, Bundman et al. 1995, Hasbani, Schlief et al. 2001), *in vivo* in mouse models (Lendvai, Stern et al. 2000, Bittner, Fuhrmann et al. 2010, Ruddy, Chen et al. 2015).

However, working with *ex vivo* brain slices has several advantages and represent a good alternative to *in vivo* systems. In contrast to cell cultures, substances can be tested in a still living cell network within a still reasonably intact neuronal circuitry. The tissue structure can be preserved and the neuronal activity with the synaptic circuits can be largely maintained (Cho, Wood et al. 2007). In cell cultures, only isolated cells can be observed and do not reflect the complexity of the whole organism (Cho, Wood et al. 2007, Humpel 2015). Furthermore, this preparation method can reduce the number of experimental animals by allowing different substances to be tested on one brain by dividing it into many sections. Another advantage is that the results can be compared with LTP experiments due to a similar experimental design.

Consistent with previously published studies (Spires, Meyer-Luehmann et al. 2005, Shankar, Bloodgood et al. 2007, Shankar, Li et al. 2008, Wei, Nguyen et al. 2010, Rammes, Seeser et al. 2018), I found $A\beta_{1-42}$ to reduce spine density significantly. Rammes, Seeser et al. (2018) found different Aβ species to decrease spine density significantly in young adult mice, but in a certain efficacy order: 3NTyrAβ > $A\beta_{1-40}$ > $A\beta_{1-42}$ ≥ AβpE3. Incubation of the slices with memantine (1 µM) before Aβ application reversed the neurotoxic effect of $A\beta_{1-42}$.
Interestingly, and consistent with my LTP results, application of xenon partially reversed the toxic effect of $A\beta_{1-42}$ on spine density in adult GFP mice. Surprisingly, also the application of 2% sevoflurane, but not of isoflurane, reversed the synaptotoxic effect, indicating a neuroprotective effect of sevoflurane as well as xenon. Nevertheless, isoflurane did not increase the loss of spines indicating no additive or synergistic toxicity.
To my knowledge, there are no other studies addressing the effect of isoflurane, sevoflurane and xenon alone and in combination with $A\beta_{1-42}$ on the density of dendritic spines in the hippocampus of adult mice. Most other studies performed tests on neonatal or very young animals (De Roo, Klauser et al. 2009, Briner, De Roo et al. 2010, Xiao, Liu et al. 2016).
Due to a lack of time I could not test further Aβ species but these experiments should be performed in future studies.

6.6 Autophagy

I aimed to determine whether $A\beta_{1-42}$ and anesthetics - either alone or in combination - have an effect on the expression of proteins involved in autophagy. Since autophagy is a complex and pivotal process for the vitality of cells in the body (Cuervo, Bergamini et al. 2005), significant changes in only a few proteins might lead to detrimental effects that may develop into neurodegenerative diseases such as AD (Komatsu, Waguri et al. 2006, Barnett and Brewer 2011, Metcalf, Garcia-Arencibia et al. 2012). Interestingly, autophagy is the main pathway for Aβ degradation (Geng, Zhang et al. 2018).

Surprisingly, the expression of none of the studied autophagy proteins changed significantly, indicating that $A\beta_{1-42}$ and inhalational anesthetics as well as the combination of both do not affect

these autophagy proteins in my experimental setup. Therefore, these results do not reveal that cognitive dysfunction after general anesthesia is caused by defects of the autophagy pathway.

Since several other studies presented relevant effects (Perucho, Casarejos et al. 2010, Geng, Zhang et al. 2018), future studies using my experimental setup could increase the time of exposure to xenon/isoflurane/sevoflurane and/or incubation with Aβ. Incubating the slices for 90 min might not be long enough to alter the levels of autophagy proteins significantly.

7. Limitations

To mimic the effect of general anesthetics on the living brain of a patient in a laboratory setting, it is crucial to work with conditions that closely represent physiological/pathophysiological conditions. It is therefore necessary to use concentrations of Aβ proteins and anesthetics that are similar to the amount of protein in the AD brain and concentrations of anesthetics/length of application that are used in the clinic.

There are several physical and molecular limitations when working with Aβ proteins and anesthetics, specifically xenon. For example, 1 MAC xenon for mice is hyperbaric at 1.61 atm (Koblin, Fang et al. 1998). Because of that, I had to use a concentration of xenon that is used in humans: 65%. Therefore, my results could underestimate the impact of a higher concentration of xenon for humans.

Regarding the change of Aβ aggregation after xenon treatment, this parameter is extremely difficult to interpret. When I used Aβ in a physiological concentration of 200 nM, xenon reduced aggregation. When I had to apply it at 100 µM due to experimental constraints, xenon had no influence on aggregation properties. But, it is physically not practicable to adapt the stoichiometry of xenon/Aβ to the Aβ concentration that is needed in silver staining experiments. These limitations have to be considered for interpretation and may explain contradictory results concerning Aβ toxicity and xenon neuroprotection.

Like many diseases, AD is sex-specific. It is more frequent in females than in males (Schmid, Rammes et al. 2019). It might a limitation that I only used male animals in my experiments.

8. Conclusion

Life expectancy in human will further increase over the next decades, which means that even more elderly will receive general anesthesia. Among these elderlies are also patients suffering from Alzheimer's disease. To ensure a safe outcome and to prevent short- and long-term effects on cognition, there is a need to find out more about the interaction between inhalational anesthetics and Aβ proteins.

The findings of my dissertation indicate that the routinely used inhalational anesthetics isoflurane and sevoflurane somehow interfere with Aβ-dependent pathophysiology of AD. Nevertheless, they no not increase Aβ protein aggregation, influence spine density or expression of autophagy proteins negatively in the study's experimental setting.
Xenon instead showed neuroprotective properties against Aβ aggregation and blockade of LTP by Aβ as well as Aβ-induced reduction of spine density.

9. References

Abramov, E., I. Dolev, H. Fogel, G. D. Ciccotosto, E. Ruff and I. Slutsky (2009). "Amyloid-beta as a positive endogenous regulator of release probability at hippocampal synapses." Nat Neurosci **12**(12): 1567-1576.

Alvarez, V. A. and B. L. Sabatini (2007). "Anatomical and physiological plasticity of dendritic spines." Annu Rev Neurosci **30**: 79-97.

Alzheimer, A. (1911). "Über eigenartige Krankheitsfälle des späteren Alters." Zeitschrift für die gesamte Neurologie und Psychiatrie.

Alzheimer, A., R. A. Stelzmann, H. N. Schnitzlein and F. R. Murtagh (1995). "Über eine eigenartige Erkrankung der Hirnrinde." Clinical Anatomy **8**: 429-431.

Amaral, D. G. (1993). "Emerging principles of intrinsic hippocampal organization." Curr Opin Neurobiol **3**(2): 225-229.

Amaral, D. G. S., H.E.; Lavenex, P. (2007). "The dentate gyrus: fundamental neuroanatomical organization (dentate gyrus for dummies)." Prog Brain Res **163**: 3-22.

Amatniek, J. C., A. Hauser, C. Del-Castillo-Castaneda, D. M. Jacobs, K. Marder, K. Bell, M. Albert, J. Brandt and Y. Stern (2006). "Incidence and Predictors of Seizures in Patients with Alzheimer's Disease." Epilepsia **47**(5): 867-872.

Androuin, A., B. Potier, U. V. Nagerl, D. Cattaert, L. Danglot, M. Thierry, I. Youssef, A. Triller, C. Duyckaerts, K. H. El Hachimi, P. Dutar, B. Delatour and S. Marty (2018). "Evidence for altered dendritic spine compartmentalization in Alzheimer's disease and functional effects in a mouse model." Acta Neuropathol **135**(6): 839-854.

Antkowiak, B. (2001). "How do general anaesthetics work?" Naturwissenschaften **88**(5): 201-213.

Association, A. s. (2021). "2021 Alzheimer's Disease Facts and Figures." Alzheimers Dement **17**(3).

Austad, S. N. (2006). "Why women live longer than men: sex differences in longevity." Gend. Med. **3**(2): 79-92.

Ballatore, C., V. M. Lee and J. Q. Trojanowski (2007). "Tau-mediated neurodegeneration in Alzheimer's disease and related disorders." Nat Rev Neurosci **8**(9): 663-672.

Barnett, A. and G. J. Brewer (2011). "Autophagy in aging and Alzheimer's disease: pathologic or protective?" J Alzheimers Dis **25**(3): 385-394.

Baumert, J. H., M. Hein, K. Hecker, J. Satlow, J. Schnoor and R. Rossaint (2007). "Autonomic cardiac control with xenon anaesthesia in patients at cardiovascular risk." British Journal of Anaesthesia **98**(6): 722-727.

Baumgart, M., H. M. Snyder, M. C. Carrillo, S. Fazio, H. Kim and H. Johns (2015). "Summary of the evidence on modifiable risk factors for cognitive decline and dementia: A population-based perspective." Alzheimers Dement **11**(6): 718-726.

Behnke, A. and O. D. Yarborough (1939). "Respiratory resistance, oil-water-solubility and mental effects of argon compared with helium and nitrogen." Am J Physiol **126**: 409-415.

Billings, L. M., S. Oddo, K. N. Green, J. L. McGaugh and F. M. LaFerla (2005). "Intraneuronal Abeta causes the onset of early Alzheimer's disease-related cognitive deficits in transgenic mice." Neuron **45**(5): 675-688.

Bischofberger, J., D. Engel, L. Li, J. R. Geiger and P. Jonas (2006). "Patch-clamp recording from mossy fiber terminals in hippocampal slices." Nat Protoc **1**(4): 2075-2081.

Bittner, E. A., Y. Yue and Z. Xie (2011). "Brief review: anesthetic neurotoxicity in the elderly, cognitive dysfunction and Alzheimer's disease." Can J Anaesth **58**(2): 216-223.

Bittner, T., M. Fuhrmann, S. Burgold, S. M. Ochs, N. Hoffmann, G. Mitteregger, H. Kretzschmar, F. M. LaFerla and J. Herms (2010). "Multiple events lead to dendritic spine loss in triple transgenic Alzheimer's disease mice." PLoS One **5**(11): e15477.

Bliss, T. V. P. and T. Lomo (1973). "Long-Lasting Potentiation of synaptic transmission in the dentate area of the anesthetized rabbit following stimulation of the perforant path." J. Physiol. **232**: 331-356.

Blum H., B. H., Gross H.J. (1987). "Improved silver staining of plant proteins, RNA and DNA in polyacrylamide gels." Electrophoresis **8**: 93-99.

Bohnen, N., M. A. Warner, E. Kokmen and L. T. Kurland (1994). "Early and midlife exposure to anesthesia and age of onset of Alzheimer's disease." Int J Neurosci **77**(3-4): 181-185.

Bohnen, N. I., M. A. Warner, E. Kokmen, C. M. Beard and L. T. Kurland (1994). "Alzheimer's disease and cumulative exposure to anesthesia: a case-control study." J Am Geriatr Soc **42**(2): 198-201.

Boros, B. D., K. M. Greathouse, E. G. Gentry, K. A. Curtis, E. L. Birchall, M. Gearing and J. H. Herskowitz (2017). "Dendritic spines provide cognitive resilience against Alzheimer's disease." Ann Neurol **82**(4): 602-614.

Boya, P., R. A. Gonzalez-Polo, N. Casares, J. L. Perfettini, P. Dessen, N. Larochette, D. Metivier, D. Meley, S. Souquere, T. Yoshimori, G. Pierron, P. Codogno and G. Kroemer (2005). "Inhibition of macroautophagy triggers apoptosis." Mol Cell Biol **25**(3): 1025-1040.

Briner, A., M. De Roo, A. Dayer, D. Muller, W. Habre and L. Vutskits (2010). "Volatile anesthetics rapidly increase dendritic spine density in the rat medial prefrontal cortex during synaptogenesis." Anesthesiology **112**(3): 546-556.

Bronco, A., P. M. Ingelmo, M. Aprigliano, M. Turella, E. Sahillioglu, M. Bucciero, M. Somaini and R. Fumagalli (2010). "Xenon anaesthesia produces better early postoperative cognitive recovery than sevoflurane anaesthesia." Eur J Anaesthesiol **27**(10): 912-916.

Brosnan, R. J. T., R. (2012). "Increased NMDA receptor inhibition at an increased Sevoflurane MAC." BMC Anesthesiol **12**: 9.

Brothers, H. M., M. L. Gosztyla and S. R. Robinson (2018). "The Physiological Roles of Amyloid-β Peptide Hint at New Ways to Treat Alzheimer's Disease." Front Aging Neurosci **10**(118).

Brown, C. E., C. Wong and T. H. Murphy (2008). "Rapid morphologic plasticity of peri-infarct dendritic spines after focal ischemic stroke." Stroke **39**(4): 1286-1291.

Brown, E. N., R. Lydic and N. D. Schiff (2010). "General anesthesia, sleep, and coma." N Engl J Med **363**(27): 2638-2650.

Brunet, A., S. R. Datta and M. E. Greenberg (2001). "Transcription-dependent and -independent control of neuronal survival by the PI3K-Akt signaling pathway." Curr Opin Neurobiol **11**(3): 297-305.

Bürge, M., S. Kratzer, C. Mattusch, C. Hofmann, M. Kreuzer, C. G. Parsons and G. Rammes (2019). "The anaesthetic xenon partially restores an amyloid beta-induced impairment in murine hippocampal synaptic plasticity." Neuropharmacology **151**: 21-32.

Burnette, W. N. (1981). "Western Blotting: Electrophoretic transfer of proteins from sodium dodecyl sulfate-polyacrylamide gels to unmodified nitrocellulose and radiographic detection with antibody and radioioninated protein A. ." Analytical Biochemistry **112**(2): 195-203.

Caccamo, A., E. Ferreira, C. Branca and S. Oddo (2017). "p62 improves AD-like pathology by increasing autophagy." Mol Psychiatry **22**(6): 865-873.

Campagna, J. A., S. A. Forman and K. W. Miller (2003). "Mechanisms of actions of inhaled anesthetics." New Engl J Med **348**(9): 2110-2124.

Cappai, R. and K. J. Barnham (2008). "Delineating the mechanism of Alzheimer's disease A beta peptide neurotoxicity." Neurochem Res **33**(3): 526-532.

Cataldo, A. M., J. L. Barnett, D. M. Mann and R. A. Nixon (1996). "Colocalization of lysosomal hydrolase and beta-amyloid in diffuse plaques of the cerebellum and striatum in Alzheimer's disease and Down's syndrome." J Neuropathol Exp Neurol **55**(6): 704-715.

Chan, E. Y., S. Kir and S. A. Tooze (2007). "siRNA screening of the kinome identifies ULK1 as a multidomain modulator of autophagy." J Biol Chem **282**(35): 25464-25474.

Chavez-Gutierrez, L., L. Bammens, I. Benilova, A. Vandersteen, M. Benurwar, M. Borgers, S. Lismont, L. Zhou, S. Van Cleynenbreugel, H. Esselmann, J. Wiltfang, L. Serneels, E. Karran, H. Gijsen, J. Schymkowitz, F. Rousseau, K. Broersen and B. De Strooper (2012). "The mechanism of gamma-Secretase dysfunction in familial Alzheimer disease." EMBO J **31**(10): 2261-2274.

Chemla, S. and F. Chavane (2010). "A biophysical cortical column model to study the multi-component origin of the VSDI signal." Neuroimage **53**(2): 420-438.

Chen, C. W., C. C. Lin, K. B. Chen, Y. C. Kuo, C. Y. Li and C. J. Chung (2014). "Increased risk of dementia in people with previous exposure to general anesthesia: a nationwide population-based case-control study." Alzheimers Dement **10**(2): 196-204.

Cho, S., A. Wood and M. R. Bowlby (2007). "Brain slices as models for neurodegenerative disease and screening platforms to identify novel therapeutics." Curr Neuropharmacol **5**(1): 19-33.

Cline, E. N., M. A. Bicca, K. L. Viola and W. L. Klein (2018). "The Amyloid-beta Oligomer Hypothesis: Beginning of the Third Decade." J Alzheimers Dis **64**(s1): S567-S610.

Coburn, M., O. Kunitz, J. H. Baumert, K. Hecker, S. Haaf, A. Zuhlsdorff, T. Beeker and R. Rossaint (2005). "Randomized controlled trial of the haemodynamic and recovery effects of xenon or propofol anaesthesia." Br J Anaesth **94**(2): 198-202.

Cooke, S. F. and T. V. Bliss (2006). "Plasticity in the human central nervous system." Brain **129**(Pt 7): 1659-1673.

Cuervo, A. M. (2004). "Autophagy: many paths to the same end." Mol Cell Biochem **263**(1-2): 55-72.

Cuervo, A. M., E. Bergamini, U. T. Brunk, W. Droge, M. Ffrench and A. Terman (2005). "Autophagy and aging: the importance of maintaining "clean" cells." Autophagy **1**(3): 131-140.

Danysz, W., C. G. Parsons, H. J. Mobius, A. Stoffler and G. Quack (2000). "Neuroprotective and symptomatological action of memantine relevant for Alzheimer's disease--a unified glutamatergic hypothesis on the mechanism of action." Neurotox Res **2**(2-3): 85-97.

Dawson, V. L. and T. M. Dawson (1996). "Nitric oxide neurotoxicity." J Chem Neuroanat **10**(3-4): 179-190.

De Roo, M., P. Klauser, A. Briner, I. Nikonenko, P. Mendez, A. Dayer, J. Z. Kiss, D. Muller and L. Vutskits (2009). "Anesthetics rapidly promote synaptogenesis during a critical period of brain development." PLoS One **4**(9): e7043.

de Sousa, S. L., R. Dickinson, W. R. Lieb and N. P. Franks (2000). "Contrasting synaptic actions of the inhalational general anesthetics isoflurane and xenon." Anesthesiology **92**(4): 1055-1066.

Degorce, F., A. Card, S. Soh, E. Trinquet, G. Knapik and B. Xie (2009). "HTRF: A Technology Tailored for Drug Discovery -A Review of Theoretical Aspects and Recent Apllications." Curr Chem Genomics **3**: 22-32.

DeKosky, S. T. and S. W. Scheff (1990). "Synapse loss in frontal cortex biopsies in Alzheimer's disease: Correlation with cognitive severity." Annals of Neurology **27**(457-464).

Dong, Y., X. Wu, G. Zhang, Z. Xu, Y. Zhang, V. Gautam, D. M. Kovacs, A. Wu, Y. Yue and Z. Xie (2013). "Isoflurane facilitates synaptic NMDA receptor endocytosis in mice primary neurons." Curr Mol Med **13**(4): 488-498.

Dong, Y., G. Zhang, B. Zhang, R. D. Moir, W. Xia, E. R. Marcantonio, D. J. Culley, G. Crosby, R. E. Tanzi and Z. Xie (2009). "The common inhalational anesthetic sevoflurane induces apoptosis and increases beta-amyloid protein levels." Arch Neurol **66**(5): 620-631.

Dorostkar, M. M., C. Zou, L. Blazquez-Llorca and J. Herms (2015). "Analyzing dendritic spine pathology in Alzheimer's disease: problems and opportunities." Acta Neuropathol **130**: 1-19.

Du, Y., M. C. Wooten and M. W. Wooten (2009). "Oxidative damage to the promoter region of SQSTM1/p62 is common to neurodegenerative disease." Neurobiol Dis **35**(2): 302-310.

Dwyer, R., H. L. Bennett, E. I. Eger, 2nd and D. Heilbron (1992). "Effects of isoflurane and nitrous oxide in subanesthetic concentrations on memory and responsiveness in volunteers." Anesthesiology **77**(5): 888-898.

Eckenhoff, R. G., J. S. Johansson, H. Wei, A. Carnini, B. Kang, W. Wei, R. Pidikiti, J. M. Keller and M. F. Eckenhoff (2004). "Inhaled anesthetic enhancement of amyloid-beta oligomerization and cytotoxicity." Anesthesiology **101**(3): 703-709.

Eckerstrom, C., U. Andreasson, E. Olsson, S. Rolstad, K. Blennow, H. Zetterberg, H. Malmgren, A. Edman and A. Wallin (2010). "Combination of hippocampal volume and cerebrospinal fluid biomarkers improves predictive value in mild cognitive impairment." Dement Geriatr Cogn Disord **29**(4): 294-300.

Economou, N. J., M. J. Giammona, T. D. Do, X. Zheng, D. B. Teplow, S. K. Buratto and M. T. Bowers (2016). "Amyloid beta-Protein Assembly and Alzheimer's Disease: Dodecamers of Abeta42, but Not of Abeta40, Seed Fibril Formation." J Am Chem Soc **138**(6): 1772-1775.

el Hachimi, K. H. and J. F. Foncin (1990). "[Loss of dendritic spines in Alzheimer's disease]." C R Acad Sci III **311**(11): 397-402.

Engert, F. and T. Bonhoeffer (1999). "Dendritic spine changes associated with hippocampal long-term synaptic plasticity." Nature **399**(6731): 66-70.

Esencan, E., S. Yuksel, Y. B. Tosun, A. Robinot, I. Solaroglu and J. H. Zhang (2013). "XENON in medical area: emphasis on neuroprotection in hypoxia and anesthesia." Med Gas Res **3**(1): 4.

Fahlenkamp, A. V., C. Stoppe, J. Cremer, I. A. Biener, D. Peters, R. Leuchter, A. Eisert, C. C. Apfel, R. Rossaint and M. Coburn (2016). "Nausea and Vomiting following Balanced Xenon Anesthesia Compared to Sevoflurane: A Post-Hoc Explorative Analysis of a Randomized Controlled Trial." PLoS One **11**(4): e0153807.

Fernandez-Vizarra, P., A. P. Fernandez, S. Castro-Blanco, J. Serrano, M. L. Bentura, R. Martinez-Murillo, A. Martinez and J. Rodrigo (2004). "Intra- and extracellular Abeta and PHF in clinically evaluated cases of Alzheimer's disease." Histol Histopathol **19**(3): 823-844.

Franks, N. P. (2008). "General anaesthesia: from molecular targets to neuronal pathways of sleep and arousal." Nat Rev Neurosci **9**(5): 370-386.

Franks, N. P., R. Dickinson, S. L. de Sousa, A. C. Hall and W. R. Lieb (1998). "How does xenon produce anaesthesia?" Nature **396**(6709): 324.

Franks, N. P. and W. R. Lieb (1993). "Selective actions of volatile general anaesthetics at molecular and cellular levels." Br J Anaesth **71**(1): 65-76.

Frink, E. J., Jr., T. P. Malan, M. Atlas, L. M. Dominguez, J. A. DiNardo and B. R. Brown, Jr. (1992). "Clinical comparison of sevoflurane and isoflurane in healthy patients." Anesth Analg **74**(2): 241-245.
Fu, M. and Y. Zuo (2011). "Experience-dependent structural plasticity in the cortex." Trends Neurosci **34**(4): 177-187.

Funderburk, S. F., Q. J. Wang and Z. Yue (2010). "The Beclin 1-VPS34 complex--at the crossroads of autophagy and beyond." Trends Cell Biol **20**(6): 355-362.

Furukawa, H., S. K. Singh, R. Mancusso and E. Gouaux (2005). "Subunit arrangement and function in NMDA receptors." Nature **438**(7065): 185-192.

Gasparini, M. V., N.; Schiaffini, C.; Brusa, L.; Panella, M.; Talarico, G.; Bruno, G. (2002). "A case-control study on Alzheimer's disease and exposure to anesthesia." Neurol Sci **23**(1): 11-14.

Gauthier, S., P. Rosa-Neto, Morais JA and C. Webster (2021). "World Alzheimer Report 2021: Journey through the diagnosis of dementia." London, 2021.

Geng, P., J. Zhang, W. Dai, X. Han, Q. Tan, D. Cheng, P. Fang and X. Liu (2018). "Autophagic Degradation Deficit Involved in Sevoflurane-Induced Amyloid Pathology and Spatial Learning Impairment in APP/PS1 Transgenic Mice." Front Cell Neurosci **12**: 185.

Giuffrida, M. L., F. Caraci, P. De Bona, G. Pappalardo, F. Nicoletti, E. Rizzarelli and A. Copani (2010). "The monomer state of beta-amyloid: where the Alzheimer's disease protein meets physiology." Rev Neurosci **21**(2): 83-93.

Giuffrida, M. L., M. F. Tomasello, G. Pandini, F. Caraci, G. Battaglia, C. Busceti, P. Di Pietro, G. Pappalardo, F. Attanasio, S. Chiechio, S. Bagnoli, B. Nacmias, S. Sorbi, R. Vigneri, E. Rizzarelli, F. Nicoletti and A. Copani (2015). "Monomeric ss-amyloid interacts with type-1 insulin-like growth factor receptors to provide energy supply to neurons." Front Cell Neurosci **9**: 297.

Glenner, G. G. and C. W. Wong (1984). "Alzheimer's disease and Down's syndrome: sharing of a unique cerebrovascular amyloid fibril protein." Biochem Biophys Res Commun **122**(3): 1131-1135.

Golomb, J., A. Kluger and S. H. Ferris (2004). "Mild cognitive impairment: historical development and summary of research." Dialogues Clin Neurosci. **6**(4): 351-367.

Gong, Y., L. Chang, K. L. Viola, P. N. Lacor, M. P. Lambert, C. E. Finch, G. A. Krafft and W. L. Klein (2003). "Alzheimer's disease-affected brain: presence of oligomeric A beta ligands (ADDLs) suggests a molecular basis for reversible memory loss." Proc Natl Acad Sci U S A **100**(18): 10417-10422.

Goto, T., H. Saito, M. Shinkai, Y. Nakata, F. Ichinose and S. Morita (1997). "Xenon provides faster emergence from anesthesia than does nitrous oxide-sevoflurane or nitrous oxide-isoflurane." Anesthesiology **86**(6): 1273-1278.

Gotz, J. and L. M. Ittner (2008). "Animal models of Alzheimer's disease and frontotemporal dementia." Nat Rev Neurosci **9**(7): 532-544.

Gouras, G. K., J. Tsai, J. Naslund, B. Vincent, M. Edgar, F. Checler, J. P. Greenfield, V. Haroutunian, J. D. Buxbaum, H. Xu, P. Greengard and N. R. Relkin (2000). "Intraneuronal Aβ42 Accumulation in Human Brain." The American Journal of Pathology **156**(1): 15-20.

Graeber, M. B., S. Kosel, E. Grasbon-Frodl, H. J. Moller and P. Mehraein (1998). "Histopathology and APOE genotype of the first Alzheimer disease patient, Auguste D." Neurogenetics **1**(3): 223-228.

Graeber, M. B. and P. Mehraein (1999). "Reanalysis of the first case of Alzheimer's disease." Eur Arch Psychiatry Clin Neurosci **249 Suppl 3**: 10-13.

Griffin, R. J., A. Moloney, M. Kelliher, J. A. Johnston, R. Ravid, P. Dockery, R. O'Connor and C. O'Neill (2005). "Activation of Akt/PKB, increased phosphorylation of Akt substrates and loss and altered distribution of Akt and PTEN are features of Alzheimer's disease pathology." J Neurochem **93**(1): 105-117.

Grinvald, A., A. Manker and M. Segal (1982). "Visualization of the spread of electrical activity in rat hippocampal slices by voltage-sensitive optical probes." J Physiol **333**: 269-291.

Guivernau, B., J. Bonet, V. Valls-Comamala, M. Bosch-Morato, J. A. Godoy, N. C. Inestrosa, A. Peralvarez-Marin, X. Fernandez-Busquets, D. Andreu, B. Oliva and F. J. Munoz (2016). "Amyloid-beta Peptide Nitrotyrosination Stabilizes Oligomers and Enhances NMDAR-Mediated Toxicity." J Neurosci **36**(46): 11693-11703.

Guix, F. X., I. Uribesalgo, M. Coma and F. J. Munoz (2005). "The physiology and pathophysiology of nitric oxide in the brain." Prog Neurobiol **76**(2): 126-152.

Guntupalli, S., J. Widago and V. Anggono (2016). "Amyloid-β-Induced Dysregulation of AMPA Receptor Trafficking." Neuronal Plasticity: 1-12.

Gupta, A., T. Stierer, R. Zuckerman, N. Sakima, S. D. Parker and L. A. Fleisher (2004). "Comparison of recovery profile after ambulatory anesthesia with propofol, isoflurane, sevoflurane and desflurane: a systematic review." Anesth Analg **98**(3): 632-641, table of contents.

Hampel, H., K. Blennow, L. M. Shaw, Y. C. Hoessler, H. Zetterberg and J. Q. Trojanowski (2010). "Total and phosphorylated tau protein as biological markers of Alzheimer's disease." Exp Gerontol **45**(1): 30-40.

Hapfelmeier, G., W. Zieglgansberger, R. Haseneder, H. Schneck and E. Kochs (2000). "Nitrous Oxide and Xenon Increase the Efficacy of GABA at Recombinant Mammalian GABAA Receptors." Anesthesia & Analgesia **91**(6): 1542-1549.

Hardy, J. and D. Allsop (1991). "Amyloid deposition as the central event in the aetiology of Alzheimer's disease." Trends Pharmacol Sci **12**(10): 383-388.

Harris, K. M. and S. B. Kater (1994). "Dendritic spines: cellular specializations imparting both stability and flexibility to synaptic function." Annu Rev Neurosci **17**: 341-371.

Hasbani, M. J., M. L. Schlief, D. A. Fisher and M. P. Goldberg (2001). "Dendritic spines lost during glutamate receptor activation reemerge at original sites of synaptic contact." J Neurosci **21**(7): 2393-2403.

Haseneder, R., E. Kochs and B. Jungwirth (2012). "[Postoperative cognitive dysfunction. Possible neuronal mechanisms and practical consequences for clinical routine]." Anaesthesist **61**(5): 437-443.

Haseneder, R., S. Kratzer, E. Kochs, V. S. Eckle, W. Zieglgansberger and G. Rammes (2008). "Xenon reduces N-methyl-D-aspartate and alpha-amino-3-hydroxy-5-methyl-4-isoxazolepropionic acid receptor-mediated synaptic transmission in the amygdala." Anesthesiology **109**(6): 998-1006.

Haseneder, R., S. Kratzer, E. Kochs, D. Hofelmann, Y. Auberson, M. Eder and G. Rammes (2009). "The xenon-mediated antagonism against the NMDA receptor is non-selective for receptors containing either NR2A or NR2B subunits in the mouse amygdala." Eur J Pharmacol **619**(1-3): 33-37.

Haseneder, R., S. Kratzer, L. von Meyer, M. Eder, E. Kochs and G. Rammes (2009). "Isoflurane and sevoflurane dose-dependently impair hippocampal long-term potentiation." Eur J Pharmacol **623**(1-3): 47-51.

Haseneder, R., L. Starker, J. Berkmann, K. Kellermann, B. Jungwirth, M. Blobner, M. Eder, E. Kochs and G. Rammes (2013). "Sevoflurane anesthesia improves cognitive performance in mice, but does not influence in vitro long-term potentation in hippocampus CA1 stratum radiatum." PLoS One **8**(5): e64732.

Head, B. P., H. H. Patel, I. R. Niesman, J. C. Drummond, D. M. Roth and P. M. Patel (2009). "Inhibition of p75 neurotrophin receptor attenuates isoflurane-mediated neuronal apoptosis in the neonatal central nervous system." Anesthesiology **110**(4): 813-825.

Hebb, D. O. (1949). "The organization of behavior; a neuropsychological theory." Oxford, England: Wiley.

Heras-Sandoval, D., J. M. Perez-Rojas, J. Hernandez-Damian and J. Pedraza-Chaverri (2014). "The role of PI3K/AKT/mTOR pathway in the modulation of autophagy and the clearance of protein aggregates in neurodegeneration." Cell Signal **26**(12): 2694-2701.

Herbert, L. E., J. Weuve, P. A. Scherr and D. A. Evans (2013). "Alzheimer disease in the United States (2010-2050) estimated using the 2010 census." Neurology **80**(19): 1778-1783.

Hering, H. and M. Sheng (2002). "Dendritic Spines: Structure, Dynamics and Regulation." Nature reviews. Neuroscience **2**(12): 880.888.

Herman, M. A. and C. E. Jahr (2007). "Extracellular glutamate concentration in hippocampal slice." J Neurosci **27**(36): 9736-9741.

Hiltunen, M., T. van Groen and J. Jolkkonen (2009). "Functional roles of amyloid-beta protein precursor and amyloid-beta peptides: evidence from experimental studies." J Alzheimers Dis **18**(2): 401-412.

Hsiao, M.-C. S., D.; Berger, T.W. (2013). "Nonlinear dynamical model based control of in vitro hippocampal output." Front Neural Circuits **7**: 20.

Hulstaert, F., K. Blennow, A. Ivanoiu, H. C. Schoonderwaldt, M. Riemenschneider, P. P. De Deyn, C. Bancher, P. Cras, J. Wiltfang, P. D. Mehta, K. Iqbal, H. Pottel, E. Vanmechelen and H. Vanderstichele (1999). "Improved discrimination of AD patients using beta-amyloid(1-42) and tau levels in CSF." Neurology **52**(8): 1555-1562.

Humpel, C. (2015). "Organotypic brain slice cultures: A review." Neuroscience **305**: 86-98.

Ishizeki, J., K. Nishikawa, K. Kubo, S. Saito and F. Goto (2008). "Amnestic concentrations of sevoflurane inhibit synaptic plasticity of hippocampal CA1 neurons through gamma-aminobutyric ac- id-mediated mechanisms." Anesthesiology **108**: 447-456.

Iwatsubo, T., A. Odaka, N. Suzuki, H. Mizushima, N. Nukina and Y. Ihara (1994). "Visualization of A beta 42(43) and A beta 40 in senile plaques with end-specific A beta monoclonals: evidence that an initially deposited species is A beta 42(43)." Neuron **13**(1): 45-53.

Jaber, N., Z. Dou, J. S. Chen, J. Catanzaro, Y. P. Jiang, L. M. Ballou, E. Selinger, X. Ouyang, R. Z. Lin, J. Zhang and W. X. Zong (2012). "Class III PI3K Vps34 plays an essential role in autophagy and in heart and liver function." Proc Natl Acad Sci U S A **109**(6): 2003-2008.

Jarrett, J. T., E. P. Berger and P. T. Lansbury, Jr. (1993). "The carboxy terminus of the beta amyloid protein is critical for the seeding of amyloid formation: implications for the pathogenesis of Alzheimer's disease." Biochemistry **32**(18): 4693-4697.

Jiang, J. and H. Jiang (2015). "Effect of the inhaled anesthetics isoflurane, sevoflurane and desflurane on the neuropathogenesis of Alzheimer's disease (review)." Mol Med Rep **12**(1): 3-12.

Jiang, M., L. Sun, D. X. Feng, Z. Q. Yu, R. Gao, Y. Z. Sun and G. Chen (2017). "Neuroprotection provided by isoflurane pre-conditioning and post-conditioning." Med Gas Res **7**(1): 48-55.

Jones, P. M., D. Bainbridge, M. W. Chu, P. S. Fernandes, S. A. Fox, I. Iglesias, B. Kiaii, R. Lavi and J. M. Murkin (2016). "Comparison of isoflurane and sevoflurane in cardiac surgery: a randomized non-inferiority comparative effectiveness trial." Can J Anaesth **63**(10): 1128-1139.

Joyce, J. A. (2000). "Xenon: anesthesia for the 21st century." AANA J **68**(3): 259-264.

Jungwirth, B., W. Zieglgansberger, E. Kochs and G. Rammes (2009). "Anesthesia and postoperative cognitive dysfunction (POCD)." Mini Rev Med Chem **9**(14): 1568-1579.

Jurado, S. (2018). "AMPA Receptor Trafficking in Natural and Pathological Aging." Front Molec Neuroscience **10: 446**: 1-14.

Kabeya, Y., N. Mizushima, T. Ueno, A. Yamamoto, T. Kirisako, T. Noda, E. Kominami, Y. Ohsumi and T. Yoshimori (2000). "LC3, a mammalian homologue of yeast Apg8p, is localized in autophagosome membranes after processing." EMBO J **19**(21): 5720-5728.

Kapila, A. K., H. R. Watts, T. Wang and D. Ma (2014). "The impact of surgery and anesthesia on post-operative cognitive decline and Alzheimer's disease development: biomarkers and preventive strategies." J Alzheimers Dis **41**(1): 1-13.

Kerenyi, L. and F. Gallyas (1973). "[Agar electrophoresis of low-protein biological fluids without previous condensation]." Orv Hetil **114**(19): 1105-1107.

Knobloch, M. and I. M. Mansuy (2008). "Dendritic spine loss and synaptic alterations in Alzheimer's disease." Mol Neurobiol **37**(1): 73-82.

Koblin, D. D., Z. Fang, E. I. Eger, 2nd, M. Laster, D. Gong, P. Ionescu, M. Halsey and J. R. Trudell (1998). "Minimum Alveolar Concentrations of Noble Gases, Nitrogen, and Sulfur Hexafluoide in Rats." Anaesthesia & Analgesia **87**(2): 419-424.

Komatsu, M., S. Waguri, T. Chiba, S. Murata, J. Iwata, I. Tanida, T. Ueno, M. Koike, Y. Uchiyama, E. Kominami and K. Tanaka (2006). "Loss of autophagy in the central nervous system causes neurodegeneration in mice." Nature **441**(7095): 880-884.

Kratzer, S., C. Mattusch, E. Kochs, M. Eder, R. Haseneder and G. Rammes (2012). "Xenon Attenuates Hippocampal Long-term Potentiation by Diminishing Synaptic and Extrasynaptic N-methyl-D-aspartate Receptor Currents." Anesthesiology **116**(3): 673-682.

Kuchibhotla, K. V., S. T. Goldman, C. R. Lattarulo, H.-Y. Wu, B. Hyman and B. J. Bacskai (2008). "Aβ Plaques Lead to Aberrant Regulation of Calcium Homeostasis In Vivo Resulting in Structural and Functional Disruption of Neuronal Networks." Neuron **59**(2): 214-225.

Kuma, A., N. Mizushima, N. Ishihara and Y. Ohsumi (2002). "Formation of the approximately 350-kDa Apg12-Apg5.Apg16 multimeric complex, mediated by Apg16 oligomerization, is essential for autophagy in yeast." J Biol Chem **277**(21): 18619-18625.

Kummer, M. P. and M. T. Heneka (2014). "Truncated and modified amyloid-beta species." Alzheimers Res Ther **6**(3): 28.

Kummer, M. P., M. Hermes, A. Delekarte, T. Hammerschmidt, S. Kumar, D. Terwel, J. Walter, H. C. Pape, S. Konig, S. Roeber, F. Jessen, T. Klockgether, M. Korte and M. T. Heneka (2011). "Nitration of tyrosine 10 critically enhances amyloid beta aggregation and plaque formation." Neuron **71**(5): 833-844.

Lai, F. and R. S. Williams (1989). "A prospective study of Alzheimer disease in Down syndrome." Arch Neurol **46**(8): 849-853.

Lambert, M. P., A. K. Barlow, B. A. Chromy, C. Edwards, R. Freed, M. Liosatos, T. E. Morgan, I. Rozovsky, B. Trommer, K. L. Viola, P. Wals, C. Zhang, C. E. Finch, G. A. Krafft and W. L. Klein (1998). "Diffusible, nonfibrillar ligands derived from Abeta1-42 are potent central nervous system neurotoxins." Proc Natl Acad Sci U S A **95**(11): 6448-6453.

Lammich, S., E. Kojro, R. Postina, S. Gilbert, R. Pfeiffer, M. Jasionowski, C. Haass and F. Fahrenholz (1999). "Constitutive and regulated alpha-secretase cleavage of Alzheimer's amyloid precursor protein by a disintegrin metalloprotease." Proc Natl Acad Sci U S A **96**(7): 3922-3927.

Lavaur, J., M. Lemaire, J. Pype, D. Le Nogue, E. C. Hirsch and P. P. Michel (2016). "Xenon-mediated neuroprotection in response to sustained, low-level excitotoxic stress." Cell Death Discov **2**: 16018.

Lei, M., H. Xu, Z. Li, Z. Wang, T. T. O'Malley, D. Zhang, D. M. Walsh, P. Xu, D. J. Selkoe and S. Li (2016). "Soluble Aβ Oligomers Impair Hippocampal LTP by Disrupting Glutamatergic/GABAergic Balance." Neurobiol Dis **85**: 111-121.

Lendvai, B., E. A. Stern, B. Chen and K. Svoboda (2000). "Experience-dependent plasticity of dendritic spines in the developing rat barrel cortex in vivo." Nature **404**(6780): 876-881.

Li, Y., H. Sun, Z. Chen, H. Xu, G. Bu and H. Zheng (2016). "Implications of GABAergic Neurotransmission in Alzheimer's Disease." Front Aging Neurosci **8**(31): 1-12.

Liu, J., L. Chang, Y. Song, H. Li and Y. Wu (2019). "The Role of NMDA Receptors in Alzheimer's Disease." Front Neurosci **13**: 43.

Liu, J., X. Zhang, W. Zhang, G. Gu and P. Wang (2015). "Effects of Sevoflurane on Young Male Adult C57BL/6 Mice Spatial Cognition." PLoS One **10**(8): e0134217.

Liu, Y., J. T. Kern, J. R. Walker, J. A. Johnson, P. G. Schultz and H. Luesch (2007). "A genomic screen for activators of the antioxidant response element." Proc Natl Acad Sci U S A **104**(12): 5205-5210.

Liu, Y., N. Pan, Y. Ma, S. Zhang, W. Guo, H. Li, J. Zhou, G. Liu and M. Gao (2013). "Inhaled sevoflurane may promote progression of amnestic mild cognitive impairment: a prospective, randomized parallel-group study." Am J Med Sci **345**(5): 355-360.

Loew, L. M. (2015). "Design and Use of Organic Voltage Sensitive Dyes." Adv Exp Med Biol **859**: 27-53.

Lu, Y., X. Wu, Y. Dong, Z. Xu, Y. Zhang and Z. Xie (2010). "Anesthetic sevoflurane causes neurotoxicity differently in neonatal naive and Alzheimer disease transgenic mice." Anesthesiology **112**(6): 1404-1416.

Luscher, C. and R. C. Malenka (2012). "NMDA receptor-dependent long-term potentiation and long-term depression (LTP/LTD)." Cold Spring Harb Perspect Biol **4**(6).

Ma, J. F., Y. Huang, S. D. Chen and G. Halliday (2010). "Immunohistochemical evidence for macroautophagy in neurones and endothelial cells in Alzheimer's disease." Neuropathol Appl Neurobiol **36**(4): 312-319.

Malenka, R. C. and R. A. Nicoll (1999). "Long-Term Potentiation - A decade of progress." Science **285**: 1870-1875.

Maletic-Savatic, M., R. Malinow and K. Svoboda (1999). "Rapid dendritic morphogenesis in CA1 hippocampal dendrites induced by synaptic activity." Science **283**(5409): 1923-1927.

Mandal, P. K. and V. Fodale (2009). "Smaller molecular-sized anaesthetics oligomerize Abeta peptide simulating Alzheimer's disease: a relevant issue." Eur J Anaesthesiol **26**(10): 805-806.

Mapleson, W. W. (1996). "Effect of age on MAC in humans." Br J Anaesth **76**: 179-185.

Martin, L. J., G. H. Oh and B. A. Orser (2009). "Etomidate targets alpha5 gamma-aminobutyric acid subtype A receptors to regulate synaptic plasticity and memory blockade." Anesthesiology **111**: 1025-1035.

Martinez-Coria, H., K. N. Green, L. M. Billings, M. Kitazawa, M. Albrecht, G. Rammes, C. G. Parsons, S. Gupta, P. Banerjee and F. M. LaFerla (2010). "Memantine Improves Cognition and Reduces Alzheimer's-Like Neuropathology in Transgenic Mice." The American Journal of Pathology **176**(2): 870-880.

Mattusch, C., S. Kratzer, M. Buerge, M. Kreuzer, T. Engel, C. Kopp, M. Biel, V. Hammelmann, S. W. Ying, P. A. Goldstein, E. Kochs, R. Haseneder and G. Rammes (2015). "Impact of Hyperpolarization-activated, Cyclic Nucleotide-gated Cation Channel Type 2 for the Xenon-mediated Anesthetic Effect: Evidence from In Vitro and In Vivo Experiments." Anesthesiology **122**(5): 1047-1059.

McCann, R. F. and D. A. Ross (2017). "A Fragile Balance: Dendritic Spines, Learning, and Memory." Biol Psychiatry **82**(2): e11-e13.

Mendez, M. F., P. Catanzaro, R. C. Doss, R. ARguello and W. H. n. Frey (1994). "Seizures in Alzheimer's disease: clinicopathologic study." J Geriatr Psychiatry Neurol. **7**(4): 230-233.

Merino-Serrais, P., S. Knafo, L. Alonso-Nanclares, I. Fernaud-Espinosa and J. DeFelipe (2011). "Layer-specific alterations to CA1 dendritic spines in a mouse model of Alzheimer's disease." Hippocampus **21**(10): 1037-1044.

Metcalf, D. J., M. Garcia-Arencibia, W. E. Hochfeld and D. C. Rubinsztein (2012). "Autophagy and misfolded proteins in neurodegeneration." Exp Neurol **238**(1): 22-28.

Mizushima, N. (2007). "Autophagy: process and function." Genes Dev **21**(22): 2861-2873.

Mizushima, N., Y. Ohsumi and T. Yoshimori (2002). "Autophagosome formation in mammalian cells." Cell Struct Funct **27**(6): 421-429.

Morad, M. and G. Salama (1979). "Optical probes of membrane potential in heart muscle." The Journal of Physiology **292**(1): 267-295.

Morris, J. C., M. Storandt, J. P. Miller, D. W. McKeel, J. L. Price, E. H. Rubin and L. Berg (2001). "Mild cognitive impairment represents early-stage Alzheimer disease." Arch Neurol **58**(3): 397-405.

Moscat, J. and M. T. Diaz-Meco (2009). "p62 at the crossroads of autophagy, apoptosis, and cancer." Cell **137**(6): 1001-1004.

Mühlpfordt, H. and K. Bachnicki (2008). "Schematic of a fluorescence microscope." Wikimedia.

Nagashima, K., C. F. Zorumski and Y. Izumi (2005). "Propofol Inhibits Long-term Potentiation but Not Long-term Depression in Rat Hippocampal Slices." Anesthesiology **103**: 318-326.

Nakata, Y., T. Goto, Y. Ishiguro, K. Terui, H. Kawakami, M. Santo, Y. Niimi and S. Morita (2001). "Minimum alveolar concentration (MAC) of xenon with sevoflurane in humans." Anesthesiology **94**(4): 611-614.

Ni, C., C. Li, Y. Dong, X. Guo, Y. Zhang and Z. Xie (2017). "Anesthetic Isoflurane Induces DNA Damage Through Oxidative Stress and p53 Pathway." Mol Neurobiol **54**(5): 3591-3605.

Nickalls, R. W. D. and W. W. Mapleson (2003). "Age-related iso-MAC charts for isoflurane, sevoflurane and desflurane in man." British Journal of Anaesthesia **91**(2): 170–174.

Nilsson, P. and T. C. Saido (2014). "Dual roles for autophagy: degradation and secretion of Alzheimer's disease Abeta peptide." Bioessays **36**(6): 570-578.

Nixon, R. A., J. Wegiel, A. Kumar, W. H. Yu, C. Peterhoff, A. Cataldo and A. M. Cuervo (2005). "Extensive involvement of autophagy in Alzheimer disease: an immuno-electron microscopy study." J Neuropathol Exp Neurol **64**(2): 113-122.

Nixon, R. A. and D. S. Yang (2011). "Autophagy failure in Alzheimer's disease--locating the primary defect." Neurobiol Dis **43**(1): 38-45.

Nussbaum, J. M., S. Schilling, H. Cynis, A. Silva, E. Swanson, T. Wangsanut, K. Tayler, B. Wiltgen, A. Hatami, R. Ronicke, K. Reymann, B. Hutter-Paier, A. Alexandru, W. Jagla, S. Graubner, C. G. Glabe, H. U. Demuth and G. S. Bloom (2012). "Prion-like behaviour and tau-dependent cytotoxicity of pyroglutamylated amyloid-beta." Nature **485**(7400): 651-655.

O' Neill, C. (2013). "PI3-kinase/Akt/mTOR signaling: Impaired on/off switches in aging, cognitive decline and Alzheimer's disease." Exp Gerontol **48**(7): 647-653.

O'Keefe, J. N., L. (1978). The Hippocampus as a Cognitive Map.

Oddo, S., A. Caccamo, J. D. Shepherd, M. P. Murphy, T. E. Golde, R. Kayed, R. Metherate, M. P. Mattson, Y. Akbari and F. M. LaFerla (2003). "Triple-transgenic model of Alzheimer's disease with plaques and tangles: intracellular Abeta and synaptic dysfunction." Neuron **39**(3): 409-421.

Ohyagi, Y., H. Asahara, D. H. Chui, Y. Tsuruta, N. Sakae, K. Miyoshi, T. Yamada, H. Kikuchi, T. Taniwaki, H. Murai, K. Ikezoe, H. Furuya, T. Kawarabayashi, M. Shoji, F. Checler, T. Iwaki, T. Makifuchi, K. Takeda, J. Kira and T. Tabira (2005). "Intracellular Abeta42 activates p53 promoter: a pathway to neurodegeneration in Alzheimer's disease." FASEB J **19**(2): 255-257.

Okasha, A. and O. Madkour (1982). "Cortical and central atrophy in chronic schizophrenia. A controlled study." Acta Psychiatr Scand **65**(1): 29-34.

Papa, M., M. C. Bundman, V. Greenberger and M. Segal (1995). "Morphological analysis of dendritic spine development in primary cultures of hippocampal neurons." J Neurosci **15**(1 Pt 1): 1-11.

Parsons, C. G. and G. Rammes (2017). "Preclinical to Phase II Amyloid beta (Aβ) peptide modulators under investigation for Alzheimer's disease." Expert Opinion on Investigational Drugs **26**(5): 579-592.

Parsons, C. G., M. Ruitenberg, C. E. Freitag, K. Sroka-Saidi, H. Russ and G. Rammes (2015). MRZ-99030 - A novel modulator of Abeta aggregation: I - Mechanism of action (MoA) underlying the potential neuroprotective treatment of Alzheimer's disease, glaucoma and age-related macular degeneration (AMD). Neuropharmacology. **92:** 158-169.

Parsons, C. G., A. Stoffler and W. Danysz (2007). "Memantine: a NMDA receptor antagonist that improves memory by restoration of homeostasis in the glutamatergic system--too little activation is bad, too much is even worse." Neuropharmacology **53**(6): 699-723.

Pearson, H. and C. Peers (2006). "Physiological roles for amyloid β peptides." J Physiol **575**(1): 5-10.

Penzes, P., M. E. Cahill, K. A. Jones, J. E. VanLeeuwen and K. M. Woolfrey (2011). "Dendritic spine pathology in neuropsychiatric disorders." Nat Neurosci **14**(3): 285-293.

Perucho, J., M. J. Casarejos, A. Gomez, J. A. Rodriguez-Navarro, R. M. Solano, J. G. De Yébenes and M. A. Mena (2010). "Anesthesia with isoflurane increases amyloid pathology in mice models of Alzheimer's disease. ." J Alzheimers Dis **19**: 1245-1257.

Perucho, J., I. Rubio, M. J. Casarejos, A. Gomez, J. A. Rodriguez-Navarro, R. M. Solano, J. G. De Yebenes and M. A. Mena (2010). "Anesthesia with isoflurane increases amyloid pathology in mice models of Alzheimer's disease." J Alzheimers Dis **19**(4): 1245-1257.

Pike, C. J., D. Burdick, A. J. Walencewicz, C. G. Glabe and C. W. Cotman (1993). "Neurodegeneration induced by beta-amyloid peptides in vitro: the role of peptide assembly state." J Neurosci **13**(4): 1676-1687.

Pini, L., M. Pievani, M. Bocchetta, D. Altomare, P. Bosco, E. Cavedo, S. Galluzzi, M. M. and G. Frisoni (2016). "Brain atrophy in Alzheimer's Disease and aging." Ageing Research Reviews **30**: 25-48.

Preckel, B., W. Schlack, T. Heibel and H. Rutten (2002). "Xenon produces minimal haemodynamic effects in rabbits with chronically compromised left ventricular function." Br J Anaesth **88**(2): 264-269.

Pryor, N. E., M. A. Moss and C. N. Hestekin (2012). "Unraveling the early events of amyloid-beta protein (Abeta) aggregation: techniques for the determination of Abeta aggregate size." Int J Mol Sci **13**(3): 3038-3072.

Puzzo, D., L. Privitera, E. Leznik, M. Fá, A. Staniszewski, A. Palmeri and O. Arancio (2008). "Picomolar Amyloid-ß Positively Modulates Synaptic Plasticity and Memory in the hippocampus." The Journal of Neuroscience **28**(53): 14537-14545.

Rammes, G., A. Gravius, M. Ruitenberg, N. Wegener, C. Chambon, K. Sroka-Saidi, R. Jeggo, L. Staniaszek, D. Spanswick, E. O'Hare, P. Palmer, E. M. Kim, W. Bywalez, V. Egger and C. G. Parsons (2015). "MRZ-99030 - A novel modulator of Abeta aggregation: II - Reversal of Abeta oligomer-induced deficits in long-term potentiation (LTP) and cognitive performance in rats and mice." Neuropharmacology **92**: 170-182.

Rammes, G., A. Hasenjager, K. Sroka-Saidi, J. M. Deussing and C. G. Parsons (2011). "Therapeutic significance of NR2B-containing NMDA receptors and mGluR5 metabotropic glutamate receptors in mediating the synaptotoxic effects of beta-amyloid oligomers on long-term potentiation (LTP) in murine hippocampal slices." Neuropharmacology **60**(6): 982-990.

Rammes, G., F. Seeser, K. Mattusch, K. Zhu, L. Haas, M. Kummer, M. Heneka, J. Herms and C. G. Parsons (2018). "The NMDA receptor antagonist Radiprodil reverses the synaptotoxic effects of different amyloid-beta (Abeta) species on long-term potentiation (LTP)." Neuropharmacology.

Rammes, G., L. K. Starker, R. Haseneder, J. Berkmann, A. Plack, W. Zieglgansberger, F. Ohl, E. F. Kochs and M. Blobner (2009). "Isoflurane anaesthesia reversibly improves cognitive function and long-term potentiation (LTP) via an up-regulation in NMDA receptor 2B subunit expression." Neuropharmacology **56**(3): 626-636.

Ramsay, W. (1903). "An attempt to estimate the relative amounts of krypton and of xenon in atmospheric air." Royal Society **71**(467-476).

Rao, Z., X. Pan, H. Zhang, J. Sun, J. Li, T. Lu, M. Gao, S. Liu, D. Yu and Z. Ding (2017). "Isoflurane Preconditioning Alleviated Murine Liver Ischemia and Reperfusion Injury by Restoring AMPK/mTOR-Mediated Autophagy." Anesth Analg **125**(4): 1355-1363.

Reisberg, B., R. Doody, A. Stoffler, F. Schmitt, S. Ferris, H. J. Mobius and G. Memantine Study (2003). "Memantine in moderate-to-severe Alzheimer's disease." N Engl J Med **348**(14): 1333-1341.

Rossi, F. and E. Bianchini (1996). "Synergistic induction of nitric oxide by beta-amyloid and cytokines in astrocytes." Biochem Biophys Res Commun **225**(2): 474-478.

Rubinstein, A. D., M. Eisenstein, Y. Ber, S. Bialik and A. Kimchi (2011). "The autophagy protein Atg12 associates with antiapoptotic Bcl-2 family members to promote mitochondrial apoptosis." Mol Cell **44**(5): 698-709.

Ruddy, R. M., Y. Chen, M. Milenkovic and A. J. Ramsey (2015). "Differential effects of NMDA receptor antagonism on spine density." Synapse **69**(1): 52-56.

Rudolph, U. and B. Antkowiak (2004). "Molecular and neuronal substrates for general anaesthetics." Nat Rev Neurosci **5**(9): 709-720.

Russell, R. C., Y. Tian, H. Yuan, H. W. Park, Y. Y. Chang, J. Kim, H. Kim, T. P. Neufeld, A. Dillin and K. L. Guan (2013). "ULK1 induces autophagy by phosphorylating Beclin-1 and activating VPS34 lipid kinase." Nat Cell Biol **15**(7): 741-750.

Russo, C., T. C. Saido, L. M. DeBusk, M. Tabaton, P. Gambetti and J. K. Teller (1997). "Heterogeneity of water-soluble amyloid beta-peptide in Alzheimer's disease and Down's syndrome brains." FEBS Lett **409**(3): 411-416.

Saglietti, L., C. Dequidt, K. Kamieniarz, M. C. Rousset, P. Valnegri, O. Thoumine, F. Beretta, L. Fagni, D. Choquet, C. Sala, M. Sheng and M. Passafaro (2007). "Extracellular interactions between GluR2 and N-cadherin in spine regulation." Neuron **54**(3): 461-477.

Salminen, A., K. Kaarniranta, A. Kauppinen, J. Ojala, A. Haapasalo, H. Soininen and M. Hiltunen (2013). "Impaired autophagy and APP processing in Alzheimer's disease: The potential role of Beclin 1 interactome." Prog Neurobiol **106-107**: 33-54.

Salzberg, B. M., D. H. V. and L. B. Cohen (1973). "Optical recording of impulses in individual neurones of an invertebrate central nervous system." Nature **246**(5434): 508-509.

Sapolsky, R. M. (2001). "Atrophy of the hippocampus in posttraumatic stress disorder: how and when?" Hippocampus **11**(2): 90-101.

Sapolsky, R. M. (2001). "Depression, antidepressants, and the shrinking hippocampus." Proc Natl Acad Sci U S A **98**(22): 12320-12322.

Schaefer, M. S., C. C. Apfel, H. J. Sachs, R. Stuttmann, B. Bein, P. H. Tonner, M. Hein, M. Neukirchen, M. Reyle-Hahn and P. Kienbaum (2015). "Predictors for postoperative nausea and vomiting after xenon-based anaesthesia." Br J Anaesth **115**(1): 61-67.

Scheff, S. W., D. A. Price, F. A. Schmitt and E. J. Mufson (2006). "Hippocampal synaptic loss in early Alzheimer's disease and mild cognitive impairment." Neurobiol Aging **27**(10): 1372-1384.

Scheff, S. W., D. L. Price, F. A. Schmitt, S. T. DeKosky and E. J. Mufson (2007). "Synaptic alterations in CA1 in mild Alzheimer disease and mild cognitive impairment." Neurology **68**(18): 1501-1508.

Schlenzig, D., S. Manhart, Y. Cinar, M. Kleinschmidt, G. Hause, D. Willbold, S. A. Funke, S. Schilling and H. U. Demuth (2009). "Pyroglutamate formation influences solubility and amyloidogenicity of amyloid peptides." Biochemistry **48**(29): 7072-7078.

Schlenzig, D., R. Ronicke, H. Cynis, H. H. Ludwig, E. Scheel, K. Reymann, T. Saido, G. Hause, S. Schilling and H. U. Demuth (2012). "N-Terminal pyroglutamate formation of Abeta38 and Abeta40 enforces oligomer formation and potency to disrupt hippocampal long-term potentiation." J Neurochem **121**(5): 774-784.

Schmid, S., G. Rammes, M. Blobner, K. Kellermann, S. Bratke, D. Fendl, Z. Kaichuan, G. Schneider and B. Jungwirth (2019). "Cognitive decline in Tg2576 mice shows sex-specific differences and correlates with cerebral amyloid-beta." Behav Brain Res **359**: 408-417.

Schmitz, C., B. P. F. Rutten, A. Pielen, S. Schäfer, O. Wirths, G. Tremp, C. Czech, V. Blanchard, G. Multhaup, P. Rezaie, H. Korr, H. W. M. Steinbusch, L. Pradier and T. A. Bayer (2004). "Hippocampal Neuron Loss Exceeds Amyloid Plaque Load in a Transgenic Mouse Model of Alzheimer's Disease." The American Journal of Pathology **164**(4): 1495-1502.

Scoville, W. B. M., B. (1957). "Loss of recent memory after bilateral hippocampal lesions." J Neurol Neurosurg Psychiatry **20**(1): 11-21.

Seitz, D. P., P. S. Shah, N. Herrmann, J. Beyene and N. Siddiqui (2011). "Exposure to general anesthesia and risk of Alzheimer's disease: a systematic review and meta-analysis." BMC Geriatr **11**: 83.

Selkoe, D. J. (2000). "Toward a comprehensive theory for Alzheimer's disease. Hypothesis: Alzheimer's disease is caused by the cerebral accumulation and cytotoxicity of amyloid beta-protein." Ann N Y Acad Sci **924**: 17-25.

Selkoe, D. J. (2001). "Alzheimer's disease results from the cerebral accumulation and cytotoxicity of amyloid beta-protein." J Alzheimers Dis **3**(1): 75-80.

Selkoe, D. J. (2001). "Alzheimer's disease: genes, proteins, and therapy." Physiol Rev **81**(2): 741-766.

Selkoe, D. J. (2005). "Defining molecular targets to prevent Alzheimer disease." Arch Neurol **62**(2): 192-195.

Serra-Batiste, M., M. Ninot-Pedrosa, M. Bayoumi, M. Gairi, G. Maglia and N. Carulla (2016). "Abeta42 assembles into specific beta-barrel pore-forming oligomers in membrane-mimicking environments." Proc Natl Acad Sci U S A **113**(39): 10866-10871.

Shankar, G. M., B. L. Bloodgood, M. Townsend, D. M. Walsh, D. J. Selkoe and B. L. Sabatini (2007). "Natural oligomers of the Alzheimer amyloid-beta protein induce reversible synapse loss by modulating an NMDA-type glutamate receptor-dependent signaling pathway." J Neurosci **27**(11): 2866-2875.

Shankar, G. M., S. Li, T. H. Mehta, A. Garcia-Munoz, N. E. Shepardson, S. I., F. M. Brett, M. A. Farrell, M. J. Rowan, C. A. Lemere, C. M. Regan, D. M. Walsh, B. L. Sabatini and D. J. Selkoe (2008). "Amyloid β-Protein Dimers Isolated Directly from Alzheimer BrainsImpair Synaptic Plasticity and Memory." Nat Med **14**(8): 837-842.

Sheng, J. G., D. L. Price and V. E. Koliatsos (2002). "Disruption of corticocortical connections ameliorates amyloid burden in terminal fields in a transgenic model of Abeta amyloidosis." J Neurosci **22**(22): 9794-9799.

Sherrington, R., E. I. Rogaev, Y. Liang, E. A. Rogaeva, G. Levesque, M. Ikeda, H. Chi, C. Lin, G. Li, K. Holman, T. Tsuda, L. Mar, J. F. Foncin, A. C. Bruni, M. P. Montesi, S. Sorbi, I. Rainero, L. Pinessi, L. Nee, I. Chumakov, D. Pollen, A. Brookes, P. Sanseau, R. J. Polinsky, W. Wasco, H. A. Da Silva, J. L. Haines, M. A. Perkicak-Vance, R. E. Tanzi, A. D. Roses, P. E. Fraser, J. M. Rommens and P. H. St George-Hyslop (1995). "Cloning of a gene bearing missense mutations in early-onset familial Alzheimer's disease." Nature **375**(6534): 754-760.

Shiomi, M., M. Miyamae, G. Takemura, K. Kaneda, Y. Inamura, A. Onishi, S. Koshinuma, Y. Momota, T. Minami and V. Figueredo (2013). "Sevoflurane induces cardioprotection through reactive oxygen species-mediated upregulation of autophagy in isolated guinea pig hearts." Journal of Anesthesia **28**: 593-600.

Simon, W., G. Hapfelmeier, E. Kochs, W. Zieglgansberger and G. Rammes (2001). "Isoflurane blocks synaptic plasticity in the mouse hippocampus." Anesthesiology **94**(6): 1058-1065.

Simon, W., G. Hapfelmeier, E. Kochs, W. Zieglgansberger and G. Rammes (2001). "Isoflurane blocks synaptic plasticity in the mouse hippocampus." Anesthesiology **94**: 1058-1065.

Sinha, S., J. P. Anderson, R. Barbour, G. S. Basi, R. Caccavello, D. Davis, M. Doan, H. F. Dovey, N. Frigon, J. Hong, K. Jacobson-Croak, N. Jewett, P. Keim, J. Knops, I. Lieberburg, M. Power, H. Tan, G. Tatsuno, J. Tung, D. Schenk, P. Seubert, S. M. Suomensaari, S. Wang, D. Walker, J. Zhao, L. McConlogue and V. John (1999). "Purification and cloning of amyloid precursor protein beta-secretase from human brain." Nature **402**(6761): 537-540.

Smith, D. L., J. Pozueta, B. Gong, O. Arancio and M. Shelanski (2009). "Reversal of long-term dendritic spine alterations in Alzheimer disease models." Proc Natl Acad Sci U S A **106**(39): 16877-16882.

Sonner, J., D. Gong and E. Edmond (2000). "Naturally Occurring Variability in Anesthetic Potency Among Inbred Mouse Strains." Anesth Analg **91**(3): 720-726.

Soscia, S. J., J. E. Kirby, K. J. Washicosky, S. M. Tucker, M. Ingelsson, B. Hyman, M. A. Burton, L. E. Goldstein, S. Duong, R. E. Tanzi and R. D. Moir (2010). "The Alzheimer's disease-associated amyloid beta-protein is an antimicrobial peptide." PLoS One **5**(3): e9505.

Spires, T. L., M. Meyer-Luehmann, E. A. Stern, P. J. McLean, J. Skoch, P. T. Nguyen, B. J. Bacskai and B. T. Hyman (2005). "Dendritic spine abnormalities in amyloid precursor protein transgenic mice demonstrated by gene transfer and intravital multiphoton microscopy." J Neurosci **25**(31): 7278-7287.

Spires-Jones, T. L. and B. Hyman (2014). "The Intersection of Amyloid Beta and Tau at Synapse in Alzheimer's Disease." Neuron **82**(4): 756-771.

Squire, L. R. (2009). "The legacy of patient H.M. for neuroscience." NEURON **61**(1): 6-9.

Squire, L. R. and C. B. Cave (1991). "The hippocampus, memory, and space." Hippocampus **1**(3): 269-271.

Stine, W. B., Jr., K. N. Dahlgren, G. A. Krafft and M. J. LaDu (2003). "In vitro characterization of conditions for amyloid-beta peptide oligomerization and fibrillogenesis." J Biol Chem **278**(13): 11612-11622.

Stolow, A. (2003). "Femtosecond Time-Resolved Photoelectron Spectroscopy of Polyatomic Molecules." Ann Rev Phys Chem **54**: 89-119.

Su, D., Y. Zhao, H. Xu, B. Wang, X. Chen, J. Chen and X. Wang (2012). "Isoflurane exposure during mid-adulthood attenuates age-related spatial memory impairment in APP/PS1 transgenic mice." PLoS One **7**(11): e50172.

Suzuki, K., Y. Kubota, T. Sekito and Y. Ohsumi (2007). "Hierarchy of Atg proteins in pre-autophagosomal structure organization." Genes Cells **12**(2): 209-218.

Takahashi, R. H., C. G. Almeida, P. F. Kearney, F. Yu, M. T. Lin, T. A. Milner and G. K. Gouras (2004). "Oligomerization of Alzheimer's beta-amyloid within processes and synapses of cultured neurons and brain." J Neurosci **24**(14): 3592-3599.

Takamura, A., M. Komatsu, T. Hara, A. Sakamoto, C. Kishi, S. Waguri, Y. Eishi, O. Hino, K. Tanaka and N. Mizushima (2011). "Autophagy-deficient mice develop multiple liver tumors." Genes Dev **25**(8): 795-800.

Takashima, S., A. Ieshima, H. Nakamura and L. E. Becker (1989). "Dendrites, dementia and the Down syndrome." Brain Dev **11**(2): 131-133.

Tan, H., R. R. Ren, Z. Q. Xiong and Y. W. Wang (2009). "Effects of ketamine and midazolam on morphology of dendritic spines in hippocampal CA1 region of neonatal mice." Chin Med J (Engl) **122**(4): 455-459.

Tang, J. X., D. Baranov, M. Hammond, L. M. Shaw, M. F. Eckenhoff and R. G. Eckenhoff (2011). "Human Alzheimer and inflammation biomarkers after anesthesia and surgery." Anesthesiology **115**(4): 727-732.

Tasaki, I., A. Watanabe, R. Sandlin and L. Carnay (1968). "Changes in fluorescence, turbidity, and birefringence associated with nerve excitation." Proc Natl Acad Sci U S A **61**(3): 883-888.

Tekirian, T. L., T. C. Saido, W. R. Markesbery, M. J. Russell, D. R. Wekstein, E. Patel and J. W. Geddes (1998). "N-terminal heterogeneity of parenchymal and cerebrovascular Abeta deposits." J Neuropathol Exp Neurol **57**(1): 76-94.

Tekirian, T. L., A. Y. Yang, C. Glabe and J. W. Geddes (1999). "Toxicity of pyroglutaminated amyloid beta-peptides 3(pE)-40 and -42 is similar to that of A beta1-40 and -42." J Neurochem **73**(4): 1584-1589.

Terry, R. D., N. K. Gonatas and M. Weiss (1964). "Ultrastructural Studies in Alzheimer's Presenile Dementia." Am J Pathol **44**: 269-297.

Texido, L., M. Martin-Satue, E. Alberdi, C. Solsona and C. Matute (2011). "Amyloid beta peptide oligomers directly activate NMDA receptors." Cell Calcium **49**(3): 184-190.

Traynelis, S. F., L. P. Wollmuth, C. J. McBain, F. S. Menniti, K. M. Vance, K. K. Ogden, K. B. Hansen, H. Yuan, S. J. Myers and R. Dingledine (2010). "Glutamate receptor ion channels: structure, regulation, and function." Pharmacol Rev **62**(3): 405-496.

Tsigelny, I. F., Y. Sharikov, V. L. Kouznetsova, J. P. Greenberg, W. Wrasidlo, T. Gonzalez, P. Desplats, S. E. Michael, M. Trejo-Morales, C. R. Overk and E. Masliah (2014). "Structural diversity of Alzheimer's disease amyloid-beta dimers and their role in oligomerization and fibril formation." J Alzheimers Dis **39**(3): 583-600.

Tu, S., S. Okamoto, S. A. Lipton and H. Xu (2014). "Oligomeric Aβ-induced synaptic dysfunction in Alzheimer's disease." Molecular Neurodegeneration **9**(48): 1-12.

Tulving, E. and H. J. Markowitsch (1998). "Episodic and declarative memory: role of the hippocampus." Hippocampus **8**(3): 198-204.

Ulbrich, M. H. and E. Y. Isacoff (2008). "Rules of engagement for NMDA receptor subunits." Proc Natl Acad Sci U S A **105**(37): 14163-14168.

Ultanir, S. K., J. E. Kim, B. J. Hall, T. Deerinck, M. Ellisman and A. Ghosh (2007). "Regulation of spine morphology and spine density by NMDA receptor signaling in vivo." Proc Natl Acad Sci U S A **104**(49): 19553-19558.

Um, J., A. Kaufman, M. Kostylev, J. Heiss, M. Stagi, H. Takahashi, M. Kerrisk, V. A., T. Wisniewski, A. Koleske, E. Gunther, H. Nygaard and S. M. Strittmatter (2013). "Metabotropic Glutamate Receptor 5 Is a Coreceptor for Alzheimer Aβ Oligomer Bound to Cellular Prion Protein." Neuron **79**(5): 887-902.

Vassar, R., B. D. Bennett, S. Babu-Khan, S. Kahn, E. A. Mendiaz, P. Denis, D. B. Teplow, S. Ross, P. Amarante, R. Loeloff, Y. Luo, S. Fisher, J. Fuller, S. Edenson, J. Lile, M. A. Jarosinski, A. L. Biere, E. Curran, T. Burgess, J. C. Louis, F. Collins, J. Treanor, G. Rogers and M. Citron (1999). "Beta-secretase cleavage of Alzheimer's amyloid precursor protein by the transmembrane aspartic protease BACE." Science **286**(5440): 735-741.

Walsh, D. M., I. Klyubin, J. V. Fadeeva, W. K. Cullen, R. Anwyl, M. S. Wolfe, M. J. Rowan and D. J. Selkoe (2002). "Naturally secreted oligomers of amyloid beta protein potently inhibit hippocampal long-term potentiation in vivo." Nature **416**(6880): 535-539.

Wang, S., M. Chen, Y. Li, Y. Shao, Y. Zhang, S. Du and J. Wu (2016). "Morphological analysis of dendrites and spines by hybridization of ridge detection with twin support vector machine." PeerJ **4**: e2207.

Watanabe, Y., E. Gould and B. S. McEwen (1992). "Stress induces atrophy of apical dendrites of hippocampal CA3 pyramidal neurons." Brain Res **588**(2): 341-345.

Weber, P. C., D. H. Ohlendorf, W. J.J. and S. F.R. (1989). "Structural origins of high-affinity biotin binding to streptavidin." Science **243**(4887): 85-88.

Wei, W., L. N. Nguyen, H. W. Kessels, H. Hagiwara, S. Sisodia and R. Malinow (2010). "Amyloid beta from axons and dendrites reduces local spine number and plasticity." Nat Neurosci **13**(2): 190-196.

Wertkin, A. M., R. S. Turner, S. J. Pleasure, T. E. Golde, S. G. Younkin, J. Q. Trojanowski and V. M. Lee (1993). "Human neurons derived from a teratocarcinoma cell line express solely the 695-amino acid amyloid precursor protein and produce intracellular beta-amyloid or A4 peptides." Proc Natl Acad Sci U S A **90**(20): 9513-9517.

White, E. (2016). "Autophagy and p53." Cold Spring Harb Perspect Med **6**(4): a026120.

White, E., J. M. Mehnert and C. S. Chan (2015). "Autophagy, Metabolism, and Cancer." Clin Cancer Res **21**(22): 5037-5046.

Wilcox, K. C., P. N. Lacor, J. Pitt and W. L. Klein (2011). "Aβ Oligomer-Induced Synapse Degeneration in Alzheimer's Disease." Cell Mol Neurobiol **31**: 939-948.

Windisch, H., W. Muller and H. A. Tritthard (1985). "Fluorescence monitoring of rapid changes in membrane potential in heart muscle." Biophys J **48**(6): 877-884.

Wirths, O., G. Multhaup and T. A. Bayer (2004). "A modified beta-amyloid hypothesis: intraneuronal accumulation of the beta-amyloid peptide--the first step of a fatal cascade." J Neurochem **91**(3): 513-520.

Wirths, O., G. Multhaup, C. Czech, N. Feldmann, V. Blanchard, G. Tremp, K. Beyreuther, L. Pradier and T. A. Bayer (2002). "Intraneuronal APP/A beta trafficking and plaque formation in beta-amyloid precursor protein and presenilin-1 transgenic mice." Brain Pathol **12**(3): 275-286.

Woods, N. K. and J. Padmanabhan (2012). "Neuronal Calcium Signaling and Alzheimer's Disease." Calcium Signaling. Advances in Experimental Medicine and Biology **740**: 1193-1217.

Xiao, H., B. Liu, Y. Chen and J. Zhang (2016). "Learning, memory and synaptic plasticity in hippocampus in rats exposed to sevoflurane." Int J Dev Neurosci **48**: 38-49.

Xie, Z., Y. Dong, U. Maeda, P. Alfille, D. J. Culley, G. Crosby and R. E. Tanzi (2006). "The common inhalation anesthetic isoflurane induces apoptosis and increases amyloid beta protein levels." Anesthesiology **104**: 988-994.

Xie, Z., Y. Dong, U. Maeda, R. D. Moir, W. Xia, D. J. Culley, G. Crosby and R. E. Tanzi (2007). "The inhalation anesthetic isoflurane induces a vicious cycle of apoptosis and amyloid beta-protein accumulation." J Neurosci **27**(6): 1247-1254.

Yan, Y. and G. Marriott (2003). "Analysis of protein interactions using fluorescence technologies." Curr Opin Chem Biol **7**(5).

Yang, C. W. and J. L. Fuh (2015). "Exposure to general anesthesia and the risk of dementia." J Pain Res **8**: 711-718.

Yang, G., P. C. Chang, A. Bekker, T. J. Blanck and W. B. Gan (2011). "Transient effects of anesthetics on dendritic spines and filopodia in the living mouse cortex." Anesthesiology **115**(4): 718-726.

Yang, T., S. Li, H. Xu, D. M. Walsh and D. J. Selkoe (2017). "Large Soluble Oligomers of Amyloid beta-Protein from Alzheimer Brain Are Far Less Neuroactive Than the Smaller Oligomers to Which They Dissociate." J Neurosci **37**(1): 152-163.

Yu, J.-T., R. C.-C. Chang and L. Tan (2009). "Calcium dysregulation in Alzheimer's disease: From mechanisms to therapeutic opportunities." Prog Neurobiol **89**(3): 240-255.

Yu, W. H., A. M. Cuervo, A. Kumar, C. M. Peterhoff, S. D. Schmidt, J. H. Lee, P. S. Mohan, M. Mercken, M. R. Farmery, L. O. Tjernberg, Y. Jiang, K. Duff, Y. Uchiyama, J. Naslund, P. M. Mathews, A. M. Cataldo

and R. A. Nixon (2005). "Macroautophagy--a novel Beta-amyloid peptide-generating pathway activated in Alzheimer's disease." J Cell Biol **171**(1): 87-98.

Zachari, M. and I. G. Ganley (2017). "The mammalian ULK1 complex and autophagy initiation." Essays Biochem **61**(6): 585-596.

Zhang, B., M. Tian, H. Zheng, Y. Zhen, Y. Yue, T. Li, S. Li, E. R. Marcantonio and Z. Xie (2013). "Effects of Anesthetic Isoflurane and Desflurane on Human Cerebrospinal Fluid Aβ and τ Level." Anesthesiology **119**(1): 52–60.

Zhang, P., A. Ohara, T. Mashimo, H. Imanaka, A. Uchiyama and I. Yoshiya (1995). "Pulmonary resistance in dogs: a comparison of xenon with nitrous oxide." Can J Anaesth **42**(6): 547-553.

Zhao, W. Q., F. G. De Felice, S. Fernandez, H. Chen, M. P. Lambert, M. J. Quon, G. A. Krafft and W. L. Klein (2008). "Amyloid beta oligomers induce impairment of neuronal insulin receptors." FASEB J **22**(1): 246-260.

Zhou, T., S. Guo, S. Wang, Q. Li and M. Zhang (2017). "Protective effect of sevoflurane on myocardial ischemia-reperfusion injury in rat hearts and its impact on HIF-1alpha and caspase-3 expression." Exp Ther Med **14**(5): 4307-4311.

Zhu, W., J. Zhu, S. Zhao, J. Li, D. Hou, Y. Zhang and H. Sun (2020). "Xenon Exerts Neuroprotective Effects on Kainic Acid-Induced Acute Generalized Seizures in Rats via Increased Autophagy." Front Cell Neurosci **14**: 582872.

10. Appendix

10.1 Animals

Mouse strain	Description	Company
C57BL/6	Wildtype mice	Charles River, Germany
Generic EGFP	Transgenic (EGFP-M) mice	Technical University of Munich, Germany

10.2 Antibodies

Primary antibodies

All primary antibodies are rabbit polyclonal antibodies.

Antibody	Dilution	Company
α-Atg12	1:1000	Cell Signaling Technology Inc., USA
α-Beclin1	1:1000	
α-Akt	1:1000	
α-pAkt	1:1000	
α-ULK1	1:500	
α-pULK1	1:500	
α-PI3K-III	1:1000	
α-p53	1:500	
α-LC3B	1:1000	

Secondary antibodies

Alexa Fluor 488 (A-21311); (Anti)-Rabbit (polyclonal); 1:200; Thermo Fisher Scientific, Germany

Anti-Rabbit IgG, HRP-linked Antibody; 1:10.000; Cell Signaling Technology

10.3 Chemicals, reagents and commercially produced sets

Substance	Details	Company
α-D-(+) Glucose- Monohydrate		Sigma Aldrich, Germany
Acetone		Merck, Germany
$A\beta_{1-42}$		Bachem Holding AG, Switzerland
$A\beta_{1-40}$		Bachem Holding AG, Switzerland
AβpE3		Bachem Holding AG, Switzerland
Ammoniumpersulfat (APS)		Sigma Aldrich, Germany
3NTyrAβ		Generously provided by Martin Kummer, Bonn, Germany
Bovine Serumalbumine (BSA)	Fraction V	Carl Roth, Germany
Biotin-labeled $A\beta_{1-42}$		AnaSpec, Fremont, CA, USA

Calcium chloride dihydrate ($CaCl_2$)		Sigma Aldrich, Germany
Carbogen	95% O_2, 5% CO_2	Linde AG, Germany
Coomassie Brilliant Blue R-250 Staining Solution	#1610436	Bio-Rad, Germany
50X Complete		Roche Deutschland Holding GmbH, Germany
Dimethylsulfoxid (DMSO)		Sigma Aldrich, Germany
Disodium phosphate		Sigma Aldrich, Germany
ECL Clarity™ Western substrate		Bio-Rad, Germany
EtOH	96%	Merck, Germany
FAM-labeled $A\beta_{1-42}$		AnaSpec, Fremont, CA, USA
Glycine		Sigma Aldrich, Germany
Guanidine Hydrochloride (HCl)		VWR, Germany
Hydrogen peroxide	30% H_2O_2	Carl Roth, Germany
Hexafluorisopropanol (HFIP)		Merck, Germany
Kaliumchlorid (KCl)		Sigma Aldrich, Germany
Dako Fluorescent Mounting Medium		Dako North America, USA
LanthaScreen® Tb-Streptavidin	1 mg/mL Kit	Life Technologies
Luminol		Sigma Aldrich, Germany
Magneisum chloride Hexahydrate		Sigma Aldrich, Germany
Milli-Q-water	Purified water Type 1	Merck Millipore, Germany
Methanol		Merck Millipore, Germany
Monopotassium phosphate		Sigma Aldrich, Germany
Sodiumhydroxide (NaOH)		VWR, Germany
Silver Nitrate BioXtra		Sigma Aldrich, Germany
Normal Goat Serum (NGS)		Sigma Aldrich, Germany
p-Coumaric acid		Sigma Aldrich, Germany
Sodiumhydrogencarbonate ($NaHCO_3$)		Sigma Aldrich, Germany
Sodiumhydrogenphosphate (NaH_2PO_4)-Monohydrate		Sigma Aldrich, Germany
Pepstatin A		Roche, Switzerland
NaCl		Sigma Aldrich, Germany
PMSF		Roche, Switzerland
Sodiumdodecylsulfate (SDS)		SERVA, Germany
Sodium bicarbonate		Sigma Aldrich, Germany
Sodium dihydrogen phosphate monohydrate		Sigma Aldrich, Germany
Pre-Diluted Protein Standard Assay	BSA Set	Thermo Fisher Scientific
Tetramethylethylendiamine (TEMED)		Sigma Aldrich, Germany
Tris		Roche, Switzerland
Triton-X-100		Sigma Aldrich, Germany
Tween-20		Sigma Aldrich, Germany
Complete, 50x	Protease Inhibitor Cocktail tablets (S2023)	Roche, Switzerland
Xenon, 65%		Linde AG, Germany
Isoflurane CP		CP-Pharma, Germany

Sevoflurane	SevoFlo	Zoetis, Belgium
DC Protein Assay		Bio-Rad, Germany
Histoacrylic	Tissue glue	B.Braun, Germany
LDS Sample Buffer		Invitrogen, Germany
Novex Sharp Pre-Stained Protein Standard		Invitrogen, Germany
phosSTOP	Phosphatase inhibitor tablets	Roche, Switzerland
Restore PLUS Western Blot Stripping Buffer		Thermo Fisher Scientific, Germany
RIPA Buffer		Sigma Aldrich, Germany
Sample Grinding Kit		GE Healthcare, Germany
Sample Reducing Agent	10% NuPAGE gel type	Invitrogen, Germany
4-(2-(6-(Dibutylamino)- 2-naphthalenyl)ethenyl)- 1-(3-sulfopropyl)- pyridinium hydroxide inner salt	Di-4-ANEPPS Staining of slices for VSDI	Sigma Aldrich, Germany
Paraformaldehyde (PFA)		Sigma Aldrich, Germany
Phenylmethylsulfonylfluoride (PMSF)		Roche, Germany
Roti®-Block		Carl Roth, Germany

10.4 Recipes

Description	Details	Concentration	
aCSF	NaCl	125	mM
	KCl	2.5	mM
	NaH_2PO_4-Monohydrate	1.25	mM
	D-(+) Glucose-Monohydrate	25	mM
	$NaHCO_3$	25	mM
	$MgCl_2$-Hexahydrate	1	mM
	$CaCl_2$-Dihydrate	2	mM
	dissolved in Milli-Q-water; pH 7.4		
Preparation buffer	NaCl	125	mM
	KCl	2.5	mM
	NaH_2PO_4-Monohydrate	1.25	mM
	D-(+) Glucose-Monohydrate	25	mM
	$NaHCO_3$	25	mM
	$MgCl_2$-Hexahydrate	6	mM
	$CaCl_2$-Dihydrate	0.25	mM
	dissolved in Milli-Q-water; pH 7.4		
Running buffer	Tris	25	mM
	Glycine	192	mM
	SDS	0.1	%
	dissolved in Milli-Q-water		
Sample buffer (4x)	LDS sample buffer, NuPAGE	1000	µl
	Sample Reducing Agent, NuPAGE	400	µl
Sample buffer (2x)	Sample buffer (4x)	500	µl

	dissolved in Milli-Q-water	1300	µl
TBS/T	Tris	25	mM
	NaCl	150	mM
	Tween-20	0.1	%
	dissolved in Milli-Q-water, pH 7.4		
Blotting Buffer	Tris	25	mM
	Glycine	192	mM
	dissolved in Milli-Q-water		
BSA, 5%	BSA (Fraction V) dissolved in TBS/T	5	%
Coumaric acid stock solution	p-Coumaric acid	14,78	mg/ml
	dissolved in DMSO		
ECL-reagent	1 M Tris (pH 8.5)	2	ml
	Coumaric stock solution	89	µl
	Luminol stock solution	200	µl
	30% H_2O_2	6.1	µl
	dissolved in Milli-Q-water	18	ml
Lysis buffer	PMSF	1	mM/ml
	Pepstatin A	2	µM/ml
	Complete, 50x	1	tablet/25 ml
	phosSTOP	1	tablet/10 ml
	dissolved in RIPA buffer		
Luminol stock solution	Luminol	44.29	mg/ml
	dissolved in DMSO		
BSA, 5%	BSA (Fraction V) dissolved in TBS/T	5	%
Blocking Buffer	Normal Goat Serum (NGS)	10	%
	Triton-X-100	0.5	%
	dissolved in PBS		
PBS	NaCl	13.7	mM
	KCl	0.27	mM
	Na2HPO4	0.8	mM
	KH2PO4	0.14	mM
	dissolved in Milli-Q-water; pH 7.4		
PFA, 4%	PFA	4	g
	PBS	50	ml
	dissolved on heat plate (50 °C); pH 7.4		
Aβ-stem-solution (TR-FRET)	$Aβ_{1-42}$	2	µM
	FAM-labeled-$Aβ_{1-42}$	2	µM
	Biotin-labeled-$Aβ_{1-42}$	2	µM
	AβpE3	2	µM
TR-FRET-assay-addition buffer $MgCl_2$(+)	MOPS/Tris base pH= 8.05	56.82	mM
	$MgCl_2$	113.64	mM

TR-FRET-assay-addition buffer $MgCl_2$(-)	MOPS/Tris base pH=8.05	56,82	mM
Aβ TR-FRET Assay solution D1	$Aβ_{1-42}$	100	nM
	FAM-labeled-$Aβ_{1-42}$	500	nM
	Biotin-labeled-$Aβ_{1-42}$	400	nM
	AβpE3	1	µM
Aβ TR-FRET Assay solution D2	$Aβ_{1-42}$	100	nM
	Biotin-labeled-$Aβ_{1-42}$	900	nM
	AβpE3	1	µM

10.5 Hardware

Description	**Details**	**Company**
Absorbance Microplate Reader		Tecan Sunrise, Switzerland
Analytic balance	LA164i	VWR, Germany
Biofuge Fresco	Microcentrifuge	Heraeus, Germany
ChemiDoc XRS+ System		Bio-Rad, Germany
Confocal microscope	BX51WI	Olympus, Hamburg, Germany
Envision		
Forane Vapour 19.3	Vapour for Isoflurane	Drägerwerk, Germany
Multi-Casting Chamber	Mini-PROTEAN System	Bio-Rad, Germany
pH electrode	SenTix 21	Xylem, Germany
ph meter	pH522	Xylem, Germany
Reference Pipettes		Eppendorf, Germany
Rocky 3D	Shaker	Fröbel Labortechnik, Germany
Sunrise reader		Tecan Group, Switzerland
Thermomixer comfort		Eppendorf, Germany
Ultrasonic bath	Bandelin Sonorex	Bandelin Electronic, Germany
Vibratome	VT1000 S	Leica, Germany
Vortexer	D-6012	NeoLab Migge, Germany
Blot filter papers		GE Health Care, Germany
Cover Slips		Menzel-Glaeser, Germany
Discofix-1, one-way	Stopcock	B. Braun, Germany
Discofix C		B. Braun, Germany
Duran laboratory bottles		VWR, Germany
Falcon centrifuge tubes		Greiner Bio-One, Germany
Filter Tip		Sarstedt, Germany
Guillotine		World Precision Instruments, Germany
Heidelberger Verlängerungen		Fresenius Kabi, Germany
Holding Chamber		Own construction
Measuring pipettes		Eppendorf, Germany
Micro tubes	1.5 ml	Sarstedt, Germany
Microscope slides	Super Frost Plus	Thermo Fisher Scientific, Germany
Pasteur Pipets	Disposable glass 230 mm	VWR, Germany
Razor blade		Wilkinson Sword, UK
Well plate	12-well, 96-well, 384-well	Brand, Germany
CCD Camera (VSDI)	MiCAM02 HR-CCD	BrainVision Inc., Japan
Glass electrodes	borosilicate glass capillaries GC150TF	Kent, UK

Horizontal glass electrode puller	DMZ-Universal Puller	Zeits Instruments, Germany
Stimulators (VSDI, LTP)	Isolated stimulator, Type 2533	Hertfordshire, UK
Light Source (VSDI)	MHAH-150 W	Moritex, China
Amplifier (VSDI)	ISO-STIM 01M	npi electronics, Germany
Microscope (VSDI, LTP)	Binocular Stemi 1000	Zeiss, Germany
Pulse generator (LTP)	Master 8	A.M.P.I., Israel
Headstage (VSDI, LTP)	CV20303BU	Axon Instruments, USA
Panel mounted pump (VSDI, LTP)	IS3124A Persistaltic pump	Ismatec, Germany
Piezomanipulator (VSDI, LTP)	PM 500-20	Frankenberger, Germany
Amplifier (LTP)	Multiplyer Axopatch 200B	Axon Instruments, USA
Plate, 384 Well	Black, Low Flange, NBS, Non-Sterile	Fisher Scientific

10.6 Software

Description	**Version**	**Company**
Excel	2018	Microsoft Corporation, USA
PraphPad Prism	6.01	GraphPad Software, USA
Image Lab	5.2	Bio-Rad, Germany
Magellan	Standard	Tecan Groups, Switzerland
EnVision multimode plate reader		Perkin Elmer
Brain Vision (VSDI)	13.04.20	Brain Vision LLC, NC, USA
Word	2018	Microsoft Corporation, USA
WinLTP 1.11b	Recording Software (LTP)	University Bristol, UK
Pulse 8.31	Recording Software (LTP)	Lamrecht, Germany
MATLAB	R2008b	The MathWorks, USA
VSDI ROI Tool (in MATLAB)	2017/2018	Customised application

11. Acknowledgements

Mein großer Dank gilt Professor Dr. Gerhard Rammes, der mir die Chance gab in seiner Arbeitsgruppe am Klinikum rechts der Isar diese Arbeit anzufertigen. Trotz mehrerer Hürden im Laufe der Jahre konnte ich immer auf seine Hilfe und Expertise vertrauen.
Auch bei der ganzen Arbeitsgruppe der Experimentellen Anästhesie möchte ich mich herzlich bedanken. Nina, Andi, Shi Dai, Xing Xing, Claudia, Tanja und viele mehr! Es war mir eine Ehre mit euch arbeiten zu dürfen.

Sebastian und Rami, danke für die Erstellung des VSDI ROI tools!

Matthias Kreuzer – was wäre diese Arbeit ohne deine Hilfe? Tausend Dank für deine allzeit schnelle Hilfe wenn ich mal wieder verzweifelt war in der Welt der Statistik!

Vielen Dank auch an die Arbeitsgruppe rund um Dr. Hadian am Helmholtz Zentrum in Großhadern – die Zusammenarbeit hat wirklich Spaß gemacht.

Chris Parsons – thank you for everything.

Widmen tue ich diese Arbeit meiner Familie – insbesondere meiner Tochter Clara Sophie und meinem Mann Peter. Ohne euch wäre das alles nicht möglich gewesen. Ich liebe euch von ganzem Herzen!